The Heemskirk granite massif, western Tasmania

- A study of chemical variability within

plutonic rocks

by

RNDr Josef Klomínský CSc

(Charles University, Prague)

A thesis submitted in partial fulfilment of

the requirements for the degree of

Doctor of Philosophy

UNIVERSITY OF TASMANIA

HOBART

June 1972

Let every student bear in mind:

that all rocks are transitional
members of series and that clear
cut boundaries are not to be
expected

Williams

This thesis contains no material which has been
accepted for the award of any other degree or
diploma in any university and to the best of my
knowledge and belief contains no copy or para-
phrase of material previously published or writ-
ten by another person except where due reference
is made in the text of the thesis.

Josef Klomínský
University of Tasmania
Hobart
1972

Frontispice

The Heemskirk granite massif with summit of Mt.
Heemskirk (2450 feet) on the left side of
the picture, viewed from Grenville Harbour. In
foreground is coastline with outcrops of the
coarse-grained white granite.

Contents   page

Summary

The Heemskirk granite massif was intruded as
a diapir about 354 m.y. ago into Precambrian and Palaeo-
zoic sediments. It fractionated into two types the red
and white granites, which are distinguished by their
colour and mineral and chemical composition. It is sug-
gested that they also differed in volatile content and
oxygen fugacity. The characteristic mineral assemblage
of the red granite (hematite – magnetite – allanite)
indicates a higher oxygen fugacity than the white type
which is characterised by tourmaline. Both rock types
are biotite or two mica granites sensu stricto (Hietanen,
1963). Differences between the granite types have deve-
loped during and after emplacement of the intrusion.

The granite body has a generally stratiform structu-
re with subhorizontal layering and the upper part of
the intrusion is characterized by a very flat dome. Its
internal structure consists of several layers of grani-
tes with slightly different mineralogical, textural and
chemical properties. Within each layer cryptic layering
can be defined by the behaviour of the trace elements.
The red granite occupies the topmost part of the intru-
sion and forms a comparatively thin layer in the eastern
part of the body; it acts as country rock, having been

consolidated earlier than most of the white granites.

Towards the west the red granite is laterally re-
placed by the white granite, which probably represents
the major part of the Heemskirk granite at depth. The
roof zone of the white granite (contact zone with the
red granite) is enriched by tourmaline nodules, which
are interpreted as originally volatile segregations in
a crystallizing magma. The white granite shows a higher
degree of geochemical and mineralogical homogeneity.

Interpretation of the granite composition in the
light of experimental data suggests that the Heemskirk
massif was emplaced at shallow depths in the crust.
A temperature of $650^{\circ}C$ is estimated for the crystalli-
zation of K-feldspars from the red granite.

The surface of the body reflects on a subdued scale
the anticlinorial structure of the original sedimentary
cover. The existence of the ghost structure of the
country rocks in the roof of the intrusion is also indica-
ted by the distribution of the contaminates and positive
anomalies of some trace elements (particularly within
the red granite).

The Heemskirk granite massif is characterized by
very regular fracture systems. Extensive greisenisation
and hydrothermal alteration follow the dominant cross
joints. The filling of the fissures is quartz, tourmaline

and commonly cassiterite in economic concentrations, and rare columbite. The majority of the tin deposits are found on the white/red granite contact. The abundance of Sn concentration at the present surface in the eastern part of the body is related to exposure of this contact and the depth of red granite cover. Where the red granite exceeds 600 feet in thickness tin mineralization is unlikely to be economic.

1. Introduction

1.1. General statement

Research in primary geochemical dispersion patterns
has been directed towards determining the distribution of
selected elements on a relatively small scale, in a parti-
cular rock type or in a suite of rocks, as for instance in
plutons which contain deposits of copper (Putman, 1962),
lead (Oftedahl 1954; Slawson 1959), gold (Montei 1967) and
uranium (Jeier 1966). In general the results of these
studies have confirmed that ore bodies are haloed by
an abnormally high content of the respective elements in
the host rocks. Hence the economic significance of regional
geochemical patterns is that they focus interest upon areas
in which the elements are enriched and it is considered
probable that these areas will form the prospecting targets
of the future. The interpretation of the patterns of
concentration has to relate the local geology, structure
and geomorphology.

Two factors made the Heemskirk massif in western
Tasmania especially appropriate for this study. First,
the high relief which provides excellent exposures and
affords an opportunity to study chemical and mineralogical
variations in three dimensions. Second, recent topographic

maps of the area are available for geological mapping on 1:31.680 scale. A generalized geological map of the Heemskirk granite massif on scale 1 : 50 000 was made as part of the present investigation.

After preliminary field work in the Heemskirk granite massif it became apparent to the writer that there was no obvious relationship between the red and white granites. It was also discovered that there was flat layering in the granite and that this had some relationship to the general structure of the body and to pre-existing structures in the host rocks. With this information, the study was turned toward complete characterization of the two units of the Heemskirk massif and determination of their inter--relationships and their relationship to the country rocks. However, problems still remain, such as the nature of the differentiation which produces granitic rocks of different character in close association and the nature, and the origin of hydrothermal solutions.

The analysis of the several hundred samples required for this study was dependent on the development of suitably rapid and precise analytical technique. The interpretation of the resulting large quantity of data was, in turn, dependent on the use of appropriate statistical methods. For these purposes the whole rocks and some of their mineral components (biotites and K-feldspars) were analysed

for trace elements by non-destructive X-ray fluorescence
and the chemical data used to construct geochemical maps
for the different rock types within the Heemskirk grani-
te. Chemical data have been also applied to the solution
of some metallogenic problems e.g. geochemical criteria
for identification of tin-bearing granites.

Appendix I contains a study on regional geochemistry
and the relationship of granitic rocks to ore deposits in
the Tasman Orogenic Zone. The work is a part of the more
detailed research project which was prepared at the de-
partment of geology of the University of Tasmania in co-
operation with Dr M.Solomon and Dr D.I.Groves. Appendix
II consist of detailed descriptions of analytical techni-
ques, and tables of chemical data.

1.2. Acknowledgments

1.3. General geology

Tasmania represents a significant block within the Tasman Orogenic zone. The island consists in general of two fundamental units, the "platform cover" and the older fundament consolidated by Variscan tectonogenesis. The "platform cover" consists of sediments and volcanics of Permian, Mesozoic, Tertiary and Quaternary age. The old fundament of this island block is composed mainly of folded unmetamorphosed and metamorphosed complexes of Precambrian and Paleozoic age. The structure of the fundament

has been outlined by Solomon and Griffiths (1972) who have suggested that the early (P€ - Ordovician) history involved formation of a new ocean followed by collision between an island arc - continental margin complex in West Tasmania and an older Precambrian block now occupying the centre of Tasmania (the Tyennan Geanticline of Solomon, 1965). Succeeding shelf sedimentation was interrupted in the mid - Devonian by the Tabberabberan Orogeny and this was followed by post orogenic granites. Crystallization of the majority of the granitic intrusives occurred between 370 million years and 338 million years (Fig. 1).
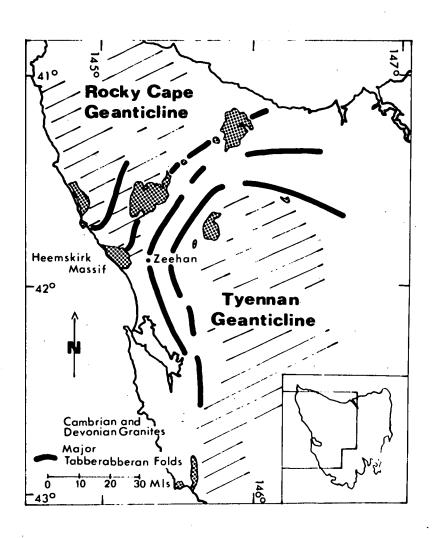
Most of the granites in the Tasmanian block outcrop in the northwest and northeast of the island, the north-western granites being predominantly of alaskite composition, whereas those in the north-east are more varied.

The north-western granites are represented by the Housetop, Meredith, Heemskirk and Pieman Heads granite massifs. The strong similarity in petrochemistry of the Heemskirk, Pieman Heads and Meredith Granite suggests that they are connected at depth (Klomínský & Groves, 1970).

The Heemskirk massif is a high-level calc-alkaline granite. It has a roughly tear-drop shaped outcrop and is emplaced in the axial zone of an anticlinorium of Precambrian metasediments which are overlain to the south

Figure 1

Major granite bodies of Western Tasmania in relation
to structure (after Carey 1953, and Solomon 1962 in
Brooks and Compston 1965).

Rocky Cape
Geanticline

Heemskirk
Massif

•Zeehan

Tyennan
Geanticline

Cambrian and
Devonian Granites

Major
Tabberabberan Folds

0   10   20   30 Mls

41°
42°
43°
145°
146°
147°

N

and east by Paleozoic formations. According to Green (1966) the Heemskirk granite intrudes Cambrian volcanics, gabbro and serpentinised dunite, and Precambrian unmetamorphosed siltstones and quartzites Precambrian age (Oonah Quartzite and Slate), as well as the Silurian Crotty Quartzite and Amber Slate Formations. The dominant country rock is the Oonah Quartzite and Slate, which consists of alternating pale grey saccharoidal quartzitic sandstone or quartzite, thin-bedded micaceous quartzite, and siltstone and laminated slate. The general trends of the country rocks are parallel to the granite margins, but down the dip the granite margin transgresses the bedding of the country rocks.

The southern contact of the body is vertical or dips steeply outward from the granite. The eastern contact has a moderate dip toward the Zeehan township, and it is possible that Ordovician and Silurian sediments to the east of the body are intruded at depth. The northern contact is undulating, with a tendency to dip gently outwards (see figure 5).

1.4. Location, access and topography

The area investigated is situated near the West Coast of Tasmania lying between the sea and the township of

Zeehan. The coastline forms the western margin of the granite from Trial Harbour (Remine) to Granville Harbour, while the eastern and northern boundaries follow the eastern slopes of the Heemskirk Range. The area is included in the geological map of the one mile series K - 55 - 5 - 50 Zeehan.

The only permanent settlement is a farm at Granville Harbour. There is a number of weekend shacks at Trial Harbour and Granville Harbour. Access to the Heemskirk granite massif consists of two gravel roads from Zeehan.

The Heemskirk massif area consists of two major physiographic units. These are the coastal plain, which extends inland for about 2 km and the Heemskirk - Agnew Range, which occupies most of the eastern part of the area (Plate 1). The coastal plain has a moderate relief, with deeper valleys and gullies close to the coast. Vegetation cover for that area consists mainly of button - - grass and thick rain forest occurs in shaltered valleys and on the slopes of the Heemskirk Range. "Horizontal" scrub is common on flatter ground and on the high gentle slopes in the area between Mt. Heemskirk and Mt. Agnew (Plate 2). This rugged depression could not be mapped because of the thick scrub cover (see Geological map).

The Heemskirk Range covers a roughly circular area in the eastern part of the region studied, with a number of peaks over 2500 feet. The highest point is Mt. Agnew, which rises to 2769 feet on the eastern edge of the Range. The second highest point is Mt. Heemskirk (2450 feet) on the north - western edge of the mountainous area.

The topography of the investigated area reflects the strong influence of recent vigorous stream erosion. The drainage pattern is roughly radial and dendritic. There is a marked water-divide running along North Heemskirk Spur via Mt. Heemskirk to Mt. Agnew. The streams flowing to the north and east belong to the Pieman and Little Henty Catchment area, while the streams on the southern and south-western slopes are part of the Coastal drainage. Major streams of the area are the Heemskirk River, Tasman River and Granite Creek. Faults and well--marked joint planes exert a local control on the stream pattern.
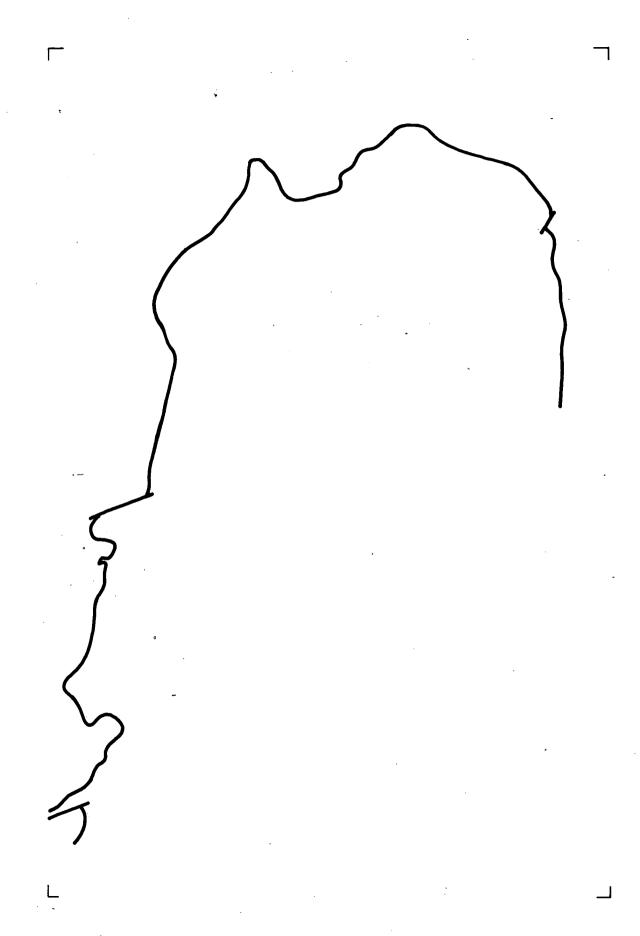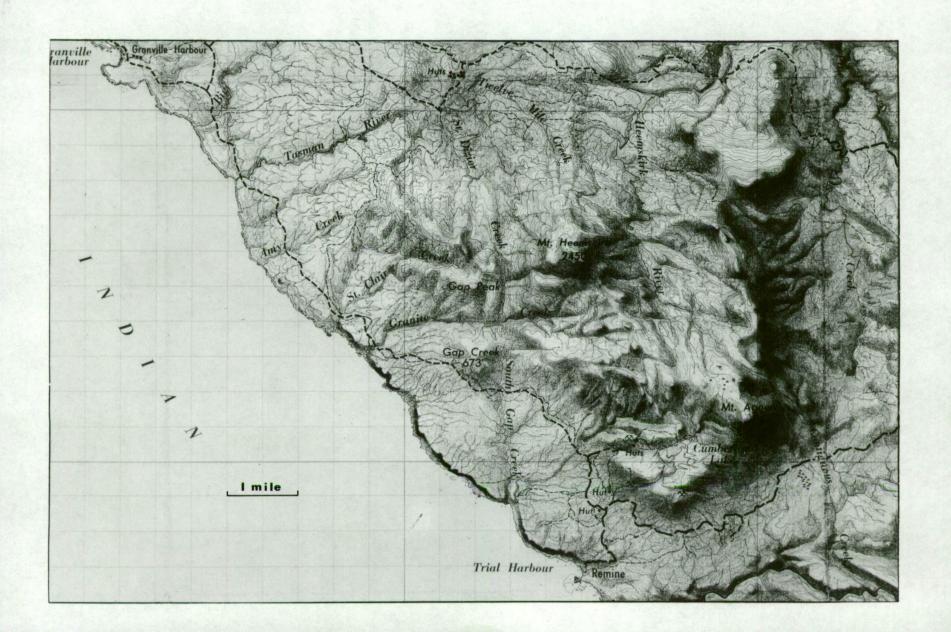
The steep slopes of the mountainous part of the Heemskirk Range, the coast line and tops of the ridges in the western part of the area are occupied by extensive outcrops of granitic rocks (Plate 1). The peneplained parts of granite (western area of the intrusion) have a thin cover of detrital quartz gravel. More intensive

Figure 2

Topographic map of Heemskirk granite massif.

Granville
Harbour

Granville Harbour

Huts

Twelve

St. Dizier

Mile

Creek

Heemskirk

Tasman

River

Creek

I   N   D   I   A   N

Amy

Creek

Creek

Creek

Creek

Mt. Heemskirk
2450

St. Clair

Gap Peak

River

Granite

Creek

Gap Creek
673'

South

Mt. Agnew

Gap

Creek

Creek

Cumberland
Lake

Huts

1 mile

Hut

Huts

Hut

Creek

Trial Harbour

Remine

weathering of the granite (kaolinisation is common in
area between Ammy Creek and Granite Creek.

1.5. Structural control of relief

The prominent relief produced by the red granite
reflects the general form the Heemskirk geanticlinal
structure. Steep slopes of the topography correspond to
the boundary of the granite body (Fig. 2). The relief of
the Mt. Heemskirk Range also reflects the general featu-
res of the topography of the topmost part of the intrusion.
In contrast, the part of the Heemskirk massif west of South
Gap Creek is represented by the gently undulating plateau
with a prominent N-W trending ridge (North Heemskirk
Spur) which is parallel to the internal structures of
the white granite.

1.6. Previous geological work

The history of geological investigation in the Heems-
kirk region began in 1876 when traces of tin were found
near Mt. Heemskirk, so openning the way for exploration
of the West Coast mineral fields.

The first report on the tin-ore deposits of Mt.Heems-
kirk was published by Waller (1902). Twelvetrees and Ward
(1910) studied the ore- bodies of the Zeehan mineral field

and their relationship to the Heemskirk granite. They
amplified Waller's observations (1904) about the zonal
distribution of ore types, and extended them to include
the Heemskirk tin field. They suggested that the ores
showed a zonal relationship to the Heemskirk granite.
A detailed study of the South Heemskirk tin field was
launched by Waterhouse (1916). His description of petro-
logy of the granite and of the mineralogy of the indivi-
dual mines and prospects is so far the most comprehensi-
ve report on this region. He first used the term
"Heemskirk granite massif".

Blissett (1962) summarised the geological history of
the Heemskirk granite massif and gave new petrological
and chemical data. He collected a complete list of
published and unpublished references concerning the
broader area of the West Coast. The Heemskirk granite and
the geology of the country rocks have been the subject
of several theses by Honorous B.Sc. students of the Uni-
versity of Tasmania in the period 1964-1968. Green (1964
and 1966a, 1966b) studied the thermal metamorphism and
geology in the Trial Harbour district. The general geology
of the western part of the intrusion was briefly described
by Palfreyman (1965).
Heier and Brooks (1966) discussed the geochemistry and
the genesis of the Heemskirk granite massif, and the geolo-

gical age and chemical composition of the different types
of the granite were studied by Brooks and Compston (1965).
A detailed study of the relationship between feldspar
alteration and the precise post-crystalization movement
of rubidium and strontium isotopes in granite was carried
out by Brooks (1968). In 1968 Coleman re-examined the
geology and ore deposits of the southern part of the
Heemskirk granite massif.

Both and Williams (1968) studied the mineral zoning in
the Zeehan mineral field and the relationship between
lead - zinc - tin mineralization and the Heemskirk granite
massif. The sulphur isotope content in ores from the
Heemskirk granite is mentioned in the study of Both et al.
(1969). Klomínský and Groves (1970) discused the chemistry
of the Heemskirk granite in the broader sence of the re-
lationship between the granitic rock types and tin and
gold mineralization in Tasmania.

1.7. Field study and sampling programme

The program of investigation on the Heemskirk granite
began with geological mapping on a scale of 1:31,680 on
topographic sheet Zeehan zone 7 no. 50A and 50C. The de-
tailed geological map covering an area of 47 square miles
(120 km^2) has been prepared on a scale of 1:50,000 (Map I).

In some areas the thickness of the bush reduced the amount
of detailed work possible and some other areas had to be
left completely unsurveyed.

The actual mapping was based on petrographic divisions
of granites according to Waterhouse (1916) and Brooks
(1966). The groups of the red and white granite were
distinguished mainly on the colour of the K-feldspar and
the characteristic appearance of biotite. The field cha-
racteristics of the red granite are pink potassium feld-
spar, the fresh character of biotite, and the absence of
muscovite. Mapping according to these criteria was parti-
cularly safe with the coarse grained facies of both grani-
tes. There were some difficulties in distinguishing the
fine-grained varieties, however, and some fine-grained
rocks were classified according to laboratory data.

Geological mapping included a revision of all known
tin deposits and prospects with respect to their accurate
geographical position. Particular attention was given to
mapping the quartz-tourmaline vein systems. Also included
in the geological map were the distribution and concentra-
tion of tourmaline nodules in both granites.

Sampling of the Heemskirk granite was carried out to-
gether with the geological mapping for the purposes of
petrographic study, separation of rock-forming minerals

and chemical analysis of trace elements. The sampling
net was determined by two factors; firstly, the occur-
rence of good outcrops, and secondly, a subjective selec-
tion based on the degree of variability of granites in a
particular area. Each sample was located on a geological
map and its position determined by geographical coordina-
tes.

The red granite area was covered by 59 samples;
the white granite area by 46. Each of the 105 samples
were 10 Kg (20 lb) in weight, as fresh as possible and
from a single outcrop. Hand specimens collected with each
sample were used for intercorrelations within each group
of rocks for photo documentation and for the preparation
of thin sections. The sampling plan used in the Heemskirk
massif could mean a loss of small scale variability. This
problem (Emerson, 1964) was tested on the basis of signi-
ficant differences between the trend map of analytical
data for a complete set of analyses and a trend map for
only three-quarters of the analytical data. Both maps
were in good agreement, proving an existence of variabi-
lity on a regional scale.

1.8. Laboratory Procedures

1.8.1. Sample preparation

All samples were pieces of granite ranging in size from 5 cm to 20 cm. These were crushed to smaller fragments about 3 cm with a hammer and hydraulic splitter. First crushing by a mechanical jaw crusher produced a fraction under 0.5 cm. One-quarter of the sample was used for the separation of K-feldspar (from red granite only). A second crushing (with jaws a minimum distance apart) produced a gravel of grainsize 0.3 cm. A quarter of this gravel was powdered in a Siebtechnik vibratory grinding mill (> 200 mesh) and was then used for all analytical work. The rest of the sample was divided by sieves into three fractions according to grainsize. The middle fraction (1-0.5 mm) was used to separate biotite, the fraction under 0.5 mm for heavy mineral separation.

1.8.2. Separation of biotite and potassium feldspar

Biotite was separated from the 95 rock samples by Franz-isodynamic magnetic separator in two stages. In the first stage biotite was separated using a vertically oriented separator at a current of 4 amps. from a grain size of 1-0.5 mm. The product thus obtained was further

separated by the same procedure with the slope at an angle of 25° (side angle 25°) and a current of 1 amp. The purity of the concentrate (after washing in water) was checked under the microscope and was found to be at least 99%.

Separation of potassium feldspars was carried out on 50 samples, mainly coarse grained red granite. Fragments of potassium feldspar several mm across (mainly phenocrysts) were picked out by hand from the coarsest fraction of the ground samples.

1.8.3. Separation of heavy minerals

The fine-grained fraction (> 0.5 mm) from several samples of each rock type was used for the separation of heavy minerals. Bromoform was then used to remove the light minerals (feldspars and quartz). The resulting concentrate was divided into three fractions by a magnet and an electromagnet. Each fraction was then analysed qualitatively.

1.8.4. XRF analysis of trace elements

Variations in the chemical composition of bulk rock samples and mineral phase separates were determined by XRF spectroscopy from pressed powder pellets. Standards were artificially prepared from pure chemicals by diluting them in powdered kaolin. The standard rocks T1, W1, G2 and

Gl were measured with the samples to check the accuracy
of the standards and method. A computer program (U949/3 -
author C.Gee) was used to compute mass absorption coef-
ficients at particular wave lengths. A detailed description
of the XRF method is given in Appendix II.

1.8.5. Structural state of the K-feldspars

In order to register differences in the structural
state of the K-feldspar megacrysts from a total of 12 dif-
ferent samples localities were examined by means of
a Müller Micro III X - ray powder diffractograph. Diffracto-
graph patterns were run over a 2Θ - range of $33.5 -36.0^{\circ}$
at $1/4^{\circ}$ (2Θ) per minute, using Cu K radiation, a diver-
gence slit of 1° and a receiving slit 0.2 mm. Peak posi-
tions were measured as described by Orville (1967).

2. Geology of the Heemskirk massif

The Heemskirk massif is an epizonal body intruded
into extensively folded Proterozoic to Cambrian rocks,
(mainly sediments). The granite body consists of the red
and the white granite (the "Pink" and "Tin" granites of
Waterhouse, 1916).

The rocks can be distinguished by their colour and
mineralogical composition. The red granite differs from
the white granite in the pink colour of its potassium
feldspar; the different colour of biotite (brown-green
pleochroism for biotite from the red granite and red-
brown pleochroism for biotite from the white granite);
presence of magnetite, sphene and allanite; absence of
muscovite and conspicuously lower content of tourmaline.
The chemical composition of both rock types is similar
(Brooks & Compston, 1965), the white granite however, is
more acidic (alaskite).

The intrusion has a generally stratiform character.
The most complete sequence of granitic layers is exposed
in the eastern part of the massif. Figure 3 shows the
scheme of stratigraphy in a W-E section. In the topmost
part of the intrusion there are small bodies of contami-
nated porphyritic granite (R_1). Individual blocks of this
contaminated granite have been preserved near the surface

Figure 3

The stratigraphical scheme of the section across
the Heemskirk granite massif

White granite: W1 contaminated porphyritic granite
W2 medium to fine-grained granite
W3 coarse-grained granite

Red granite: R1 contaminated porphyritic granite
R2 coarse-grained granite
R3 medium to fine-grained granite

W   E

W_1 W_1 W_2 R_1 R_2 R_3 R_2

W_3 W_2 W_3 R_2 R_3 W_2 W_2

W_3 R_3 W_2 W_3 W_3

W_2 W_3

W_3

70/11/21

of the cupola within both the red and white granite.
They result from incomplete assimilation of small bo-
dies of mafic rocks derived from the local country rock.
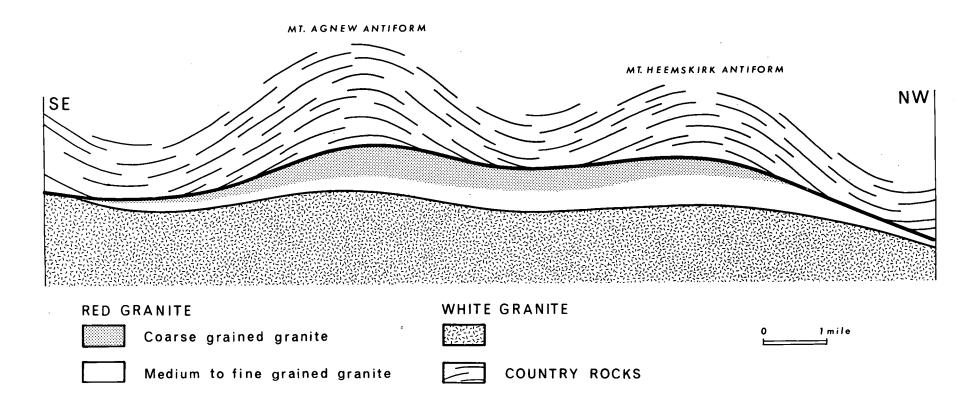
On the contact with the country rocks there is
a coarse-grained red granite (R_2). This is underlain by
a medium- to fine-grained red granite (R_3), which is in
turn underlain by a group of the white granites which
outcrop mostly in the western part of the body and form
the major mass of the Heemskirk intrusion. On the contact
between the red and white granites there is a nodular
facies of medium- to fine-grained granite (with nodules
of tourmaline) (W_2) which changes progressively to a
coarse-grained muscovite-biotite granite (W_3) at depth.
All rock types within the massif are granites according
to the classification of A.Hietanen (1963).

Figure 4 shows a cross-section through a model of
the Heemskirk intrusion before erosion of the overlying
sediments. The upper part of the body has a flat cupola-
like structure. The surface of the body appears to
reflect on a subdued scale the double anticlinorial
structure of the original sedimentary cover. The indivi-
dual anticlines and synclines of the country rocks have
axes plunging generally ESE, and the pattern of layering
within the granite indicates that the same general type
of structure persists.

Figure 4

A cross-section through a model of the Heemskirk
intrusion before erosion of the overlying sediments.

MT. AGNEW ANTIFORM

MT. HEEMSKIRK ANTIFORM

SE

NW

RED GRANITE

Coarse grained granite

Medium to fine grained granite

WHITE GRANITE

COUNTRY ROCKS

0   1 mile

20/11.64

Wide-spread tin mineralisation in the eastern part of the Heemskirk massif has taken place in a contact zone between the red and white granite and is accentuated by the relief of this contact (map·III). Cassiterite occurs mainly in quartz-tourmaline, or greisen fissure-veins. Rich concentrations of tin are erratic, and tend to form short ore shoots at the intersection of two vein·systems. According to Baumann's classification (1970) of the cassiterite deposits in silicate rocks of the Erzgebirge (central Europe), the tin mineralisation within the Heemskirk massif belongs to the "pure vein" type, mainly developed as mineralised fissure veins in the top zones of granites with very gently-dipping flanks.

3. Internal structure and tectonics of the Heemskirk massif

The Heemskirk granite massif is characterized by a remarkable layered structure and well developed fracture systems. Layering of the intrusion was detected by geological mapping and was confirmed by chemical analyses of the rocks and their minerals. Fracture systems were studied on a statistical basis by the measurement of the joints systems in the field and interpretation of the air photographs.
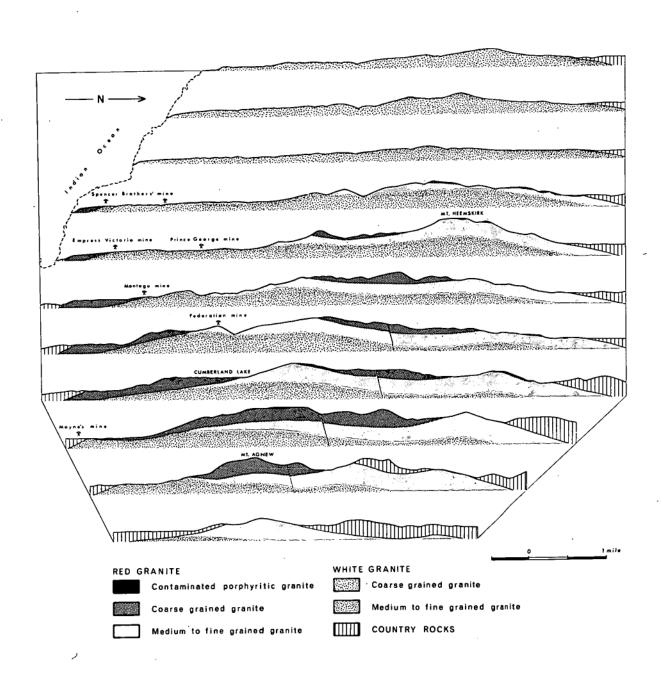
3.1. Layering

Wager and Brown (1968) have defined the layering as an igneous phenomenon and, moreover, a planar feature dependent for its origin largely upon the physical effects of gravity and the chemical effects of magmatic fractionation.

The layering of the Heemskirk granite massif in terms of the mineralogical and grainsize changes is shown in figure 5. The upper part of the intrusion is characterized by a very flat dome. Its internal structure consists of several layers of granites with slightly different mineralogical and chemical properties. Within each layer,

Figure 5

Geological cross-sections
through the Heemskirk granite massif.

RED GRANITE

■ Contaminated porphyritic granite

▨ Coarse grained granite

☐ Medium to fine grained granite

WHITE GRANITE

▨ Coarse grained granite

▨ Medium to fine grained granite

▥ COUNTRY ROCKS

exists also cryptic layering which can be defined by the behaviour of trace elements.

In the eastern part of the intrusion the topmost strata are formed by the red granite which is underlain by the white granite. The red granite strata consist of coarse grained granite and medium-to fine grained granite. The coarse grained layer occupies the upper part of the red granite strata in the southeast region of the massif. This layer pinches out toward the north and is replaced by the underlaying layer of the medium-to fine grained granite. In general the red granite strata thin away also toward the west and are replaced by the fine-grained white granite. The layer of the medium-to fine grained white granite passes into the coarse-grained white granite further to the west.

3.2. Planar structures of local scale

It has long been postulated that planar structures in granites reflect the motion of the magma during emplacement (R.Balk, 1948). Experimental studies have demonstrated that repeated intrusive movements of the crystal-rich magma over a period of time may have produced the prominent grain-size layering in marginal zones of high shear--stress. Primary planar structures within the Heemskirk granite are not abundant. Flow layers (schlieren) are very

rare, and, if present, they are concentrated close to the contact of the intrusion with the country rocks. They were described as a biotite banding by T.H.Green (1966) from the Trial Harbour area. Platy flow structures consist of schlieren of mafic minerals or biotite banding associated with aplite layering. Schlieren are more common within the contact zone of the red granite (type R2) with the country rocks. Several of them have been found in the shoreline outcrops 1 km N from Trial Harbour. Schlieren consist essentially of those minerals that make up the surrounding rocks, but in different proportions (remarkable prevalence of biotite and hornblende). The upper boundaries of some of them are gradational and the schlieren are often curved. They dip and strike parallel to the contact of the intrusion.

Another type of planar structure consists of biotite bands associated with aplite layering which is very characteristic of the contact of type R2 with R3 and of R3 or R2 with W3. Most bands strike at about 65° and dip to the south at 30°. Biotite banding on the contact between the pink granite (type R2) and the white granite (type W3) was described in detail by T.H.Green (1964).

A very similar type of platy flow structure was observed on the contact between granite types R2 and R3, near the sample point 5 (Plate 3-2). The contact zone is

up to 1 m wide with very flat dip and consists of paral-
lel layers of aplite (aplite schlieren?) and layers of
the coarse - to medium-grained granite which are in gene-
ral richer in biotite. Tourmaline nodules are concentrated
along the flow layers on the bottom of the contact zone.
Shearing in the plane of flow or on the contact of compo-
sitional boundaries might be the best explanation for the
repeated layering and variation in width of the layered
zones.

3.3. Parallelism of xenoliths and tourmaline nodules

A few xenoliths occur in the topmost parts of the red
and white granite, closely associated with the contact of
the intrusion and the country rocks. In general the xenoliths
are represented by two groups of rocks; granites of dif-
ferent composition, and xenoliths of metamorphosed country
rocks. The parallelism of xenoliths is more obvious near
the steeper contact of the granite intrusion. The largest
xenoliths within the red granite in the Mt. Heemskirk and
Mt.Agnew area have the character of relatively thin plates
with horizontal arrangement. Their orientation indicates
the existence of planar structure on the roof of the
Heemskirk granite massif. The largest xenoliths within
the white granite consist of two major types: xenoliths

of the red granite, and xenoliths of contaminated porphy-
ritic granite. The xenoliths of red granite near Gap
Peak and around Falconer Creek (see geological map) are
thin plates with horizontal arrangement, and represent
remnants of the originally more extensive red granite
layer. Their characteristic position also indicates the
orientation of the planar structures within the Heemskirk
granite massif. The large xenoliths of contaminated por-
phyritic granite in the white granite are concentrated in
the NW part of the intrusion and strike parallel to the
contact with the country rocks.

The tourmaline nodules are   particularly characte-
ristic part of the medium-to fine-grained white granite
(Plate 4-1). They are concentrated in the upper part of
the white granite (type W2). The nodules usually form re-
markably spherical bodies up to 30 cm in diameter (Plate
12). The best development of the nodular layer, up to 20 m
in thickness appears in the boundary zone between the whi-
te granite (W2) and the red granite (R2 or R3 respective-
ly). In detail the arrangement of the tourmaline nodules
within the intrusion is not typical flow structure but
on the regional scale it indicates the existence of the
layering and planar structures within the massif.

3.4. Primary fracture systems

The Heemskirk granite massif is characterised by
regular fracture systems.
In figure 6 is shown a frequency of the total length of
the quartz-tourmaline veins (in black) which in general
follow the primary fracture systems. There are five major
systems, NNE-SSW, WNW-ESE, N-S, NE-SW and W-E, of which
the most important are the NNE-SSW and the perpendicu-
-lar WNW-ESE systems. The origin of the fracture systems is
a difficult problem open to several interpretations.
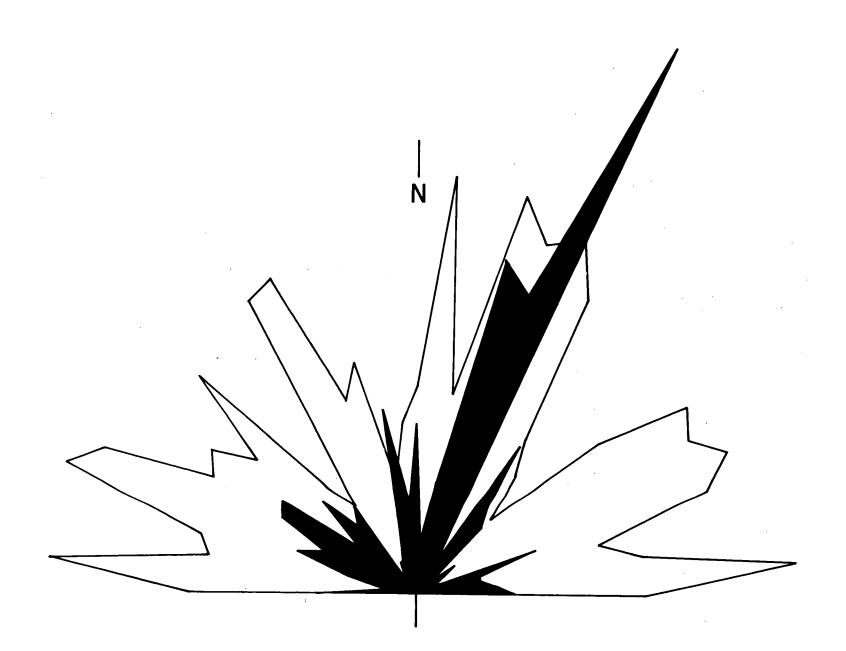
Two two major joint systems are a function of planar
(flow) structures, (1) cross joints and (2) longitudinal
joints and the basic structure of the primary fracture
systems is shown in map II. The interpretation is based
on airphotographs and detailed measurement of the quartz-
tourmaline vein system in the field.

1) Cross joints

Flow lines in the Heemskirk granite massif trend
north-west and south-east. They are traversed by the system
of long, partially curved joints which strike NNE predomi-
nantly. The opening of the fissures due to the contraction
of the granite mass after consolidation was associated
with extensive greisenisation and hydrothermal alteration.

Figure 6

Diagram of the frequency of the total length of
the quartz-tourmaline veins systems in the Heems-
kirk granite massif (in black) and the fault pat-
tern in the Zeehan mineral field.

The fissures are usually filled with quartz-tourmaline veins (Plate 3-1). Scores of quartz-tourmaline veins with cassiterite and greisens occupy cross joints predominantly in the red granite. Systems of cross joints show fan-like form reflecting the presence of an arch or dome in the flow lines. In the marginal zones of the red granite, the cross joints show a fan-like structure in the map plane. The splitting or bending of the cross joints systems could be due to topographic effects.

2) Longitudinal joints (S-joints of H.Cloos, 1923).

Like the cross joints, the longitudinal fractures depend on the direction of linear flow or the principal direction of shear. They are oriented perpendicularly to the cross joints. Many of them are rougher and shorter and lack the smooth surfaces of the cross joints. Their traces on the map plane in the red granite area are conformable with the boundaries of the intrusion. Many of them have a moderate dip and some of them appear to be bent.

The formation of the longitudinal joints and their opening may be due to upward expansion of the earlier consolidated red granite. Quartz-tourmaline veins, as a filling of the longitudinal joint system, are more abundant in the red granite.

3.5. Faults

Within the Heemskirk granite massif it is possible
to recognize three fault systems: 1) N-S or NNW-SSE,
2) NE-SW, and 3) NW-SE.

The first of these (N-W or NNW-SSE) is most important
and one of the major faults crosses the massif following
South Gap Creek and St.Dizier Creek. This fault could be
responsible for the greater uplift of the eastern part
of the intrusion in comparison with the western part.

The second system is represented by the fault fol-
lowing the Tasman River valley in the western part of
the intrusion. This fault has a regional character and it
is also an important tectonic feature of the country rocks.

The third system (NW-SE) contains the thrust faults
which are concentrated predominantly in the eastern part
of the massif.

4. Petrography

The Heemskirk granite massif can be divided into two
broad divisions, the red and the white granite, as has
been recognized by all investigators of the massif.
Table 1 shows the details of the subdivision of the red
and white granite according to Waterhouse (1916), Green
(1966), Brooks (1965) and this study.

According to colour and grain size of K-feldspar,
pleochroism of biotite, grain size of the ground mass and
the prevalence of characteristic accessory minerals, six
fairly distinctive types may be recognized within the red
and white granite.

White granite: W1 - Contaminated porphyritic granite

W3 - coarse-grained granite

W2 - medium-to fine-grained granite

Red granite: R1 - Contaminated porphyritic granite

R2 - coarse-grained granite

R3 - medium-to fine-grained granite

Photographs (Plates 6-12) show the overall texture
of the red and white types in sequence from the porphyri-
tic types through the coarse-grained types to medium - and
fine-grained granites.

Table 1

Comparison of petrographic subdivisions of the Heemskirk granite

massif of previous authors and this study

Waterhouse (1916)	Green (1966)	Brooks (1965)	this study
pink granite	gray granite	gray granite	contaminated red granite
	pink granite	red granite	coarse-grained red granite
fine-grained tourmaline granite	porphyritic aplite tourmaline nodular aplite	porphyritic aplite microgranite	medium-to fine-grained red gran.
			medium-to fine-grained white gr.
white granite	white granite	white granite A	coarse-grained white granite
		white granite B	contaminated white granite

4.1. White granite

This has the greatest surface extent of the two major types (62 km^2 of total 120 km^2) and it is probably the dominant rock in the subsurface part of the Heemskirk granite massif.

4.1.1. W1 – Contaminated porphyritic granite (Plate 5-2)

This type has white K-feldspar and quartz phenocrysts (about 10 per cent by volume) set in a grey phaneric matrix. The K-feldspar phenocrysts are twinned on the Carlsbad law and va_ry from 10-15 mm x 10 mm to 5x3 mm. Quartz phenocrysts vary from 5 to 3 mm.

The even-grained matrix is composed essentially of K-feldspar, plagioclase, quartz, biotite and muscovite, most crystals being hypidiomorphic.

This granite forms a minor rock type in the white granite mass, and occurs mainly as large inclusions within the white granite in the western part of intrusion. The best outcrop of this rock occurs in the granite-hornfels contact on the shoreline at Granville Harbour (sample locality no.1).

Plagioclase (20%) is an important constituent of the groundmass. Some of the grains are zonal with cores

altered to sericite. Bulk composition ranges between An_{15} - An_{25}. Plagioclase also occurs as mantles (An_{20}) about orthoclase phenocrysts and as inclusions in K-feldspar phenocrysts. The mantles usually consist of single minute crystals, c-axes being orientated perpendicularly to the margins of the K-feldspar phenocrysts. Plagioclase (An_{25}), occuring as inclusions within K-feldspar, has a parallel orientation. Most grains (about 0.5 mm in size) have rims of albite. Most of plagioclase (An_5) in perthitic arrangement occurs as irregularly branching veins and regular films.

K-feldspar (25%) occurs as subhedral phenocrysts (Plate 5-2) and anhedral patches in the groundmass. Quartz (2o%) grains have markedly undulose extinction. Biotite (6%) forms subhedral crystals varying from 0.5 to 2 mm across and locally occurs in clusters. The mica contains inclusions of apatite, and zircon. The pleochroism is α = pale straw, γ = red-brown. Some chlorite occurs in layers parallel to cleavage.

4.1.2. W3 - coarse-grained granite (Plate 6-2 and 7-2)

This has the greatest surface extent of the six major types, and outcrops as shoreline cliffs. There are two variants: muscovite-biotite granite and tourmaline-biotite

granite. Two-mica granite occurs in the western part of
the white granite area. Tourmaline-biotite granite occu-
pies the central part of the white granite and towards
the east passes gradually into medium-to fine-grained
tourmaline granite (see map I). The boundary between the
two variants has a transitional nature and coincides with
the line marking the difference in color of biotite
(Fig. 7).

The coarse-grained granite is an even-grained rock
(specimens 68, 82, 83). White k-feldspar, milky-white
plagioclase and pale-brown glassy quartz form an evenly
dispersed mixture that is speckled with brown flecks of
biotite. Tourmaline occurs as disseminated crystals or
nodules or as irregular segregations (up to 5 cm in size).
Most grains are between 2 - 10 mm in length, with some
feldspar about 20 mm long.
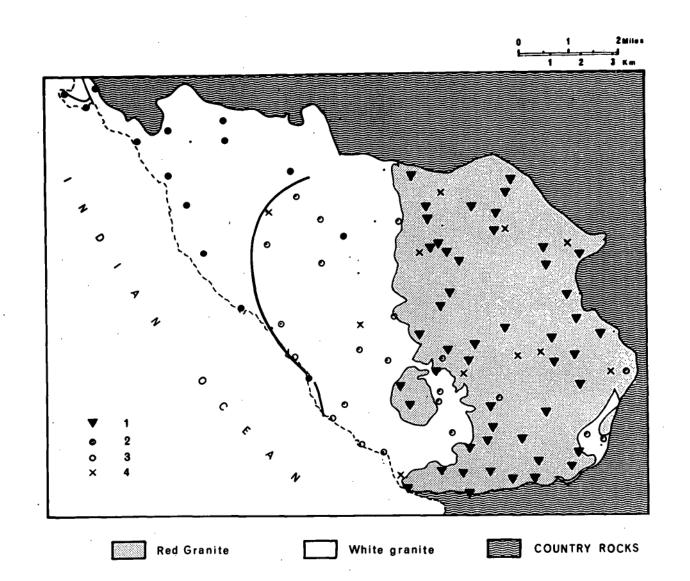
Quartz (38%) grains are anhedral. They aggregate and
interlock. Extinction is usually even but large quartz
grains are strained. K-feldspar (37%) forms subhedral and
anhedral crystals. Some grains have developed Carlsbad
twins. Basal sections show fine-hatched twinning. The feld-
spar is coarsely microperthitic and clouded.

Plagioclase An_{10} (17%) is generally euhedral or sub-
hedral and tabular. Crystals are commonly clouded by de-

Figure 7

Colour of biotites from granites of the Heemskirk
massif (powdered samples)

1 - black-green

2 - light grey

3 - brown

4 - green (altered biotites)

INDIAN

OCEAN

▼	1
◉	2
○	3
✕	4

0   1   2 Miles

1   2   3 Km

Red Granite   White granite   COUNTRY ROCKS

composition to sericite and clay. Twinning is universal, the commonest low being albite.

Biotite (4%) forms ragged subhedral flakes which aggregate and intergrow with muscovite. Inclusions are of apatite, zircon and monazite. The pleochroism is α = pale straw, β = pale brown and γ = red-brown. In altered rock the biotite is intensely chloritized with α = pale straw, β = γ = pale green. Among the included minerals are fluorite and rutile (sagenite).

Muscovite (1 %) is present in varying amounts as reaction rims between biotite and K-feldspar crystals or as interstitial crystal aggregates between the felsic constituents. Tourmaline (2%) is in most cases the dominant accessory. Black tourmaline is most common but green, blue and brown varieties have also been observed. It is found as interstitial crystals set between the felsic constituents and replacing K-feldspars (Plate 14-1). In some cases the tourmaline is intergrown with the green variety of mica or chlorite.

4.1.3. W2 - medium - to fine-grained tourmaline granite

(Plate 8-2, 9-2, 10-2 and 11-2)

This type occupies the roof zone of the white granite (specimens 100, 51, 85 and 38). The body of that granite

type has the form of flat layers and a sharp contact with the overlying red granite and/or Precambrian country rocks. Towards the bottom of the layer the rock passes gradually into the coarse-grained white granite (W3) by increasing the grain-size. The roof zone of the granite is enriched with tourmaline nodules (tourmaline nodular aplite of Green 1966). (They occur in such abundance that the weathered granite-soil surface is a venner of tourmaline nodules.) This part of the rock may be classified as an orbicular granite in the sense of Leveson (1966). The concentration of the nodules is highest (over 100 per m^2) close to the contact with the red granite (Plate 4-1). Towards the coarse-grained granite their quantity decreases. The tourmaline nodules range from 1 cm to 25 cm in diameter (Plates 9-2, 10-2, 11-2 and 12). They form spherical bodies usually surrounded by quartz-felsic rims lacking the biotite which is otherwise a common component of the granite (Plate 10-2). Black tourmaline and quartz are the most common component minerals, but occasionally green tourmaline (outer parts of the nodules), fluorite and cassiterite also occur in the nodules. The tourmaline nodules are more resistent to weathering than the granite mass, and frequently stand out several inches in relief. The effect is illustrated in Plate 4-1 and 4-2.

Medium - to fine-grained granite is a cream-coloured rock and has several varieties including porphyritic and aplitic types. They are millimetre-grained rocks whose texture ranges from hypidiomorphic-equigranular to inequigranular-seriate. In some specimens, "pools" of millimetre-grained felsic material are set in a network of aplitic material (grain size less than 0.5 mm). In the porphyritic variety quartz and K-feldspar occur as subhedral phenocrysts.

Quartz (40%) is clear and colourless and occurs in two forms: as subhedral phenocrysts, and as anhedral grains only 0.2 mm in size commonly forming myrmekitic intergrowth with albite. Some phenocrysts of quartz have myrmekitic rims.

Potash feldspar (35%) occurs as interlocking anhedral-subhedral crystals with quartz, or as small (up to 5 mm) phenocrysts. It is usually very dusty in contrast to the clear quartz. Unaltered crystals are perthitic and exhibit the cross-hatched twinning of a microcline.

The plagioclase (20%) is nearly pure albite, and is subhedral to euhedral with albite and pericline twins. Sericitization is a common feature of the majority of plagioclase crystals.

Biotite (3%) forms ragged, thin, subhedral flakes which are usually completely altered to chlorite. Dark brown mica may be either biotite or the paler lithionite. The pleo-

chroism of unaltered biotite is α = pale straw, β = yellow-brown and γ = brown. The many inclusions in the biotite or chlorite usually contain inclusions of fluorite and opaque ore, and occur in association with tourmaline. The pleochroism of the altered biotite is α = pale straw and β = γ = brown-green.

Tourmaline (1-3%) appears replacing K-feldspar, while quartz exhibits straight margins against the tourmaline (Plate 4-2). The pleochroism of tourmaline is ϵ = indigo blue, ω = green-yellow or brown-yellow.

Muscovite occurs as an accessory disseminated throughout the rock and usually interstitial to feldspars.

4.2. Red granite

The red granite forms a relatively thin layer consisting of three rock types. On the surface the most abundant type is coarse-grained granite R2. The red granite covers 57 km^2 of the total 120 km^2.

4.2.1. R1 - contaminated porphyritic granite (Plate 5-1)

Type R1 (specimens 36 and 78) forms small sheet-like bodies in the vicinity of the roof of the intrusion, and occurs as large inclusions within types R2 and R3. There are abundant inhomogeneities and rapid changes in texture. The granite is a brown-red coloured medium-grained rock

with phenocrysts of K-feldspar, quartz and plagioclase
set in a groundmass of essentially K-feldspar, plagioclase,
quartz, biotite, hornblende, abundant magnetite and sphene.
Accessories are represented by zircon, apatite and fluorite.

The red-coloured K-feldspar occurs in two forms:
as subhedral phenocrysts and as anhedral grains only about
1 mm in size. The phenocrysts are commonly twinned on
the Carlsbad law and vary from 20 x 10 mm to 5 x 3 mm.
They are frequently mantled by a rim of white-coloured
albite which may be as thick as the whole diameter of
the K-feldspar core. Both phenocrysts and groundmass
grains are perthitic, and are frequently dusty with clay.
Plagioclase (20%) forms a few subhedral phenocrysts, and
is an essential constituent of the groundmass. Bulk com-
position ranges between An_5 - An_{35}. Plagioclase (An_{27})
also occurs as inclusions within K-feldspar (small simply-
zoned crystals).

Quartz (20%) occurs in two forms: as anhedral-sub-
hedral smoky-coloured phenocrysts (up to 10 mm in size),
and as anhedral grains only about 0.2 mm in size in the
groundmass. The groundmass quartz frequently forms inter-
growths with orthoclase to give graphic texture.
Hornblende (up to 3%) occurs as subhedral poikilitic

crystals 1 mm in size. It may be present as single crystals or as "matted" clots. Minerals found within the hornblende are magnet ə, sphene, zircon, apatite, biotite, fluorite and alla: ɔ. Pleochroic colours are patchy but α = yellow, β = b: ɯn-green, γ = green.

Biotite (2-5 %) forms subhedral crystals often associated with hornblende. Pleochroism is α = straw, β = γ = yellow-green. In some samples (specimen 12), biotite is more abundant (hornblende is absent) and unaltered biotite exhibits the pleochroism α = dark straw, β = γ = almost opaque.

Magnetite is the most abundant accessory in the rock. It is usually concentrated in hornblende and K-feldspar as minute subhedral crystals (Plate 16-1) which are frequently mantled by sphene.

Zircons are often zoned. Magmatic zircons contain inclusions of older zircons which may be derived from the assimilated country rock (Plate 20 and 21).

Sphene (1%) is euhedral or anhedral and appears to be an alteration product of the mafic minerals (together with magnetite) from the country rocks.

Apatite, as well as violet fluorite and allanite are common accessories.

4.2.2. R2 Coarse-grained granite (Plate 6-1 and 7-1)

Outcrops of this type occupy the southern margin of

the intrusion and the major part of the area between Mt. Heemskirk and Mt. Agnew and have the greatest surface extent of the red granite group. The coarse-grained granite is an even-grained rock with slightly varying grain-size. Texture is typically hypidiomorphic granular.

Pink-coloured potash feldspar (38%, mostly orthoclase) occurs as subhedral and anhedral grains from 5-20 mm in size. In the upper part of the coarse-grained granite layer K-feldspars are generally mantled by albite. Albite rims are largely sericitized. Twinning on the Carlsbad law is almost universal and usually the feldspar is coarsely microperthitic and clouded (haematite pigment and kaolinization). Quartz (37%) is anhedral with frequent large crystals (up to 5 mm in size). These grains are often unstrained but small grains are usually strained. A typical feature of the rock is a net of tourmaline needles in the quartz grains (Plate 15).

Plagioclase (18%) is generally subhedral and tabular. Albite twinning is universal. Some crystals shows diffuse zonation in the range (An_{35}-An_5). Sericitization is a common feature of the plagioclase.

Biotite (6%) forms subhedral crystals varying from 0.2-2mm in width. Pleochroism is $\propto$ = dark straw, β = green-brown and γ = dark brown to opaque (some minor chlorite forms in layers along the cleavage).

Sphene, magnetite, zircon and apatite occur within the biotite. Pleochroism of altered biotite is α = dark straw, $\beta = \gamma$ = dark green. This type of mica contains violet fluorite. A typical accessory of type R2 is allanite, which occurs in the upper part of the coarse-grained granite layer (Plate 13-2).

4.2.3. R-3 Medium-to fine-grained granite (Plate 8-1, 9-1, 10-1 and 11-1)

Type R3 usually occupies the lower part of the red granite layer. This pink to red coloured granite is underlain by white granite (type W2) and overlain by coarse-grained red granite (usually R2). On the western margin of the Heemskirk massif the granite intrudes Precambrian sediments. Both upper and lower contacts of R3 are sharp and distinct for geological mapping. There is generally a passage from fine- to medium-grained granite. The compositional and textural range of the rock is wide, and a comprehensive account is difficult. Broadly, however, it may be considered as belonging to two main categories:

a) fine-grained aplite granite, which usually occurs close to the contact of the red granite with sedimentary country rocks or with the white granite

b) medium-grained granite, which frequently occupies the upper part of the R3 layer and shows a great similarity to type R2.

Both rock varieties are essentially equigranular rocks.

The R3 type very commonly contains segregations of tourmaline. As previously mentioned, at the red-white granite contact, tourmaline is concentrated into spherical nodules. Some varieties of type R3 are very light coloured and are very similar to type W3. In such cases it is difficult to find field criteria to distinquish the types.

Potash feldspar is generally interstitial and slightly perthitic. It is usually very dusty (clay and Fe pigment) in contrast to the clear quartz. Graphic texture is a common feature of K-feldspar (Plate 13-1).
Quartz is anhedral and interstitial and almost unstrained.
Myrmekite is a common form of the quartz grains.
Plagioclase (An_{20-0}) is subhedral with albite and pericline twins. The cores of the grains are often sericitized, and some crystals show a diffuse zonal structure.
Biotite forms subhedral flakes or agregates with pleochroism α = dark straw, β = yellow-green, γ = dark brown to opaque. It is generally associated with magnetite. Biotite flakes are usually chloritized along the cleavage. Accessories are represented by magnetite, tourmaline, zircon and apatite.

4.3. Dykes

Dyke of granitic rocks occur within both granite

types, while sills of aplite or tourmaline aplite granite
are common in the red granite (in the Mt. Agnew area).
In general they are identical to the aplitic variety of
the white granite (type W3). A flesh-pink coloured variety
of aplite shows a close relationship to the fine-grained
red granite (type R3) (Plate 11-2).

Pegmatite is not abundant within the Heemskirk granite
massif, and usually occurs intimately associated with apli-
te. Pegmatite centres of the aplite dykes (up to 30 cm in
width) consist of crystals of orthoclase, quartz, tourma-
line and albite. Pegmatite patches and streaks are more
abundant within the white granite and consist of quartz
crystals up to 10 cm in size and aggregates of albite and
orthoclase.

Unusual basic dykes with axinite occur within the red
granite. They outcrop on the coast 1 mile north of Trial
Harbour. This rock type has been described in detail by
Waterhouse (1916) and Green (1966). According to Green
(1966) the diopside-rich rocks are derived from the assimi-
lated mafic country rocks by the magmatic activity of
the granite.

4.4. Postmagmatic products of the Heemskirk granite massif

4.4.1. Tourmaline fissures, quartz-tourmaline veins, dykes and greisens within the granite

Map II shows the distribution of the major postmagmatic vein systems. It is obvious that the fissures and veins were formed and filled with quartz and tourmaline after consolidation of all the granite rocks. Greisens are rare and are mostly concentrated within the white granite. A few quartz-tourmaline dykes occur in the red granite predominantly (Plate 5-1). Prominent individual veins or swarms of parallel veinlets are common near the contact of the red and white granite (see map II). The width of the major veins and dykes varies from 1 to 10 m. The intersections of tourmaline fissures and quartz-tourmaline veins do not usually show appreciable displacement, but in rare cases the N-S system of veins is slightly displaced by a similar one striking E-W. This is in agreement with the observations of Waterhouse (1916). The majority of the veins and large dykes were tested or mined for their content of cassiterite. Detailed descriptions of the veins and their mineralogical variability were published by Waterhouse (1916).

The essential component mineral is quartz, with coarse

grained black tourmaline and green tourmaline varieties
being less common. The tourmaline crystals commonly form
radiating clusters (tourmaline suns) (Plate 19). Wolframite
and newly discovered columbite are minor constituents. On
some veins, pyrite (Federation mine) and arsenopyrite
(Spencer Brothers' workings) are common sulphides. Fluorite
is a characteric accessory mineral of the majority of quartz-
tourmaline veins and dykes. Greisen veinlets and veins
usually consist of quartz, Li-bearing mica, tourmaline and
rare cassiterite. In one case the presence of lepidolite
was discovered (see map II).

4.4.2. Quartz-tourmaline veins in the country rocks

A few brecciated quartz-tourmaline veins occur along
faults and fissures in the country rocks in the vicinity
of the northern margin of the Heemskirk granite. The ce-
menting material of the sharp fragments of banded quartz-
-tourmaline consists of quartz crystals and needles of
tourmaline, with the latter usually concentrated near the
outside of the quartzose fragments, giving them a zonal
structure (Plate 18).

4.5. Thermal metamorphism

In general the metamorphism of the Precambrian sedi-
ments is slight and an andalusite- or chiastolite- bearing

hornfels and a pelitic hornfels is the only characteristic
assemblage. One of the major effects of the granite in-
trusion appears to have been the silicification and tourma-
linisation of the sedimentary rocks. On the north and NE
flanks of the intrusion there is widespread tourmalinisa-
tion (up to 1 km from the contact) of interbedded slates.

The original slates and quartzites have been widely
replaced by quartz and tourmaline, the resulting rock
being a striking banded black and white rock (Plate 17-1).
Argillaceous bands have been replaced by tourmaline, while
the arenaceous bands are represented by quartz bands, the
resulting banded rock being composed entirely of these two
minerals (Plate 16-2). The least-altered rocks have cross-
-cutting tourmaline veinlets, and it is noticeable that
the tourmaline and quartz have impregnated the quartzite
to a large extent on either side of the vein fissure
(Plate 17-2). It seems clear that the composition of the
sedimentary rocks has determined the type of alteration.
These banded quartz-tourmaline replacement rocks were
described in detail by Waterhouse (1916). Selective
weathering of the intensively tourmalinised sediments pro-
duces a cellular structure.

More pronounced contact effects of the Heemskirk gra-
nite on the mafic and ultramafic rocks have produced a va-
riety of mineral assemblages. According to Green (1966)

they are lime-and ferromagnesia-rich (hypersthene, cum-
mingtonite-labradorite; diopside-hornblende-diopside),
magnesia rich (cordierite - hypersthene; cordierite-
-anthophyllite), and ultramafic (olivine- and/or pleo-
naste). Biotite (or phlogopite) is an almost invariable
component and garnet and sphene may also be present in
these groups. These rocks are noted here because they
suggest a source for mafic xenoliths in the red granite
as well as in the white granite. Some outcrops of the
contaminated porphyritic granite indicate that the mafic
rocks were resistant to assimilation and bring into promi-
nence the idea that the type Rl and Wl formed by hybridi-
zation. Green (1966) and Waterhouse (1916) described
the occurrence of diopside-rich bodies and dykes with
axinite within the granite body near the southern margin
of the granite mass.

4.6. Ghost structure of the country rocks within
the Heemskirk granite massif

In general the internal structure of the intrusion is
stratiform. The layering shows a diminishing influence of
the structure of the country rocks with depth (Fig. 4).
The structure of the country rocks has the form of a brachy-
anticlinorium which consists of several semi-parallel
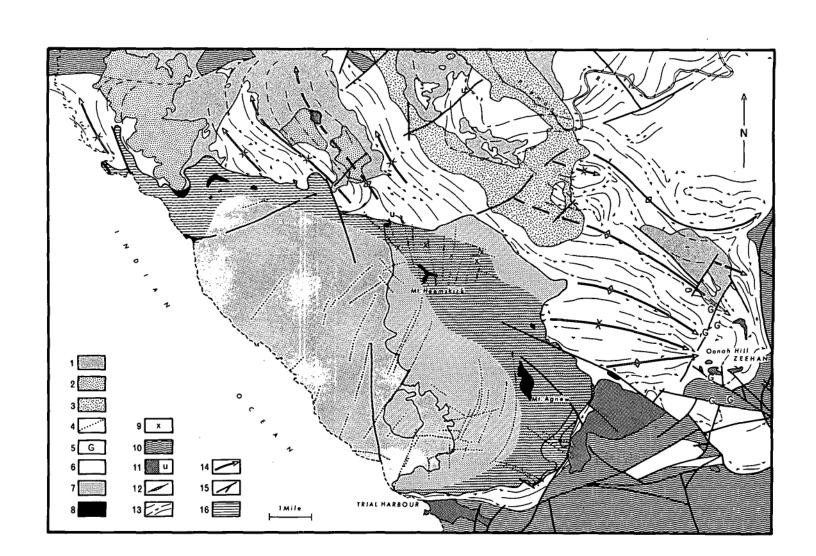
brachysynclines and brachyanticlines (the Heemskirk Anticlinorium according to Blissett, 1962). The axes of these structures trend in the ESE and NW respectively, with the apex of the structure in the centre of the granite massif. On the eastern side the brachysynclinorial closure terminates in the area of the Oonah Hill (Zeehan), 3 miles easterly of the Heemskirk granite massif (anticlinal nose, of the Heemskirk Anticlinorium according to Blissett, 1962). It is evident that the structure of the country rocks has been partly copied by the intrusion and is reflected in the internal structure of the granite body (see figure 4). The geological evidence for it is in the distribution of the small bodies of contaminated porphyritic granite (R1 and W1) and a few large xenoliths which are derived from the local country rock (mafic and ultramafic rocks) as the result of incomplete assimilation of the roof rocks. The geochemical evidence for it is in the distribution of the positive anomalies of some trace elements particularly within the red granite (see figure 43).

The pattern of the ghost structure of the country rock in the roof of the intrusion is shown in figure 8. There is an obvious close relationship between the position of the outcrops of mafic rocks on the southern, eastern and northern margin of the intrusion and the pattern of the contamination of the toplayer of the intrusion.

Figure 8

Schematic tectonic map of the Heemskirk-Zeehan area

1) Tertiary - Permian sedimentary cover

2) Tertiary basalts

3) Jurassic dolerite

4) Quartz-tourmaline veins and greisens

5) Aplitic granite rocks from Zeehan

6) White granite

7) Red granite

8) Contaminated granite

9) Magnetite-rich rocks or solid martite ore

10) Older Paleozoic sedimentary rocks

11) Ultramafic and mafic rocks

12) Magnetite or Fe sulphide bodies

13) Structure (foliation) of Precambrian rocks;
    structure of Precambrian rocks underneath of
    the sedimentary cover

14) Major synclines and anticlines with trend
    of plunge

15) Faults

16) Ghost-structure of the country rocks reflected
    in the Heemskirk granite intrusion

Legend

1		9	x
2		10	
3		11	u
4		12	
5	G	13	
6		14	
7		15	
8		16	

Map labels: INDIAN OCEAN, Mt. Heemskirk, Mt. Agnew, Oonah Hill, ZEEHAN, TRIAL HARBOUR

Scale: 1 Mile

N (north arrow)

This agreement indicates the existence of palimpsestic ghost-stratigraphy in sense of Whitten (1960) within the Heemskirk granite massif.

The longitudial axis of the dome structure of the intrusion is oriented WNW-ESE. In the western part of the body the axis dips very gently towards the WNW while in the eastern part of the intrusion the axis dips towards the ESE. The apex of the axis arch is situated aproximately at Gap Peak.

5. Mineralogy

5.1. Feldspars

5.1.1. The composition of plagioclases in the rock types
of the Heemskirk granite massif was studied by means of
the universal stage (Becke - Becker method).

R1 (sample 36 - 27 % An);

R2 (sample 11 - 0, 11, 12 % An, sample 48 - 35, 31, 32 % An);

R3 (sample 19 - 6, 6, 9, 21 % An, sample 24 - 6, 0 % An);

W2 (sample 68 - 14, 16, 6 % An, sample 83 - 29, 28,

rim 0, 9 % An);

W3 (sample 100 - 0, 0 % An).

According to Brooks (1968) the plagioclase in the red
granite differ clearly in color and specific gravity.
The fresh plagioclase (75% of total plagioclase content)
is green with s.g. 2.660 and altered plagioclase of s.g.
2.640 being distinctly pink. Brooks (1968) used the powder
X -ray technique according to Smith (1956) to determine
plagioclase compositions in the coarse-grained red granite
(approximate An_{25}).

5.1.2. The composition of K-feldspars was studied only in
the red granite. The Na_2O content was used to calculate
the total amount of albite in K-feldspars. The average

Na_2O content (3.44%) is roughly equal to 30% albite and hence the perthite has composition close to Or_{70} Ab_{30}. According to the distribution pattern of the Na_2O in the K-feldspars of the red granite. the higher Na_2O content is in the upper part of the red granite layer. It could be interpreted. as increase of the albite content in the K-feldspars. (up to Or_{60} Ab_{40}). It coincides with increasing of An content in coexisting plagioclases.

Assuming that K-feldspar and associated plagioclase (average for the red granite An_{20}) were in, or were close to, a state of equilibrium, the K - ratio of Barth (1956) may be used to obtain the approximate temperature at which equilibrium was established. For the two feldspars k=0.38 and using Barth' data (see also Winkler 1961) the temperature of crystalization of K - feldspars in the red granite is about 650° C.

5.1.3. Triclinicity of potassium feldspars

The triclinicity Δ , as defined by Goldsmith and Laves (1954) may be regarded as a measure of the degree of the order of the Si/Al arrangement in the tedrahedral sites of the K-feldspar lattice. It is calculated as $\Delta = 12,5x$ [d [131] - d [1$\bar{3}$1]] and varies from $\Delta = 0$ in disordered structure of the monoclinic sanidine to $\Delta = 1$ in the

completely ordered triclinic maximum microcline. In nature there is a continuous gradation between the monoclinic and triclinic potash feldspars.

It is known that disordered modifications of feldspars are formed at higher temperatures than are ordered ones (Goldsmith and Laves 1956, Spencer 1952, Mac Kenzie 1957). Thus monoclinic alkali feldspar is formed at temperatures greater than 500° C (Goldsmith and Laves, 1956, Barth 1959). The natural alkali feldspars are very often mixtures of structural variants, differing in triclinicity within the rock of grains or parts of grains (Dietrich 1962).

12 samples of K-feldspars from the red granite and 2 samples from the white granite were examined (Fig. 9). Triclinicities measured according to the method of Goldsmith and Laves (1954) are given in figure 10.
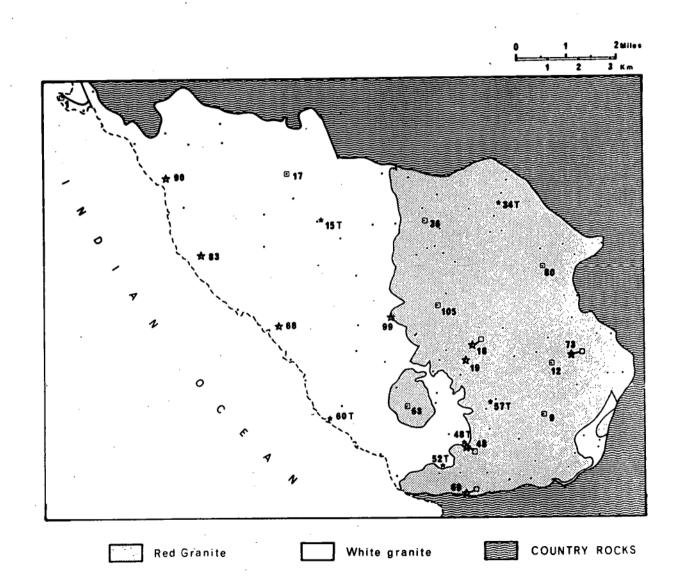
Careful tests of K - feldspars of the Heemskirk granite showed no separation or broadening of the $131 - 1\bar{3}1$ reflections for most of the samples. Slight triclinicity was find only in sample No. 80, 105 (the red granite) and 17 (the white granite/see figure 10). The majority of samples were prepared from the red granite, including type R1 with 2 samples, type 2 with 6 samples and type R3 with 1 sample. The white granites, type W1 and W3 are represented by 1 sample each. The total range of Δ values for selected samples is 0.0 - 0.33. Only the single peak 131 is

Figure 9

Distribution of samples for chemical analyses and
determinations of triclinicity of K-feldspars
(Tab. 2, 5 and 13).

Open stars - chemical analyses of rocks and bioti-
tes (chlorites)
Black stars - chemical analyses of tourmalines
Open squares - triclinicity of K-feldspars

| | Red Granite | | White granite | | COUNTRY ROCKS |

Figure 10

Diffraction patterns in range of 131 - 1$\bar{3}$1 reflections
for alkali feldspars of the Heemskirk granite, showing
triclinicities from 0.0 to 0.33. Number of samples cor-
respond to sampling net in the map I and figure 9.
36, 12 - contaminated red granite
69,73,9,48,80 - coarse-grained red granite
63,18,105 - medium-to fine - grained red granite
17 - coarse-grained white granite
1 - contaminated white granite
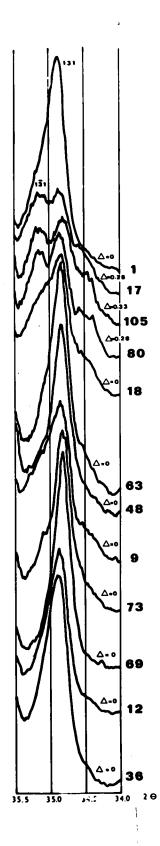
observed in all specimens for type R1, R2 (except 105-R3, 17-W2) and W1. According to monoclinic symmetry the pheno-crysts of the potash feldspars may be described as perti-thitic "ortoclase".

5.2. Biotite

5.2.1. Biotite colour

According to Rimšaite (1967) the colour of mica de-pens on the amount of colouring ions present and on the proportion of Ti and $Fe^{'''}$ ions.
Black-green coloured biotites (colour of powdered dry samples) of the Heemskirk red granites have considerably lower Al content than the bright brown coloured biotites of the white granite. It is in agreement with results of Rimšaite (1967) that aluminum exerts a bleaching effect and yields brighter colour.
Brown, black-green and gray colours (colour of biotite powders) commonly observed in the biotites of the Heemskirk granite are related to the state of oxidation of iron and to the proportion of titanium and manganese in the octa-hedral layer. A comparison of colour of mica with the ra-tios $Fe^{'''}$(Ti and $Fe^{''}$) $Fe^{''}$ is as follows.

Most prominent colour		Sample No.	Fe'''/Ti	Fe'''/Fe''
Gray	(type W2)	99, 68	1.86	0.16
Brown	(type W3)	83, 90	0.72	0.12
Black-green	(type R2)	73, 69, 48	1.13	0.16
Black-green	(type R3)	19	1.61	0.28

The relationship between the colour and ratios Fe'''/Ti and Fe'''/Fe'' confirms the observations of Rimšaite (1967) and Hayama (1959). According to Rimšaite (1967) ferric iron, when present in octahedral coordination in the proportions exceeding $Fe'''/Ti = 1.0$ and Fe'''/Fe'' 0.17 imparts a greenish colour to mica. It is in good agreement with black green colour and average $Fe'''/Ti - 1.5$ and $Fe'''/Fe'' - 0.25$ ratios for the red granite.

5.2.2. Refractive Indices

Refractive index γ/β was measured by bivariate method on nine samples of biotites of both granite types (Tab.13). Results of samples 18, 19 and 69 were checked by immersion method. The range and mean values of indices of the biotites from the red granite differs of those for the white granite biotite. In general the red granite biotites show

higher refractive indices. Within the red granite group
biotite of the coarse-grained granite shows lower refracti-
ve indices (except sample 69) than biotite of the medium-
grained granite (19).

5.3. Tourmaline

Tourmaline occurs in aggregates occasionally with whi-
te granite, and commonly in masses of slender prismatic
crystals radiating from a centre. It is usually black mine-
ral in hand specimens; not uncommonly dark green, dark brown
and blue in colour. The tourmaline nodules are sometimes zo-
nated with black cores and green rims. Green tourmaline
occurs generally in association with cassiterite.

Tourmaline from the Heemskirk granite massif is com-
monly refered to as "schorl" in the literature (Blissett
1962, Green 1965). From analyses of Table 2 it seems pro-
per to use this term for all tourmalines tested from both
red and white granites (Fig. 9). Tourmalines of the white
granite show higher Al content and generally lower Mg
and Fe content. Tourmalines from the red granite are cha-
racterized by higher Fe content predominantely. In figure
11 the chemical analyses of tourmaline are plotted in the
triangle diagram MgO- FeO-Al_2O_3 together with main end-
-members of the schorl type of the tourmaline group : dra-
vite and schorl (elbaite und uvite are omitted for low Li

Figure 11

MgO-FeO-Al$_2$O$_3$ diagram for composition of tourmalines

D - theoretical composition of dravite
S - theoretical composition of schorl

Open stars - Tourmalines from the white granite
Black stars - Tourmalines from the red granite
Number of samples are marked in the figure 9.
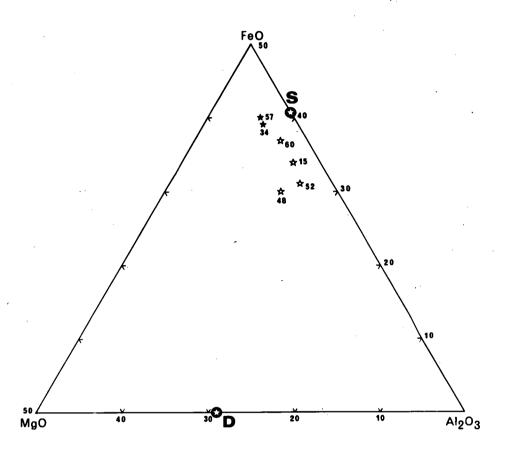
TABLE 2.

Partial Chemical Analyses of Tourmaline

Area	White granite				Red granite	
colour	black	black	black green	green	black	black
No.of Sample	15	60	52	48	3	34
SiO_2	33.11	34.91	34.64	34.70	31.82	33.64
Al_2O_3	32.62	31.33	33.54	33.30	30.50	29.16
Fe_2O_3	19.40	21.30	17.93	17.46	24.25	22.47
TiO_2	0.35	0.26	0.36	0.35	0.20	0.23
CaO	1.16	1.05	1.14	1.18	1.36	1.42
MgO	1.63	1.59	1.89	3.39	2.22	2.14
Na_2O	2.10	2.13	2.03	2.03	2.05	2.00
K_2O	0.21	0.23	0.30	0.18	0.30	0.23
Li_2O	0.03	0.04	0.04	0.03	0.07	0.03
Loss on ignition	0.40	0.60	0.55	0.50	0.55	0.65

and Ca contents in the analyses).
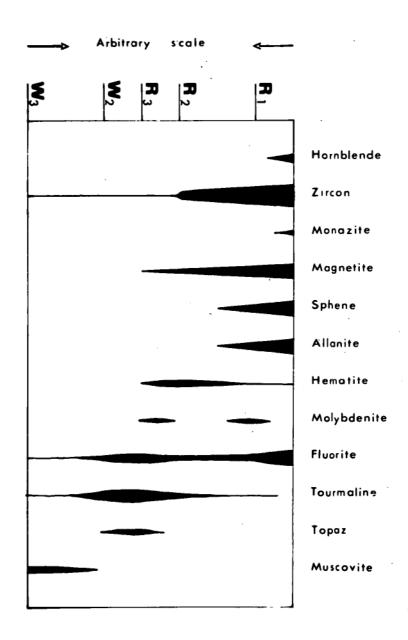
Tourmalines of the red granite show a low variation
in the chemical composition and they lie close to the
theoretical pole of schorl. Higher variability in compo-
sition is obvious in the group of the tourmalines from
the white granite. Their schorl molecule contains up to
25 per cent of dravite (sample no. 48). Tourmaline from
the red granite show an excess in total iron content. Ac-
cording to cell dimensions of the sample no 3 (a - 15.98 Å,
c - 7.18 Å) there is some similarity to ferric iron tourma-
line or buegerite (other type of feric tourmaline). Further
analytical data are needed to clarify this speculation.

5.4. Distribution of accessories in the Heemskirk granites

Accessory mineral components of the Heemskirk grani-
tes were studied in thin sections of the rocks. From nine
samples of the principal rock types and their varieties
the heavy minerals were concentrated and separated for
quantitative modal analyses. Both the red and white granite
are characterized by specific mineral assemblages of acces-
sories.

Assemblage of magnetite - sphene - allanite - heama-
tite - zircon (- fluorite and hornblende) represents the
red granite and assemblage of tourmaline - muscovite -
- fluorite represents the white granite. A relative distri-

Figure 12

Distribution of major accessory minerals in
the Heemskirk granites.

Arbitrary scale

W₃ W₂ R₃ R₂ R₁

Hornblende

Zircon

Monazite

Magnetite

Sphene

Allanite

Hematite

Molybdenite

Fluorite

Tourmaline

Topaz

Muscovite

bution of accessory minerals in the vertical scale is shown in figure 12 from which it is obvious that there is a more varied mineral assemblage in the red granite. This observation in compatible with the mode of origin of the red granite. Quantitative modal analyses of heavy minerals in the red and white granites are shown in Table 3 (opaque minerals - magnetite and ilmenite are not included). In the red granite a decrease of hornblende, apatite and zircon content is apparent in the sequence of rock types R1-R2-R3. A reverse relationship was found in the fluorite content.

Tourmaline is the dominant mineral in the white granite. There is a decrease in the fluorite content in the sequence of the rock types, W3→W2. The presence of andalusite, hornblende and Ti-minerals in some white granite samples indicates the contamination of the white granite magma (by country rocks). The occurence of andalusite indicates a high Al content in the white granite (see table 2). This is compatible with the composition of country rocks where an andalusite or chiastolite-bearing hornfels is characteristic assemblage.

5.5. Mineralogy of quartz-tourmaline veins and greisens

Occurences of cassiterite, tourmaline (schorl), fluorite, wolframite, pyrite, chalcopyrite, arsenopyrite,

Accessory Minerals* of the Heemskirk Granites

TABLE 3.

Rock Type	Red granite					White granite			
	R_1	R_2	R_2	R_3	R_3	W_3	W_3	W_2	W_2
mineral in % sample	36	69	48	18	19	68	83	90	99
Tourmaline	—	—	—	—	15	81	8	79	94
Fluorite	2	12	4	53	13	7	7	2	—
Zircon	6	55	72	23	49	7	52	13	4
Apatite	7	25	11	4	1	2	12	3	2
Epidote	—	—	—	1	2	—	—	—	—
Monazite	—	—	—	—	—	1	—	—	—
Hornblende	38	7	5	1	1	—	12	1	—
Ti minerals (Sphene, Anatase)	47	1	8	18	19	2	9	1	—
Andalusite	—	—	—	—	—	—	—	1	—

*(Opaque minerals are not included)

molybdenite, bismuthinite, galena, stibnite (?), spha-
lerite, pyrrhotite were discribed in detail by Waterhouse
(1916) from quartz-tourmaline veins and greisens of the
Heemskirk granite massif. The principal localities of
those minerals are marked in the geological and minera-
logical maps (see map I and II) and they are completed by
some occurences which were discovered during the author's
field work. The most interesting discovery is abundant
cassiterite on the eastern slopes of the Mt.Heemskirk -
Mt. Agnew Range in country rocks immediately adjacent to
the contact of the Heemskirk granite.

Cassiterite was found in the quartz-tourmaline veins
on the ridge which is parallel to the latitude of
$41^{o}52'30''$ (see map II and Plate 17-2).
XRF study of some samples proved occurence columbite,
lepidolite, Ag- tetrahedrite, jamesonite and heamatite-
-magnetite in some old workings and outcrops as new mine-
rals for the Heemskirk granite massif (see map II).

Columbite was found in the trench close to Allison's
Workings (in vicinity of the sample point no. 20), 1 ki-
lometer northwesterly of Federation mine. Old trench is
situated on the ridge above main adit of Allison's
Workings. The system of quartz-tourmaline veins and
greisens runs in the north-east dirrection. Material with

columbite is a fragment of the vein in 10 cm of thickness. The sample shows banded texture. The vein consists of the older quartz-tourmaline fillings (outer zone) and tourmaline rich agregate needle-like crystals as a inner zone of the vein filling. In centre of the vein there are abundant crystals of columbite up to 10 mm in size, sitting on tourmaline as a youngest mineral of the vein.

Lepidolite was found in the detritus of the greisens veins in the northwestern part of the Heemskirk granite massif (ee the map I). The samples consists of quartz, tourmaline, Li-mica and lepidolite. Lilac-coloured lepidolite is concentrated in the centre of the vein in association with Li-mica and quartz. Boulders of vein material (up to 30 cm in size) were collected on the old track crossing Tasman river approximately 600 meters further to south.

Ag - tetrahedrite was identified in samples from Spencer Brothers' working and Woodings' workings approximately 2 km northwesterly of Trial Harbour. Tetrahedrite occurs in association with arsenopyrite, chalcopyrite, tourmaline, fluorite, quartz and Li-mica.

Jamesonite was identified in samples from Sweeney's mine as a very abundant mineral occuring in association with pyrite, cassiterite and fluorite in the quartz-chlorite- talc matrix. Fine-grained needle-like agregates of

the Sb - mineral has been probably described from
the same locality as stibnite by Waterhouse (1916).

6. Chemistry of rocks and minerals

6.1. Chemical composition and distribution of trace elements in rocks

The chemical composition of the Heemskirk granite
rocks has been studied by Heier and Brooks (1966), and
Brooks and Compston (1965); other chemical analyses are
contained in studies by Rattigan (1968) and Blissett
(1962). The mean chemical compositions of the red and
white granite shown in Table 4 according to Klominsky
and Groves (1970) are based on the data of Brooks and
Compston (1965) and Blissett (1962). Table also shows
ranges of percentages of the individual oxides. The ma-
ximum and minimum concentrations of the oxides indicate
a considerable fluctuation in both rock groups. These
differences reflect the difference in mineralogical com-
position of each petrographic type within both rock groups.
For comparison in table 5 there are shown new chemical
analyses of the major rock types of the Heemskirk massif.

TABLE 4.

Average chemical analyses of the red and white granite and average chemical composition of the Heemskirk granite massif[x]

	The red granite		The white granite		The Heemskirk massif mean
	mean	range	mean	range	mean
SiO_2	75.24	76.8 - 73.2	74.44	76.6 - 72.9	74.84
TiO_2	0.20	0.30-0.08	0.19	0.30 - 0.07	0.20
Al_2O_3	12.68	12.8 - 12.39	13.55	14.3 - 12.6	13.12
Fe_2O_3	0.62	0.96-0.16	0.31	0.78 - 0.01	0.46
FeO	1.27	2.12 - 0.36	1.50	2.00 - 0.83	1.38
MnO	0.04	0.05-0.02	0.04	0.07 - tr.	0.04
MgO	0.31	0.65-0.09	0.37	0.58 - 0.13	0.34
CaO	0.74	1.64 - 0.18	0.82	1.13 - 0.47	0.78
Na_2O	2.91	3.65-2.40	2.75	3.18 - 2.19	2.83
K_2O	5.21	5.80 - 4.95	4.96	6.04 - 3.69	5.08
P_2O_5	0.04	0.07 -0.01	0.10	0.13 - 0.04	0.07
H_2O^+	0.56	0.66 - 0.47	0.68	0.98 - 0.50	0.62
H_2O^-	0.25	0.70 - 0.19	0.16	0.30 - 0.05	0.20
Sum	100.07		99.87		99.96
Number of analyses	7		7		14

[x] after Rattigan (1964)

TABLE 5.

Chemical analyses of the Heemskirk granites

Rock Type	Red granite					White granite			
	R_2			R_3		W_2		W_3	
No. Sample	69	73	48	18	19	99	90	68	83
SiO_2	73.96	73.85	73.85	75.15	76.75	75.19	74.30	75.10	74.57
TiO_2	0.31	0.35	0.30	0.20	0.15	0.07	0.13	0.12	0.20
Al_2O_3	12.64	12.73	12.87	12.37	11.78	13.29	13.00	13.09	13.14
Fe_2O_3	0.19	0.60	0.25	0.71	0.78	0.47	0.15	0.27	0.22
FeO	1.90	1.65	1.94	1.25	1.00	0.93	1.22	1.11	1.43
MnO	0.03	0.04	0.02	0.03	0.01	0.02	0.03	0.02	0.03
MgO	0.32	0.06	0.12	0.43	0.22	0.17	0.27	0.35	0.12
CaO	0.84	0.08	0.18	0.81	0.36	0.55	0.59	0.66	0.43
Li_2O	0.019	0.01	0.016	0.01	0.0088	0.013	0.02	0.02	0.02
Na_2O	3.00	3.22	3.18	3.06	2.92	3.08	4.70	3.14	2.88
K_2O	5.30	5.02	5.12	5.18	5.50	5.10	5.10	5.12	5.20
P_2O_5	0.03	0.04	0.09	0.02	tr.	0.01	0.07	0.03	0.06
CO_2	0.22	0.11	0.20	0.14	0.17	0.03	0.15	0.14	0.04
H_2O^+	0.47	1.00	0.91	0.66	0.52	0.80	0.35	0.75	0.83
H_2O^-	0.28	0.39	0.32	0.29	0.22	0.30	0.24	0.32	0.24
F	0.17	0.21	0.20	0.10	0.04	0.08	0.12	0.22	0.12
S	0.01	tr.	tr.	tr.	tr.	tr.	tr.	tr.	tr.
Σ	99.68	99.36	99.56	100.41	100.42	100.20	100.44	100.56	99.55

From a comparison of the averages for the red and white granite it can be seen that the chemical data of both granites are very similar. There are some differences in content of Al_2O_3, Fe_2O_3, and TiO_2, SiO_2, Li_2O. In general the red granite is richer in Al_2O_3, Fe_2O_3 and TiO_2 content and poorer in SiO_2 and Li_2O content in comparison with the composition of the white granite. Figure 13a shows the position of the mean and the range of analyses in the classification of granitic rocks according to Tuttle and Bowen (1958) and Hietanen (1963).

A diagram of normative Ab-Or-Q (Fig. 13b) shows the Heemskirk intrusion as a true granite. The mean and close cluster of analyses lie in the inner triangle which limits the spread of granites sensu stricto. In diagrams of normative Ab-Or-An according to Hietanen (1963) the mean and the majority of analyses also lie in the field of granites sensu stricto.

Regional variations within the granite were studied by means of trace elements. According to the generally accepted view, the behaviour pattern of trace elements is a magnification of the major element pattern in monotonous granites, where in some cases the response of major elements is rather insignificant or undetectable.

The content of selected trace elements and Na_2O was studied in 105 rock samples of the red and white granite.

Figure 13

A) Triangular diagram An-Ab-Or according to Tuttle
and Bowen (1958). Inner triangle limits the range
of the granite field.
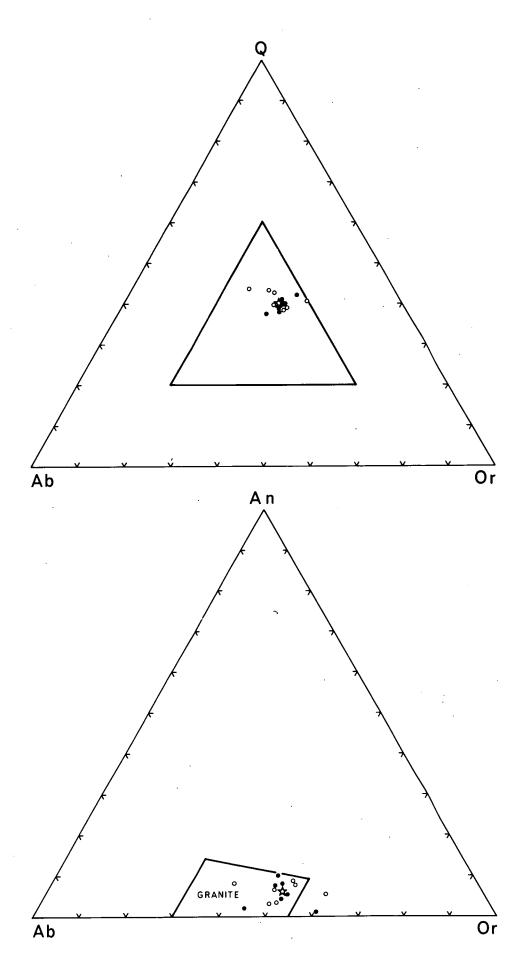
B) Triangular diagram An-Ab-Or according to Hietanen
(1963).
Classification of coarse-grained calc-alkalic
igneous rocks on the basis of their normative
feldspar content. Ab, An and Or refer to the mole-
cular norms of albite, anorthite and orthoclase.
The plots of the weight norm would fall a short
distance father from the Ab corner.
Open circles - White granite
Black circles - Red granite
Star - Average composition of the Heemskirk
granite massif

Q

Ab   Or

An

GRANITE

Ab   Or

70/9/18 6

The concentrations of Rb, Sc, Na_2O, Zr, F, Nb, Pb, Ba and Sn are shown in Tables A-1 and A-2 of Appendix II. Table 6 shows the arithmetic means, and range of content of elements studied. Figure 14 indicates interfacial trends of the mean concentration of elements studied in individual rock types (R2, R3, W2, W3). A correlation between the elements studied (log base) in rock is given in Table 7.

The differences in the average contents of the elements studied in the red and white granites (Table 6) are markedly distinguishable in the content of Rb, Zr, Sr, Pb and Ba. The differences in the concentration of Sn, Nb, F and Na_2O are less marked or are within the range of analytical error (Nb). These arithmetic means in heterogeneous groups of the white and red granite mask the differences in the concentration of elements in each individual rock type (R2-R3 and W2-W3). Figure 14 shows the differences in the average content of the elements studied in the basic petrographic types W3-W2-R3-R2 in stratigraphic sequence from the underlying to the overlying rocks. A continuity between the chemical trends of the red and white granite is marked by a broken line.

Rb In the sequence of rock types W3 W2 R3 R2 there is a gradual decrease in the Rb content towards R2. As can be seen from Table 6, the white granite is richer in Rb.

TABLE 6.

ROCKS

Mean (ppm) * in %	Red Granite	White Granite	Heemskirk Granite
Rb	379 ppm	499 ppm	439 ppm
Sr	24 ppm	15 ppm	20 ppm
Na_2O *	3.26 %	3.30 %	3.28 %
Zr	202 ppm	91 ppm	146 ppm
F	0.17 %	0.16 %	0.17 %
Nb	14 ppm	13 ppm	14 ppm
Pb	42 ppm	51 ppm	46 ppm
Ba	152 ppm	85 ppm	118 ppm
Sn	22 ppm	26 ppm	24 ppm
Standard Deviation			
Rb	74	97	85
Sr	17	21	19
Na	0.26	0.34	0.30
Zr	44	36	40
F	0.04	0.04	0.04
Nb	8	9	9
Pb	8	12	10
Ba	100	94	97
Sn	6	8	7
Number of samples	59	46	105

TABLE 7.

Correlation matrix
(Data in log base 10.)

Red granite
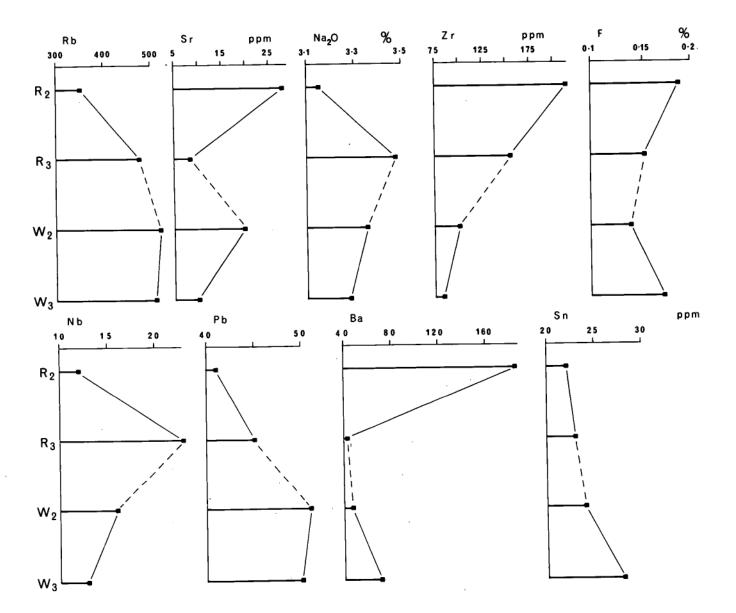
y \ x	Rb	Sr	Na$_2$O	Zr	F	Nb	Pb	Ba	Sn
Rb		-0.831	0.249	-0.645	-0.081	0.550	0.309	-0.770	0.013
Sr	-0.826		-0.343	0.685	0.221	-0.438	-0.200	0.778	0.021
Na$_2$O	0.284	-0.560		-0.219	-0.309	0.064	0.127	-0.449	-0.100
Zr	-0.570	0.789	-0.704		0.075	-0.187	-0.268	0.725	0.052
F	0.336	-0.132	-0.225	-0.083		0.027	0.088	0.237	0.238
Nb	0.577	-0.614	0.526	-0.493	0.116		0.225	-0.365	0.104
Pb	0.424	-0.287	-0.164	-0.054	0.182	0.145		-0.299	0.107
Ba	-0.572	0.822	-0.732	0.765	0.046	-0.549	-0.065		0.120
Sn	0.141	-0.064	0.119	-0.176	0.057	0.121	0.360	0.050	

White granite x = f (y)

Figure 14

Méan concentration of trace elements and Na_2O in the main rock types of the Heemskirk granite massif. Abscissa is on an arbitrary scale.

20/11/18

The Rb content in the rocks of the Heemskirk massif is closely related to the chemical composition and modal concentration of biotite and potassium feldspar. In both minerals Rb (diadochically) replaces the potassium. The degree of dependence of the Rb content in host rocks, and the content in biotite and potassium feldspar, was studied in the red granite.
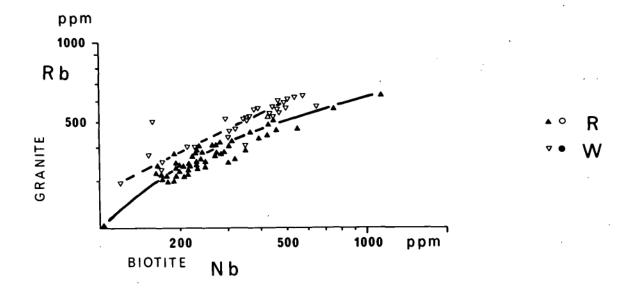
Rb in rocks is in positive correlation to Rb in potassium feldspar but in an antipathetic relation to Rb in co-existing biotites. In both granites Rb is in positive relationship to Zr, Na, Pb and negative correlation to Zr, Sr, and Ba. The weak positive correlation of Rb with F is obvious only in the white granite. A remarkable antipathetic relationship between Rb and Zr was found also by Hahn-Weinheimer and Johanning (1969) on granite plutons in Schwarzwald (Black Forest) in Germany. According to these authors the characteristic relationship between the Rb and Zr probably corresponds to the trend of differentiation of the studied plutons.
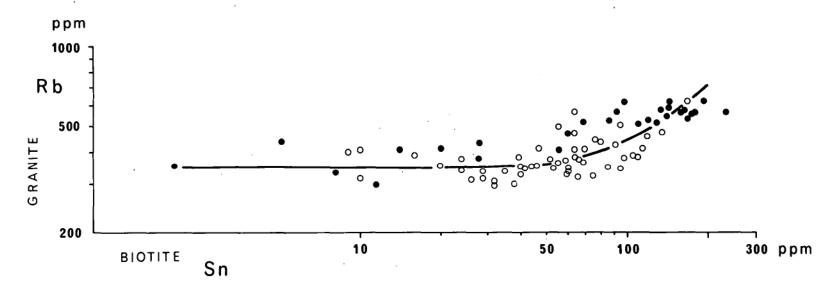
Rb in the red and white granites is also related to Nb and Sn in biotites (Fig.15). From the figure it is obvious that the Rb content in the host rocks remains stable (300 ppm) with increasing Sn content in biotite up to 50 ppm Sn. The Sn contents above 50 ppm correspond exactly to the higher concentration of Rb in rocks. These trends

Figure 15

A) Plots of Rb content in granites vs. Nb content
   in their biotites.

B) Plots of Rb content in granites vs. Sn content
   in their biotites.

   black triangles and open circles - Red granite
   open triangles and black circles - White granite

in the Heemskirk massif can be important for the localization of the more promising Sn mineralization areas.

<u>Sr</u>   The Sr content of the rocks of the Heemskirk massif is remarkably variable with the highest concentrations occurring in the R2 phase of the granite.

In white granite there is on the average a lower concentration of Sr in the coarse grained type W3. Higher values of Sr with considerable variation in range were found in rocks of the Heemskirk massif by Brooks and Compston (1965). Sr in both rock groups is closely positively related to Zr, Ba and antipathetically related to Nb, Rb and also to Na_2O in the white granite.

<u>Na_2O</u>   The Na_2O concentration represents the albite content in the Heemskirk massif rocks. The mean concentrations of Na_2O for the red and white granite are nearly identical, but within both rock groups there exist remarkable difference as can be seen in figure 14.

The lowest Na_2O contents are in coarse-grained red granite (R2) and the highest concentrations are in the type R3. The Na_2O content in the white granite lies between the two extremes and tends to increase from W3 to W2.

Na_2O in the white granite has an antipathetic relationship to Zr, Sr and Ba and positive correlation only with Nb.

In the red granite the negative correlation of Na_2O with Zr, Sr and Ba, is considerably less important. There is a complete lack of correlation between Na_2O and Nb.

Zr   Zr in the Heemskirk massif rocks occurs only in zircon. A marked variation in the Zr content exists not only between the individual rock group (Table 6) but also within each of the groups.

As can be seen from figure 14 Zr concentration increases in the sequence of rock W3-W2-R3-R2.

In the white and red granite Zr has a positive correlation with Sr and Ba and an antipathetic relationship with Na_2O, Rb and Nb (with the exception of Rb in the white granite).

F   The total F content in the Heemskirk massif rocks has a remarkable complex character. F is present in muscovite, biotite, tourmaline, accessory fluorite, apatite, and topaz.

The mean F content in both granites masks the more marked variations within both these groups based mainly on the total content of biotite. A lower content of biotite in type R3 and W2 corresponds to lower F concentrations, whereas in types W3 and R2 - biotite richer rocks - the F contents are remarkably higher.

In the white granite F has a tendency towards a weak positive relationship with Rb and a weak negative relation-

ship with Na_2O. In the red granite F has a weak positive correlation with Sr, Ba and Sn and negative correlation to Na_2O.

Nb Most Nb occurs in biotite, with some in accessories (sphene, zircon, magnetite). The tight bonding of Nb in biotite is obvious from the positive correlation of Nb in the host rock vs. Nb in biotite in both granites. From Table 6 it can be seen that the mean Nb contents are practically the same for the red and white granite. Within both granite groups there are marked variations in the Nb content. The highest inhomogeneity of Nb data is in the red granite. From figure 14 of the interfacial trends of trace elements in granites it is obvious that there is a remarkable difference in the Nb content in type R2 (120ppm) and R3 (23ppm). In the white granite there is a similar trend (higher content in type W2) but it is less marked.

In the white granite Nb has a positive correlation with Rb and Na_2O and an antipathetic relation to Sr, Zr and Ba. The same applies for the red granite except for Na_2O, which shows no correlation with Nb.

Pb In the rocks of the Heemskirk massif Pb is mainly in K-feldspars. On the average it is more concentrated in the white granite. Within each individual granite group there is an increase in the Pb content from type R2 to R3, W3 to W2 respectively. Between the two granitic types there is

a considerable break.

From the correlation matrix (Table 7) it is obvious that the Pb does not have any marked correlation with any of the studied elements in either the red or the white granite. In both granites Pb is only weakly positively correlated to Rb. In the white granite Pb has a tendency towards positive correlation with Sn and in the red grani- te a very weak correlation between Pb and Nb exists.

Ba   As is generally accepted, Ba has a tendency to be clo- sely related to Sr in K-feldspars (Heier and Taylor 1959). In the Heemskirk granite rocks there are generally high Ba contents in the red granites. From Fig. 14 it can be seen that a high concentration of Ba belongs only to type R2 while in type R3 the Ba content is the lowest of all observed types in the Heemskirk massif. In the white gra- nite it is obvious that there is a decrease in Ba content from type W3 to W2. In general the lowest Ba contents are in the medium to fine grained types of both granite groups.

From the correlation matrix it can be seen that the Ba in the red and white granite is in positive correlation with Sr and Zr and in antipathetic correlation with Nb, Na_2O and Rb.

Sn   The presence of Sn in the rocks of the Heemskirk mas- sif has a complicated character. The greatest part of the tin is bound up in the biotite but a considerable amount

is also present in the potassium feldspar of the red granite. Other concentrations of Sn are in the Ti acces-sory minerals (sphene, rutile) and muscovite in the white granite.

Accessory cassiterite was detected in some samples of both granites. On the average the higher concentrations of Sn occur in the white granite. Figure 14 shows a de-creasing trend in Sn content from type W3 to R2. The mean Sn contents of rocks in the Heemskirk massif correspond to the lower boundary of Sn concentration in typical Sn bearing granites (see figure 8).

From the correlation matrix (Table 7) it is obvious that there is a weak positive correlation of Sn with Pb in the white granite and with F in the red granite.

The relationships to other elements are not statisti-cally significant in the same way as F and Pb.

6.2. Bulk composition and trace elements of biotites

The content of selected trace elements was studied in 96 samples of biotite from red and white granite. The element concentrations of Rb, Sr, Sc, Ni, Cr, F, Cl, Zn, Nb and Sn are shown in Table A-5 and A-4 in Appendix II. Table 8 shows the arithmetic means and standard deviation of elements studied. The relationship between the trace

TABLE 8.

Biotites

Mean (ppm) *in%	Red Granite	White Granite	Heemskirk Granite
Rb	736	1066	901
Sr	6	6	6
Sc	89	97	93
Ni	232	231	232
Cr	59	65	62
F*	0.74	0.55	0.64
Cl	3404	1730	2567
Zn	345	382	363
Nb	288	372	330
Sn	63	103	83
Standard Deviation			
Rb	351	533	442
Sr	6	7	7
Sc	18	19	19
Ni	117	90	103
Cr	11	23	17
F*	0.37	0.30	0.33
Cl	1835	1757	
Zn	152	192	
Nb	161	134	
Sn	37	74	
number of samples	54	39	93

Correlation matrix
(Data in log base 10)

TABLE 9.

Biotite of the red granite

x / y	Rb	Sr	Sc	Ni	Cr	F	Cl	Zn	Nb	Sn
Rb		-0.359	-0.218	-0.332	-0.569	0.673	0.784	-0.379	-0.334	-0.093
Sr	-0.146		0.191	0.339	-0.157	-0.234	-0.284	0.031	0.296	0.361
Sc	-0.256	0.139		0.187	0.177	-0.271	-0.341	-0.005	0.416	0.038
Ni	0.117	0.049	0.358		0.644	-0.503	-0.558	0.329	0.660	0.496
Cr	-0.473	0.183	-0.430	-0.094		-0.557	-0.621	0.389	0.346	0.265
F	0.259	0.193	-0.288	-0.189	-0.010		0.748	-0.426	-0.568	-0.176
Cl	0.493	-0.114	-0.716	-0.402	0.280	0.431		0.594	-0.615	-0.220
Zn	-0.256	0.295	0.497	0.226	-0.120	-0.285	-0.537		0.471	-0.049
Nb	0.222	-0.019	0.675	0.566	-0.719	-0.132	-0.597	0.295		0.380
Sn	-0.068	0.113	0.504	0.564	-0.436	-0.118	-0.671	0.407	0.731	

Biotite of the white granite

$x = f(y)$

TABLE 10. A - B

Correlation matrix
(Data in log base 10)

Red granite

"Red" biotite

y \ x	Rb	Sr	F	Nb	Sn
Rb	-0.344	0.276	0.329	-0.072	0.145
Sr	0.274	-0.177	-0.196	0.109	-0.240
F	-0.557	0.593	0.496	-0.160	-0.199
Nb	0.924	-0.890	-0.283	0.382	-0.066
Sn	0.379	-0.249	-0.240	0.181	0.019

White granite

"White" biotite

y \ x	Rb	Sr	F	Nb	Sn
Rb	0.071	-0.174	0.002	0.030	-0.344
Sr	-0.040	0.019	0.319	-0.160	0.165
F	-0.238	0.239	0.692	-0.163	-0.246
Nb	0.888	-0.863	0.212	0.731	0.131
Sn	0.784	-0.705	0.283	0.412	0.131

$x = f(y)$

TABLE 11. A – B

Correlation matrix
(Data in log base 10)

Red granite

y \ x	Rb	Sr	Na	Pb	Ba	Sn
Rb	0.695	-0.699	-0.365	0.244	-0.750	0.186
Sr	-0.510	0.737	0.273	-0.191	0.709	-0.231
Na	-0.393	0.450	0.654	0.012	0.373	-0.039
Pb	0.560	-0.535	-0.432	0.288	-0.485	-0.085
Ba	-0.462	0.622	0.202	-0.203	0.647	-0.228
Sn	0.165	-0.200	-0.119	-0.006	-0.096	0.058

K-feldspar

"Red" biotite

y \ x	Rb	Sr	Sn
Rb	0.007	-0.401	0.116
Sr	0.170	0.173	-0.033
Sn	0.690	-0.132	0.238

K-feldspar

$x = f(y)$

TABLE 12 A-B

Chemical Analyses of Biotites

	1[*]	2[*]	3[*]
SiO_2	35.93	36.54	36.38
TiO_2	1.8?	1.78	3.25
Al_2O_3	15.8?	14.05	16.15
Fe_2O_3	4.42	4.42	3.58
FeO	23.52	22.55	18.16
MgO	3.82	4.39	6.00
MnO	0.29	0.50	0.60
CaO	0.62	0.97	0.11
Na_2O	0.41	0.50	0.35
K_2O	8.21	7.83	9.57
P_2O_5	-	-	-
H_2O^+	2.49	2.90	3.26
F	1.85	1.65	1.45
Li_2O	0.39	0.28	0.32
Total ξ	99.63	99.36	99.18

[*] I.H. Rattigan
1 - White granite
2 - Red granite
3 - Red granite (marginal contact phase)

K-Feldspars

	mean (ppm)	std. dev.
Rb	610	102
Sr	76	29
Na_2O	3.44%	0.28
Pb	79	21
Ba	1135	422
Sn	29	9

Chemical Analyses of Biotites

TABLE 13.

	Red granite					White granite			
	R$_2$			R$_3$		W$_2$		W$_3$	
	69	73	48	18	19	99	90	68	83
SiO$_2$	35.20	34.23	33.33	29.86	35.13	33.01	34.95	29.32	33.28
TiO$_2$	4.28	3.75	3.63	3.80	3.80	1.85	2.75	2.45	3.27
Al$_2$O$_3$	12.58	12.51	14.26	16.22	16.69	23.04	19.75	20.65	21.49
Fe$_2$O$_3$	3.74	5.30	3.74	10.33	6.40	3.22	2.45	5.54	2.79
FeO	24.30	21.72	25.00	20.30	20.30	23.85	22.87	24.80	21.80
MnO	0.38	0.41	0.32	0.57	0.34	0.62	0.55	0.70	0.50
MgO	5.15	7.05	5.50	4.47	3.73	1.71	3.02	3.33	4.43
CaO	1.01	2.80	1.69	2.52	0.38	0.056	0.48	2.00	0.79
Li$_2$O	0.20	0.14	0.19	0.12	0.19	0.15	0.35	0.28	0.26
K$_2$O	7.74	4.68	5.92	1.30	5.23	2.65	6.96	2.33	6.55
Na$_2$O	0.23	0.31	0.15	0.45	0.20	0.27	0.29	0.12	0.13
P$_2$O$_5$	0.45	0.41	0.40	0.44	0.21	0.10	0.08	0.12	0.12
CO$_2$	0.14	0.17	0.26	0.26	0.32	0.22	0.20	0.16	0.27
H$_2$O$^+$	2.69	5.06	4.18	8.00	5.91	8.39	4.31	6.49	4.31
H$_2$O$^-$	0.25	0.23	0.22	0.74	0.39	0.21	0.19	0.36	tr.
F	1.49	1.73	1.54	0.52	0.75	0.23	1.08	1.30	0.79
S	0.03	0.006	0.01	0.02	0.02	0.009	0.009	0.05	0.02
Σ	99.86	100.51	100.34	99.92	99.99	99.59	100.29	100.00	100.80
γ/β	1.6707	1.6553	1.6573	1.6651	1.6677	1.6477	1.6545	1.6576	1.6481
Mean γ/β			1.6632					1.6519	

TABLE 14.

Average Chemical Analyses of Biotites

	Red granite		White granite	
	Range	Mean	Range	Mean
SiO_2	35.20 - 33.33	34.47	34.95 - 33.28	34.12
TiO_2	4.28 - 3.63	3.87	3.45 - 2.75	3.10
Al_2O_3	16.69 - 12.51	14.01	21.49 - 19.75	20.62
Fe_2O_3	6.40 - 3.74	4.80	2.79 - 2.45	2.62
FeO	25.00 - 20.30	22.83	22.87 - 21.80	22.33
MnO	0.41 - 0.32	0.36	0.55 - 0.50	0.52
MgO	7.05 - 3.73	5.36	4.43 - 3.02	3.73
CaO	2.80 - 0.38	1.47	0.79 - 0.48	0.64
Li_2O	0.20 - 0.14	0.18	0.35 - 0.26	0.29
K_2O	7.74 - 4.68	5.89	6.96 - 6.55	6.76
Na_2O	0.31 - 0.15	0.22	0.29 - 0.13	0.21
P_2O_5	0.45 - 0.21	0.37	0.12 - 0.08	0.10
CO_2	0.32 - 0.14	0.22	0.27 - 0.20	0.23
H_2O^+	5.91 - 2.69	4.46	4.31 - 4.31	4.31
H_2O^-	0.39 - 0.22	0.27	0.19 - tr.	0.10
F	1.73 - 0.75	1.38	1.08 - 0.79	0.94
Σ		100.16		100.6
Number of analyses		4		2

elements (in log base 10) is given in a correlation matrix (Table 9). Table 10 shows the intercorrelation of these elements (in log base 10) between host rocks and biotite and Table 11b between biotite and potassium feldspar.

Bulk chemical analyses of biotites from both granites (Rattigan, 1968) are shown in Table 12. Sample no. 1 represents the composition of biotite from the white granite and Sample No. 2 represents the composition of biotite from the red granite. Table 13 shows new chemical analyses of biotites from the major rock types of the Heemskirk granite massif. From a comparison of the averages for biotite – R and biotite – W (Table 14) it can be seen remarkable difference in content of Al_2O_3, Fe_2O_3 and MgO. In general higher Fe_2O_3 and MgO content is in biotite – R and higher Al_2O_3 content is in biotite – W. Relative high content of H_2O+ in both biotites indicates significant alteration of some samples (chloritisation).

According to the classification of trioctahedral micas (Foster, 1960) the analysed samples of white and red biotite lie on the lower periphery of the Fe-biotite field. The red biotite (mainly the biotite from contaminated granite) is closer to the Mg pole (Fig. 16a).
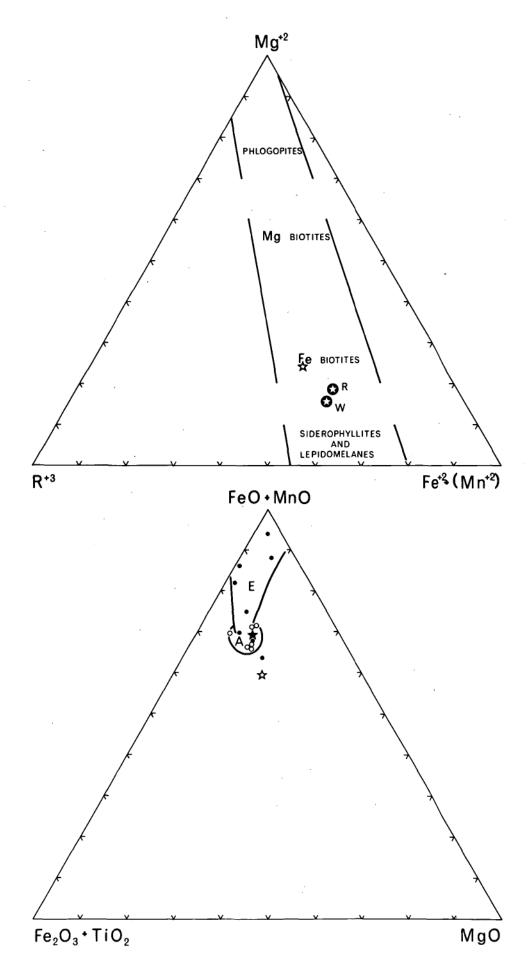
The differences in chemistry are due among other things to the mineralogical association of each granite.

Figure 16

A) Triangular diagram of R^3 ($Fe_2O_3 + Al_2O_3 + TiO_2$) - MgO and FeO (+MnO) according to the classification of trioctahedral micas (Foster 1960).

Open star - average composition of biotites from the Heemskirk massif (according to the data of Rattigan 1964)

Open star on black background - R - biotite of the red granite

- W - biotite of the white granite

B) Triangular diagram FeO + MnO - $Fe_2O_3 + TiO_2$ - MgO

Black circles - biotites from Erzgebirge tin-bearing granites (Central Europe) according to Bräuer (1967).

Open circles - biotites from australian tin-bearing granites according to Rattigan (1964)

Black star - average composition of the biotites from the Heemskirk granite

Open star - composition of the biotite from the contaminated red granite (Heemskirk granite massif).

Top triangle:
- Mg^{+2}
- R^{+3}
- Fe^{+2}(Mn^{+2})
- PHLOGOPITES
- Mg BIOTITES
- Fe BIOTITES
- R
- W
- SIDEROPHYLLITES AND LEPIDOMELANES

Bottom triangle:
- FeO + MnO
- Fe$_2$O$_3$ + TiO$_2$
- MgO
- E
- A

20/11/16

Biotite in white granite occurs in association with musco-
vite while the biotite in red granite occurs alone.

A high content of Al_2O_3 and a lower SiO_2 content in
biotite W[+] agrees with the results of Nockolds (1948).
He suggested the same relationship for biotites associat-
ed with muscovite. A low MgO content and high FeO in bioti-
te W is in agreement with the general chemical trend in
both rocks.

Mean contents of trace elements in Table 8 for bioti-
tes R[+] and W show marked differences in Rb, F, Cl, Nb and
Sn. On the other hand the contents of Sr, Ni and Cr are
approximately equal in both biotites. These mean values
mask differences in the concentration within each group of
biotites. In figure 17 the interfacial trends of mean
contents in the rock types W3 - W2 - R3 - R2 can be seen.
Rb is the trace element that is most ideally camouflaged
on the biotite structure and it exhibits a well known
coherence with K. The mean content of Rb (Table 8) is of
the same order as the concentration of Rb in Sn-bearing
granites in southern England which were published by
Bradshaw (1967).
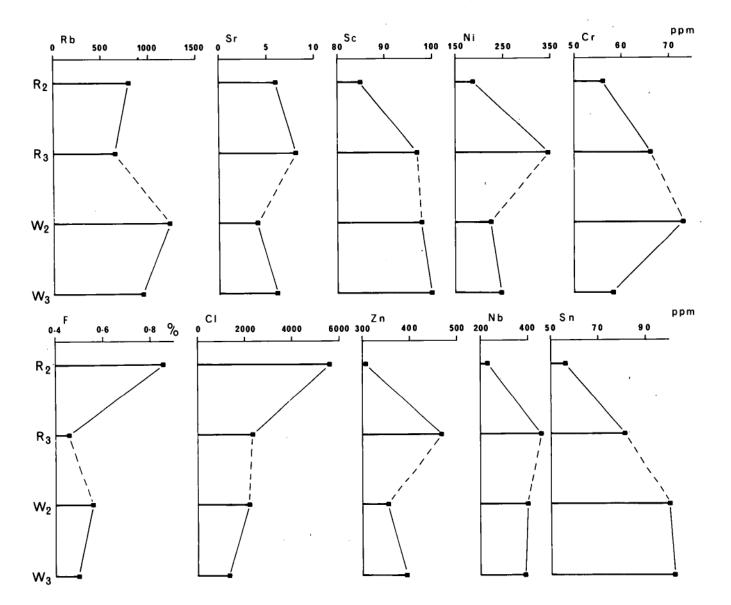
In the biotite R group the concentration of Rb increa-
se from type R3 to R2. The same trend is obvious in the

[+] Biotite W and biotite R from the white (W) and red (R)
granite.

Figure 17

Mean concentration of the trace elements in biotites
of the main rock types of the Heemskirk granite mas-
sif. Abscissa is on an arbitrary scale.

20/11/17

biotite W from type W3 to W2. In both cases the Rb concentration increases from underlying to the overlying rocks, with a marked increase in absolute values between the biotite R and W.

In Table 9 it can be seen that the Rb in the biotite R shows a marked positive correlation with F, Cl and an antipathetic relationship to Cr. Rb in biotite W has a positive correlation only with Cl, and a negative one with Cr. The Rb concentration in the biotite R is negatively correlated with Rb and positively correlated to F in host rocks. Rb in the biotite W shows only a weak antipathetic relationship with Rb in the host rock.

<u>Sr</u> In the biotite structure Sr occurs in the interlayer with Na, Ca and Ba. The Sr content in the biotites of the Heemskirk massif is of the same order as in the Catrige Pass pluton of the Sierra Nevada Batholith (Dodge and Moore, 1968). In the sequence of the rock types in the Heemskirk massif the lowest Sr contents are in type W2 and the highest in type R3. Types R2 and W3 have approximately the same concentration of Sr. From Table 9 it can be seen that Sr does not show any marked correlation with other elements in either the biotite R or biotite W. The same applies to the correlation of Sr between biotites and bulk rocks (tab. 10).

Sc The main features of the geochemistry of scandium are known through the studies of Goldschmidt and Peters (1931), Kvalheim and Strock (1939), Borisenko (1961). According to these studies Sc^{3+} replaces Mg^{2+} and Fe^{2+} in crystal structures. In the problem of the dispersion of scandium in ferromagnesian minerals of the early stage of crystallization of magmatic rocks Ringwood (1955) postulated that scandium enters them at the expense of Fe^{2+} and not at the expense of Mg^{2+}. Ringwood explains the possibility of replacement of a ferrous ion by a scandium ion by the fact that Sc^{3+} has a considerably larger ionic radius and also a higher electronegativity than Mg^{2+}.

In the rocks of the Heemskirk massif biotite is the only ferromagnesium mineral, and indeed it contains the majority of the Sc content in the rock.

Data on scandium are relatively abundant (Dodge, Smith and Mays, 1969; Tilling, Greenland and Gottfried, 1969; Dodge and Moore, 1968). Some of the previous studies have indicated that the Sc content of biotite increases with decreasing temperature of crystallization (Oftedal, 1943; Ingerson, 1955; Herz and Dutra, 1964).

The mean Sc content for biotites studied is somewhat higher than in data published by Herz and Dutra (1964) and Ingerson (1955) for biotites from alkaline granites.

In general the biotite R has a lower Sc content than
the biotite W. Figure 17 demonstrates a gradual decrease
in Sc concentration from the lower part of the massif to
the overlying rocks (W3 — W2 — R3 — R2).

Table 9 shows the positive correlation of Sc with
Zn, Nb and the negative correlation with Cl and Cr for
the biotite W. In the biotite R Sc can only be correlated
with Nb.

Ni According to Herz and Dutra (1964), in the early sta-
ges of differentiation Ni can substitute readily for Fe
as both have similar ionic radius and electronegativity.
In later differentiation Ni may form complexes depending
upon the availability of O and volatiles (Herz and Dutra
1964).

The mean content of Ni is practically the same for
both types of biotite, corresponds to the maximum values
in granitic biotites published by Haack (1967) and
greatly exceeds the values published for biotites by
Hertz (1964).

Figure 17 shows that there is an increasing concentra-
tion of Ni from type W3 to type R3 and a steep decrease
from type R3 to type R2. A similar trend is obvious for
Zn and Nb (see p. 28 and 29). Ni in biotites R is in
positive correlation with Cr, Nb and Sn, and negative
correlation with F and Cl.

In the biotite W Ni shows positive relationship to
Nb and Sn and negative correlation with Cl.

$\underline{Cr}$ substitutes for Fe^{3+} in the octahedral position in
the structure of biotite. The concentration of Cr in
biotites of the Heemskirk massif is relatively lower than
the averages published by Haack (1969) for biotites of
some European granites.

In the sequence of rock types W3 W2 R3 R2 there
is a remarkable increase in the concentration of Cr from
W3 to W2 and considerable decrease from R3 to R2. A simi-
lar trend is obvious for Ni and Nb (see p.102 and105).
Cr in the biotite R is in positive correlation with Ni
and negative correlation with F, Cl and Rb. In biotites W
Cr has an antipathetic relationship to Sn, Rb and Sc.

$\underline{F}$ In the biotite structure F isomorphically replaces the
OH group. In biotites of the Heemskirk massif a minor part
of the fluorine can be bonded in fluorite which is a com-
mon impurity in biotite W. Another impurity in the biotite
is apatite which cannot be completely removed for the
purposed of analysis and hence its F content contributes
to the determined concentration of fluorine in the biotite.

Figure 17 illustrates the increasing trend of F
content from the biotites W to biotites R. The highest
fluorine concentrations are in Type R2. A similar trend
is shown by Cl (see p.104). F in the biotite R has a po-

sitive relationship to Rb, Cl and negative correlation
with Cr, Zn, Nb. In the biotite W F shows a positive cor-
relation only with Cl.

In the correlation matrix (Table 10) fluorine in the
biotite R is in positive correlation with Sc, F, and nega-
tive correlation with Rb in the host rocks. In the case
of the correlation of trace elements of the biotite W and
the white granite fluorine of biotites shows only a posi-
tive correlation with Cl of the bulk rocks.

- Cl In the same way as F, Cl also replaces the OH group
isomorphically, both in the biotite and apatite.

Part of the Cl content of biotites can be related to
the aqueous inclusions in that mineral. Some studies on
fluid inclusions in other granites support the view
that most of the ore fluids are chloride solutions
(Roeder, 1960). According to Sainsbury and Hamilton (1967)
the volatile compounds SnF_4 and $SnCl_4$ are important
transport agents of Sn.

Cl shows the same increasing trends in its concentra-
tion as F in sequence of rock types from W3 to R2·which
has the highest Cl content. From the correlation matrix
(Table 9) it can be seen that the Cl in the biotite R is in
a close positive correlation with Rb, F and has an anti-
pathetic relationship to Ni, Cr, Zn and Nb. In the bioti-
te W Cl is in positive correlation with Rb, F and in a ne-

gative relationship to Sc, Ni, Zn, Nb and Sn.

Zn   The mean Zn content of both types of biotites is very
similar to average concentration of Zn in biotites for
Cornwall (350 ppm) reported by Bradshaw (1967).

In the sequence of rock types W3—W2—R3—R2 (Fig.17)
the Zn content varies markedly mainly in biotites R. In
the biotite W the Zn content is higher in type W3. The
highest Zn content is in biotite R (type R3) and decreases
in type R2. Zn in the biotite R has a positive correlation
with Nb and partially also with Cr and Ni. An antipathetic
relationship exists between Zn and F, Cl.

In the white biotite Zn is in positive correlation
with Sc and Sn, and in negative correlation with Cl.

Nb   The heterovalent isomorphism of niobium is very pro-
nounced. Nb replaces certain quadrivalent cations (Ti, Zr,
Sn) and some trivalent cations (Fe). In granites the most
common substitution of Nb is for Ti and Zr. In the bioti-
tes of the Heemskirk massif the Nb content increases in
the sequence of rock types W3 W2 R3 from 380 to 450ppm.
There is a marked decrease from R3 to R2 (down to 220ppm).

Nb in the biotite R positively correlates with Sc,
Ni, Zn, Sn and negatively correlates with Cl, F and partly
with Rb.

In the biotite W Nb has a positive correlation also
with Sc, Ni and an antipathetic relationship to Cr and Cl.

In the correlation matrix biotites versus granites
(Table 10) the Nb from biotites R and W has a positive
correlation with Rb, Nb and negative correlation with
Sr from the host rocks.

Sn The highest concentrations of Sn in granites are
to be found in the micas, and some accessory minerals
(magnetite, sphene).

In the literature the Sn content in biotite is gene-
rally accepted as a useful metallogenic indicator of pos-
sible Sn mineralisation. Higher concentrations of Sn are
generally found in biotites from Sn-bearing granites, and
may be as much as ten times higher than the concentration
of Sn in the host rocks (Hesp, 1970).

The incorporation of tin into biotite is generally
explained by diadochic substitution for cations occupying
octahedral sites in the biotite structure. The character
of diadochic substitution has not yet been exactly defined
mainly because of lack of experimental data.

Vendel (1945, 1956) and Neubauer have claimed that
Sn^{4+} (also Sn^{2+}) can substitute for Mg^{2+}. According to
Hellwege (1956) in the diadochic bond of Sn in biotite,
Fe^{2+}, Fe^{3+} and Ti^{4+} also play a role. Barsukov (1957)
assumes the bond of Sn in the structure of biotite to
show a two-step isomorphism:

1) $Li^{+}Fe^{3+} \rightleftharpoons Mg^{2+} + Fe^{2+}$

2) $Li^{+}Sn^{4+} \rightleftharpoons Mg^{2+} + Fe^{3+}$

The bonding of Sn in the biotite structure has an apparently complex character.

The Sn contents in the biotites of the Heemskirk massif are on the average lower than those published by Bradshaw (1967) for the biotites of the Sn-bearing granites of Southern England.

On the other hand the averages for the red biotite (60 ppm) and white biotite (100 ppm) are in agreement with the values published by Jedwab (1955) for biotites from non-mineralized and mineralized granites respectively in France.

In the sequence of rock types W3 — W2 — R3 — R2 the Sn content decreases from 100 ppm to 60 ppm. Sn content is generally higher in the biotite W. Sn in the biotite R has positive correlation only with Ni, Nb and Sr. On the other hand Sn content in the biotite W shows closer relationships to the chemical composition of the biotite.

Correlation matrix (Table 9) shows the positive relationship of Sn to Sc, Nb and Zn and negative correlation to Cl and Cr.

In the correlation of bulk rocks and their biotites Sn in biotites shows a positive relationship to Rb, Nb and antipathetic relationship to Sr in bulk rocks. In

the biotite R versus red granite correlation Sn in biotite
has a weak correlation only with Rb from bulk rocks.

According to Vendel (1949), Sattran and Klominsky
(1970), Rattigan (1963), Hosking (1967) and others stan-
niferous granites are characterized by very low Mg and Fe
contents. This results from a low content of biotite which
is the only mafic mineral in these rocks. As shown in
figure 16b the composition of biotite in both Erzgebirge
area (M.Bräuer, 1967) and the major tin-bearing granite
provinces of Eastern Australia (data according to Rattigan)
is concentrated close to the Fe pole of the $Fe_2O_3 + TiO_2 -$
$- MgO - FeO + MnO$ diagram. From this diagram (Fig.16b)
it can be seen that the composition of biotite from the
Heemskirk granite is practically identical with the compo-
sition of biotites from these tin-bearing granites.

Cations of Mg, Fe and Ti used in the formation of
micas in tin-bearing granites are not numerous enough to
camouflage all Sn, so that scattered accessory cassiterite
arises. From this point of view it is obvious that the tin
content of biotites should be related directly to the
availability of tin and inversely to the modal content
of biotite in the source rock. This type of calculation
was done by H.Bräuer (1967), Sattran and Klominsky (1970)
and Hesp (1970).

On the basis of the Sn concentration in the host rocks, the Sn content in biotite and the modal concentration of biotite in the tin-bearing granites of Erzgebirge (Central Europe), Sattran and Klominsky (1970) established on an empirical basis the saturation limit of the diadochic bond of Sn in biotite crystal structure. Granites which can be considered as potential sources of Sn accumulations and contain free cassiterite have less than 25 g of Sn captured by the biotite in one ton of granite and more than 25-30 g in the host rock (Fig. 18). From figure 18 it can be seen that the white granite completely satisfied these conditions for a potential source of Sn mineralisation.

6.3. Distribution of Na_2O and trace elements in K-feldspars

The content of Na_2O, Rb, Sr, Pb, Ba and Sn was studied on 43 samples of K-feldspar from the coarse grained red granite. The elemental concentrations of these elements are presented in Table A-5 of Appendix II.
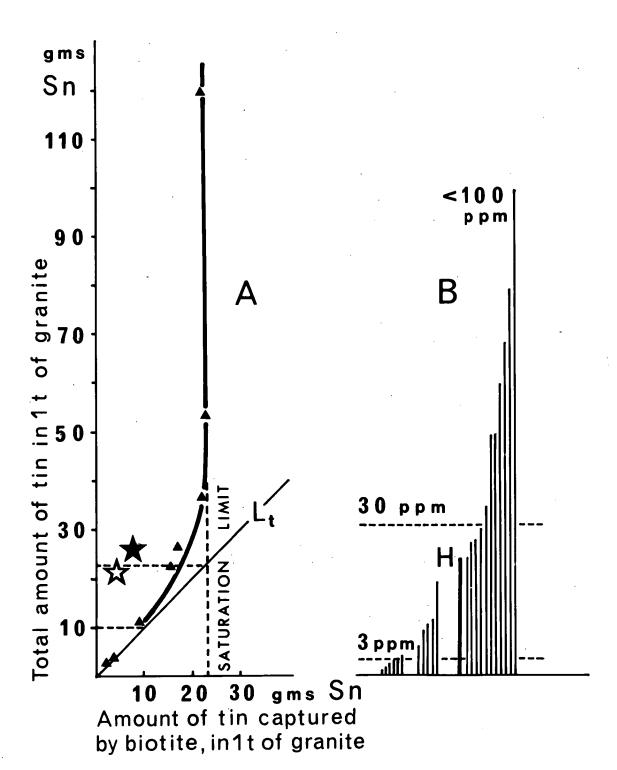
Table 12b shows their arithmetic mean and standard deviation. Intercorrelations of elements in log base 10 are given in correlation matrix (Table 15). Table 11 shows the correlation coefficients of selected elements in log base 10 between potassium feldspar and red granite and potassium feldspar and the biotite R.

110

Figure 18

Tin saturation limit in granites of the Saxo-
-Thuringian zone (A) and distribution of tin in
the different granitic rocks (B) according to
Sattran and Klomínský (1970).

Black star - average for biotite from the white
                granite

Open star - average for biotite from the ed
                granite

H - average Sn content in the Heemskirk granite
    massif.

70/9/185

Correlation matrix
(Data in log base 10)

K-feldspars of the red granite

TABLE 15.

x / y	Rb	Sr	Na	Pb	Ba	Sn
Rb		-0.846	-0.369	0.275	-0.796	0.123
Sr	-0.795		0.425	-0.398	0.917	0.012
Na	-0.405	0.348		-0.296	0.291	-0.153
Pb	0.362	-0.419	-0.356		-0.378	-0.039
Ba	-0.726	0.910	0.242	-0.376		0.068
Sn	0.089	0.078	-0.106	-0.067	0.035	

x = f (y)

Except for Sn the elements considered are those that can occupy the potassium site in the feldspar structure.

Rb exhibits its well known association with the K^{1+}. According to Taylor and Heier (1960) a large scale fractionation process must operate to produce an effective enrichment of Rb vs. K. The mean value of 600 ppm corresponds to the lower boundary of the Rb content of K-feldspar from the tin-bearing granites of south England which were studied by Bradshaw (1967).

A marked negative correlation between the Rb, Ba and Sr proves the antipathetic relationship of these elements in K-feldspars and also in the bulk rocks. The weak positive correlation between the Rb and Pb is supported by Bradshaw's results (1967). From Table 10 it can be seen that the Rb content in K-feldspars appears to be dependent on the whole rock composition. Rb of K-feldspars is negatively correlated with Sr, Na_2O, Ba and negatively correlated with Rb from the bulk rocks.

Sr is often regarded as a close associate of Ca. According to Heier and Taylor (1959) Sr in K-feldspars shows close association with Ba and a much weaker relation to Ca. In the correlation matrix (Table 15) Sr shows a marked antipathetic relationship with Pb and also partly with Na_2O.

The positive correlation with Pb lies on the boundary of statistical significance. From Table 11a it can be seen that Sr in K-feldspar has a close relationship to the Sr and Ba content of the bulk rocks and weaker antipathetic relationship with Rb in bulk rocks. On the other hand in the correlation matrix for K-feldspar and biotite R the Sr does not show any statistically significant relationship with either Rb or Sn.

Na_2O From Table 15 it can be seen that Na has a weaker antipathetic relationship with Rb. A positive correlation between the Na and Ba is on the boundary of statistical significance. A similar antipathetic relationship exists between Na and Pb. From the table it is obvious that Na in K-feldspar has a marked positive correlation with the Sr and Ba and an antipathetic relationship with Rb in bulk rocks. The mean value of Na in the K-feldspar of red granite shows a content very similar to the unmineralized granites of Dartmoor in Great Britain (Bradshaw, 1967).

Pb according to Heier (1962) Pb does not show any simple relation to any of the other elements substituting for K in potassium feldspars. In our case Pb exhibits a weak antipathetic relationship to Sr. The correlations of Pb with other selected elements are nearly all statistically non-significant. From Table 11 it can be seen that Pb in

red granite K-feldspar has a positive relationship to Rb and negative correlation with Sr, Na and Ba of the bulk rocks is statistically insignificant. The mean and range of Pb content for these feldspars are minimal to the determinations of the lead content of mineralised granites of Bradshaw (1967), Slawson and Nackowski (1959) (50ppm) and Wedepohl (1956) (100 ppm).

Ba according to Heier (1962) and Engelhardt (1936) Ba forms a strong ionic bond with oxygen which causes Ba to be markedly captured in the early formed K-feldspars. This marked tendency for capture was also found in this study (see section on regional variation of Ba). In Table 15 there is a strong correlation between Ba and Sr and an antipathetic relation between the Ba in K-feldspar and Rb in host rocks. The mean range for Ba in the K-feldspars overlaps with the lower range of variation in the Pb content in granitic feldspars (Heier, 1960).

Sn the mean Sn content in red granite K-feldspars is similar to the reported means of 16-32 ppm Sn (Ivanova, 1963) and 29 ppm Sn (Bradshaw, 1967) for K-feldspars from unmineralized granites. Sn does not show any important correlation with other elements in K-feldspar. Similarly there is no correlation between K-feldspar versus bulk rocks and K-feldspar versus biotite.

7. Statistical models of analytical data from rocks
and minerals

The aim of the geological mapping of the Heemskirk massif was to determine by field criteria the degree of homogeneity or heterogeneity in the various rock types. The majority of these criteria - colour, grain size and mineralogical associations - have a semiquantitative character, and hence, despite its accepted importance, geological mapping remains a rather subjective method for investigation of granites.

An attempt to solve the disadvantages of geological mapping on an objective basis, results in the quantification of geological data and the application of statistical methods propagated by Whitten and others. Trend surface analysis, factor analysis and discriminant analysis, are the basic statistical techniques used to study the areal variation of granites and to test the significance of the already established rock groups in the field part of study.

7.1. Trend surface analysis

Trend surface analysis belongs to the series of methods that have been used to express the distribution of data in space. Any measured geological variable

which is defined by space coordinates is called the regionalized variable. These variables are not strictly independent of each other. They influence each other up to some distance which it is necessary to consider for interpretations of the results obtained by mathematical and statistical methods. The theory of the regionalized variables has been studied by G.Matheron (1965) and J.Serў (1967).

In this study the standard trend surface analysis was used to distinguish large - scale regional variation from the complex pattern of local fluctuations and to define the geochemical anomalies within the Heemskirk granite massif.

7.1.1. Principles of the method

Trend surface analysis is a potentially useful quantitative analytical technique whereby the underlying area trend, or background, may be separated from random local variations to give a trend surface and residuals. In theory there are various types of mathematical functions which can be regression fitted to a series of points, with varying success. In common usage, however, trend surface analysis implies least-squares fitting of polynomial surfaces. Many applications of this

method in geology and geophysics were published by Whitten (1959), Peikert (1962) etc. Irregular spacing within the grid of samples points necessitates use of non-orthogonal polynomial analysis (Krumbein 1959).

Polynomial regression

We may designate a single map observation as Z_{ij} in a two-dimensional field with coordinates U and V (provided that the U-axis is normal to the V-axis).

then: $\quad Z_{ij} = \tau_{ij} + e_{ij}, \quad i, j = 1, 2....., n$

where $\quad_{ij}$ is the trend in the point (U_i, V_j) and e_{ij} the random component. The trend τ has unknown parameters in the general point and may be expressed as

$$\tau = \alpha_{oo} + \alpha_{10}U + \alpha_{o1}V + ... \alpha_{pq} U^p V^q$$

the polynomial coefficients may be found by a least-squares linear-model techniques.

Thus for the linear surface, the matrix and vectors concerned are

$$S = \begin{bmatrix} n & \Sigma U & \Sigma V \\ \Sigma U & \Sigma U^2 & \Sigma UV \\ \Sigma V & \Sigma UV & \Sigma V^2 \end{bmatrix}, \quad \hat{\beta} = \begin{bmatrix} \hat{\alpha} \\ \hat{\alpha} \\ \hat{\alpha} \end{bmatrix} \quad b = \begin{bmatrix} \Sigma\Sigma Z_{ij} \\ \Sigma U_i Z_{ij} \\ \Sigma V_j Z_{ij} \end{bmatrix}$$

For the quadratic surface the trend may be expressed as

$$\tau^{(2)} = \alpha_{oo} + \alpha_{1o}U + \alpha_{o1}V + \alpha_{2o}U^2 + \alpha_{11}UV + \alpha_{o2}V^2$$

The matrix and vectors concerned are

$$
\begin{bmatrix}
n & \sum U_i & \sum V_j & \sum U_i^2 & \sum U_i V_j & \sum V_j^2 \\
\sum U_i & \sum U_i^2 & \sum\sum U_i V_j & \sum U_i^3 & \sum U_i^2 V_j & \sum\sum U_i V_j^2 \\
\sum V_j & \sum\sum U_i V_j & \sum V_j^2 & \sum\sum U_i^2 V_j & \sum U_i V_j^2 & \sum V_j^3 \\
\sum U_i^2 & \sum U_i^3 & \sum\sum U_i^2 V_j & \sum U_i^4 & \sum U_i^3 V_j & \sum\sum U_i^2 V_j^2 \\
\sum\sum U_i V_j & \sum\sum U_i^2 V_j & \sum\sum U_i V_j^2 & \sum\sum U_i^3 V_j & \sum\sum U_i^2 V_j^2 & \sum\sum U_i V_j^3 \\
\sum V_j^2 & \sum\sum U_i V_j^2 & \sum V_j^3 & \sum\sum U_i^2 V_j^2 & \sum\sum U_i V_j^3 & \sum V_j^4
\end{bmatrix}
\begin{bmatrix}
\propto_{00} \\
\propto_{10} \\
\propto_{01} \\
\propto_{20} \\
\propto_{11} \\
\propto_{02}
\end{bmatrix}
=
\begin{bmatrix}
\sum Z_{ij} \\
\sum U_i Z_{ij} \\
\sum V_j Z_{ij} \\
\sum U_i^2 Z_{ij} \\
\sum\sum U_i V_j Z_{ij} \\
\sum V_j^2 Z_{ij}
\end{bmatrix}
$$

For the cubic surface the trend may be expressed as

$$
\hat{z}^{(3)} = \propto_{00} + \propto_{10} U + \propto_{01} V + \propto_{20} U^2 + \propto_{11} UV + \propto_{02} V^2 +
$$
$$
+ \propto_{30} U^3 + \propto_{12} U^2 V + \propto_{12} UV^2 + \propto_{03} V^3
$$

Matrix equation for this surface is derived by extension of the matrix for quadratic surface.

For any contour-type map a measure of the total variability is given by the sum of squares, designated as SS of the mapped variable computed as $SS = (X_o - \bar{X}_o)^2$ where X_o is the observed value of the mapped variable at a point of observation, $\bar{X}_o$ is the average of all observed values. When a surface is fitted to a map the total sum of squares

is divided into two parts, one (part A) associated with
the fitted surface and the other (part B) with the de-
viations from that surface. The percentage of the total
sum of squares is 100 x $(\frac{\text{part A}}{\text{part B}})$ called "the reduction in
the sum of squares attributable to the fitted surface".

Only third order (cubic) surfaces are considered
pertinent because:

1) trace elements have an erratic nature

2) planar surfaces do not seem adequate because curved or
   concentric patterns are common in many classical
   examples of the granite structure.

Cubic trends were determined for all minor elements in
both the red and white granite for rocks and their minerals.

7.1.2. Some problems and limitations of the method

As with other technique there are certain problems and li-
mitations to trend surface analysis.

Trend surface analysis of geological variables deals usual-
ly with ungridded sample points. From this point of view
according to Doveton and Parsley (1970) the modification
requires that the distribution of data points satisfies
three basic criteria: 1) a reasonable number of points;
2) an even distribution of points and 3) a map strip which
is not greatly longer than wide.

If these basic conditions for useful application of trend surface analysis are not observed a more or less progressive distortion of the computed surfaces from their theoretical ideal is obvious. Critical remarks on the method were published also by Chayes and Suzuki (1963). A criticism of the existence of the trend in geology was launched by Matheron (1965).

Perhaps one of the most serious difficulties is that of determining whether certain trends obtained are significant. If a low degree of polynomial surface is used the deviations contain some part of the trend which is not necessarily separate.

7.1.3. Regional trends of elements and their positive deviations in the rocks

The trend surface analysis demonstrates the existence of very strong and consistent gradients (trends) for each trace element examined within the Heemskirk massif. In this way the statistically significant variability has been proved within both the whole body and the particular rock types. These trends appear to have a geological significance for the following reasons:-

1) Major axes of the trend surfaces are parallel and superimposed,

2) virtually identical trends were found for a large

number of trace elements patterns,

3) total variance of trend surfaces indicates that all
   are non-random.

Only third order surfaces (linear + quadratic + cubic
trends) were considered for Rb, Sr, Na_2O, Zr, F, Nb, Pb,
Ba and Sn in both the red and white granites.
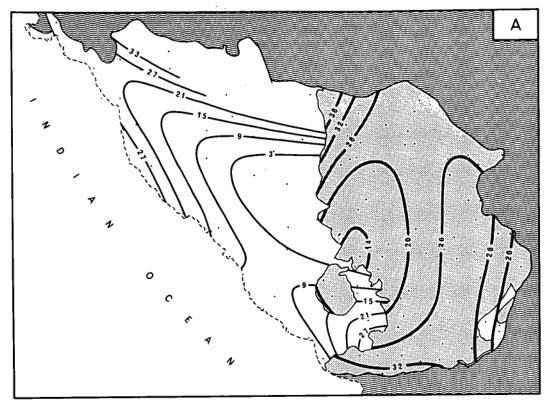
Strontium, zirconium and barium
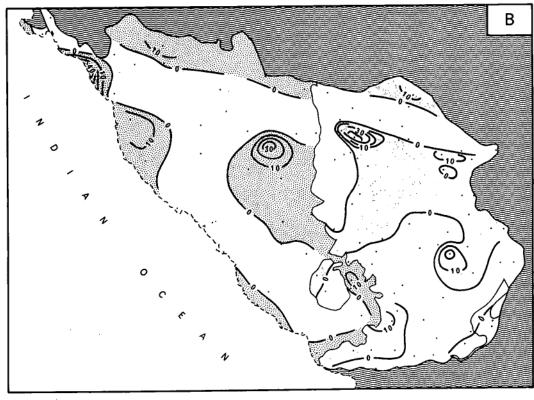
The trend surface analysis for Sr, Zr and Ba is shown
in figures 19, 20, 21. A distinctive feature is that the
linear plus quadratic plus cubic partial trend surfaces
for these elements are remarkably similar to one another.
The pattern of surfaces has the character of flat troughs
with low Sr, Zr and Ba content in the highest structural
and altitudinal level of the white granite (mainly fine
grained granite - type W2). Complementary ridges of high
Sr, Zr and Ba contents occur in the SE part of the white
granite - in the area rich in indications of tin minera-
lisation.
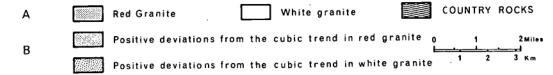
The surfaces for the red granite consist of ridges of
high Sr, Zr and Ba content in the highest structural le-
vels of the red granite and complementary troughs of low
Sr, Zr and Ba content on the bottom of the red granite
layer. The shapes of these trend surfaces show a general
N-S trend.

Figure 19

A – trend surface analysis (third degree) and
B – positive deviations for Sr in rocks of the
Heemskirk granite massif (values in ppm).
Per cent sum of squares accounted for by the
trend surfaces of the red granite 13.4 and the
white granite 53.1.

A   ▨ Red Granite   ☐ White granite   ▨ COUNTRY ROCKS

    ▨ Positive deviations from the cubic trend in red granite   0   1   2 Miles

B   ▨ Positive deviations from the cubic trend in white granite   1   2   3 Km

Figure 20

A - trend surface analysis (third degree) and
B - positive deviations for Zr in rocks of
the Heemskirk granite massif (values in ppm).
Per cent sum of squares accounted for by the
trend surfaces of the red granite 19.4 and
the white granite 45.2.

A

INDIAN

O C E A N

B

INDIAN

O C E A N

A   Red Granite   White granite   COUNTRY ROCKS

    Positive deviations from the cubic trend in red granite   0   1   2 Miles

B   Positive deviations from the cubic trend in white granite   1   2   3 Km

70/7/15-3

Figure 21

A - trend surface analysis (third degree) and
B - positive deviations for Ba in rocks of the
Heemskirk granite massif (values in ppm).
Per cent sum of squares accounted for by
the trend surfaces of the red granite 17.8 and
the white granite 37.0.

A

INDIAN

OCEAN

150
100
50
300
250
200
150
200
50
50
100
250

B

INDIAN

OCEAN

50
0
100
50
0
0
0
0
50
100
50
50
50
0
0
0
0
50
50
50
0
0
50

A   Red Granite   White granite   COUNTRY ROCKS

B   Positive deviations from the cubic trend in red granite

Positive deviations from the cubic trend in white granite

0   1   2 Miles

1   2   3 Km
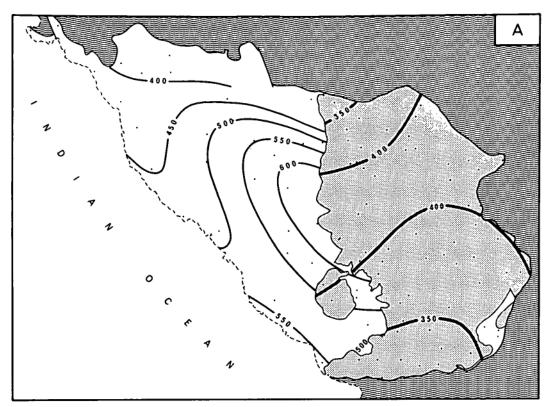
Positive deviations for Sr, Zr and Ba are located in the topmost part of the type R2 (including type R1). The maximum anomalies correspond with the occurrence of the contaminated porphyritic granite (type R1) with abundant magnetite, sphene and zircon. The correlation between the distribution of the deviations and internal structure of the topmost part of the red granite indicates the existence of an eastward plunging ghost syncline within the rocks of the Heemskirk granite massif. In the white granite the position of the positive deviations for Sr is in agreement with the location of the positive deviations for Ba.
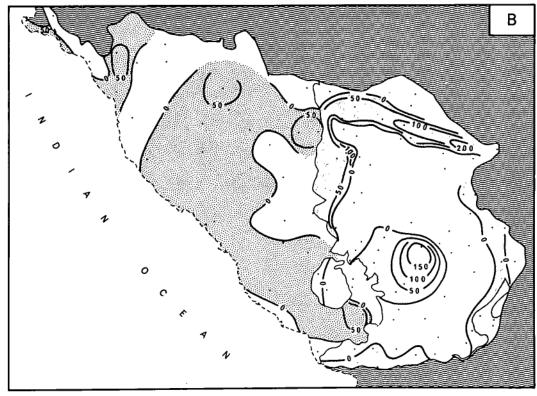
Rubidium, sodium and niobium
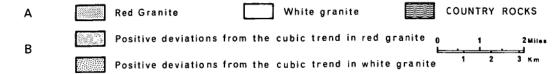
The trend surface analysis for Rb, Na_2O and Nb is shown in figures 22, 23, 24. General features of the trend surfaces for these elements are similar. In the cupola--like trend surfaces the maximum Rb, Na_2O and Nb contents roughly correspond with the highest structural parts of the white granite (the fine grained granite - type W2). Contours of the trend surface show a tendency to continue underneath the red granite layer. The area occupied by the type R3 coincides with an elevation in the trend surfaces, and the region with prevalence of the types R2 and R1 is indicated by the depression in the Na_2O and Nb trend surfaces. High Rb content corresponds with the lower part

Figure 22

A – trend surface analysis (third degree) and
B – positive deviations for Rb in rocks of the
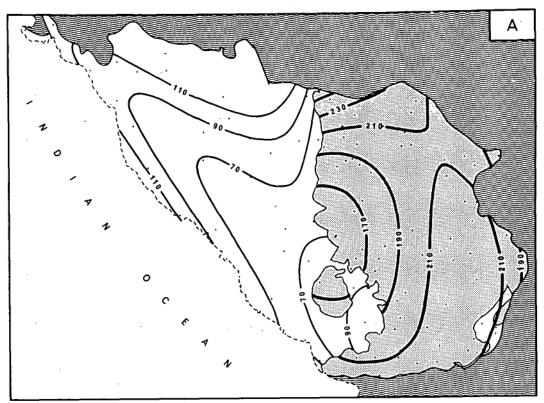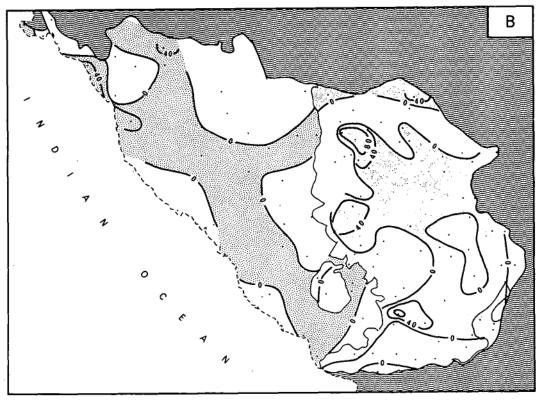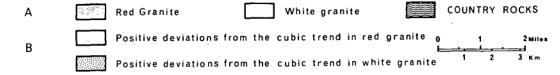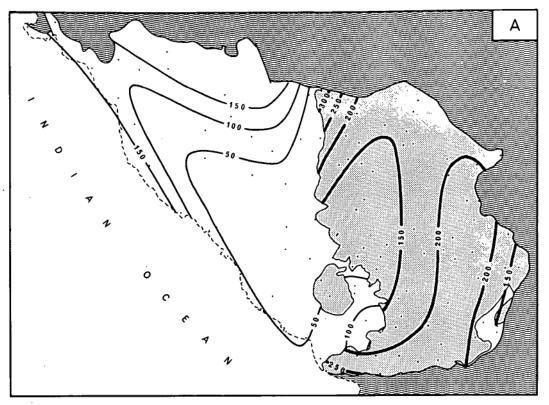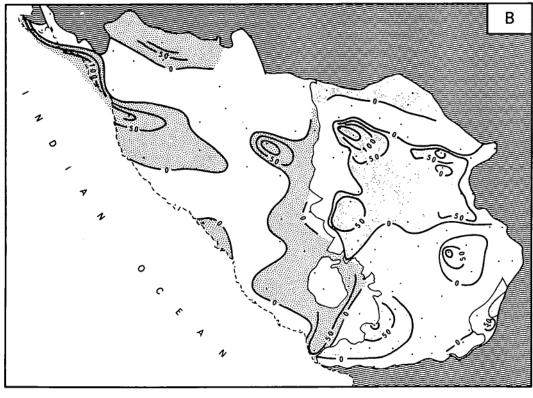Heemskirk granite massif (values in ppm).
Per cent sum of squares accounted for by
the trend surfaces of the red granite 18.4 and
the white granite 66.8.

A — Red Granite — White granite — COUNTRY ROCKS

B — Positive deviations from the cubic trend in red granite

Positive deviations from the cubic trend in white granite

0   1   2Miles

1   2   3 Km

Figure 23

A - trend surface analysis (third degree) and
B - positive deviations for Na_2O in rocks of
the Heemskirk granite massif (values in %).
Per cent sum of squares accounted for by
the trend surfaces of the red granite 47.4 and
the white granite 52.4.

A	Red Granite		White granite		COUNTRY ROCKS
B	Positive deviations from the cubic trend in red granite				
	Positive deviations from the cubic trend in white granite				

0   1   2 Miles

1   2   3 Km

Figure 24

A - trend surface analysis (third degree and
B - positive deviations for Nb in rocks of
the Heemskirk granite massif (values in ppm).
Per cent sum of squares accounted for by
the trend surfaces of the red granite 7.3 and
the white granite 55.0.

A

B

Red Granite   White granite   COUNTRY ROCKS

Positive deviations from the cubic trend in red granite

Positive deviations from the cubic trend in white granite

0   1   2 Miles

1   2   3 Km

of the red granite layer (type R3) while the upper part
of the red granite (type R2 and R1) shows a low Rb content.
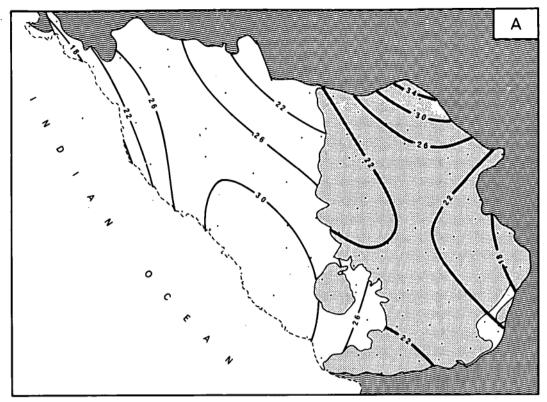
Distribution patterns of the Rb, Na_2O and Nb positive
deviations for the red granite mostly cover the outcrops
of the type R3 or indicate a thin layer of the type R2.
Rb deviations are remarkably high in comparison to the
white granite area. In the case of Na_2O in the southern
part of the red granite the positive deviations cover
a part of the type R2 - in which there is a high concen-
tration of tin mineralisation. These anomalies may repre-
sent the process of albitisation within the mineralized
area. In general the Rb, Na_2O and Nb positive deviations
lie in the areas which are occupied by the Sr, Zr and Ba
negative deviations and vice versa.

Tin
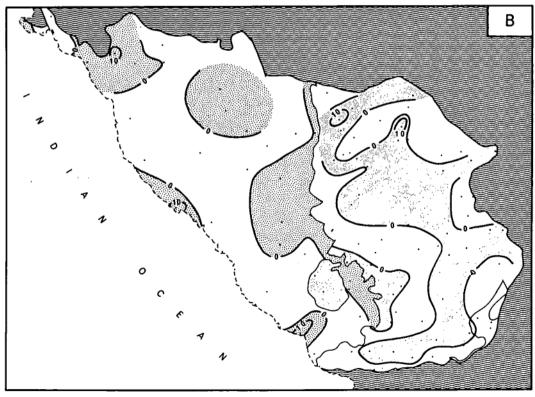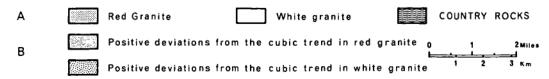
The trend surface analysis for Sn is shown in figure
25. Clearly, the main variations in the Sn content occur
in the white granite only. The Sn surface for the red
granite is very flat without distinct variation except for
the northern part of the area.

Positive deviations for Sn in the white granite oc-
cur mainly over the outcrops of the type W3. Positive de-
viations in the red granite are more complex, partly si-
tuated within the type R3 and partly within the type R2
and R1 respectively. The major part of the anomaly is si-
tuated in the mountainous part of the Heemskirk massif.

Figure 25

A - trend surface analysis (third degree) and
B - positive deviations for Sn in rocks of
the Heemskirk granite massif (values in ppm).
Per cent sum of squares accounted for by
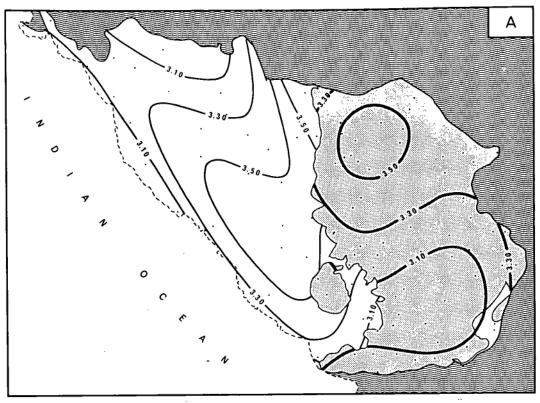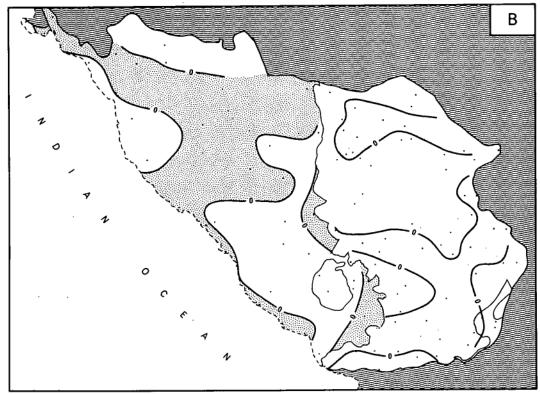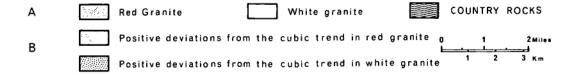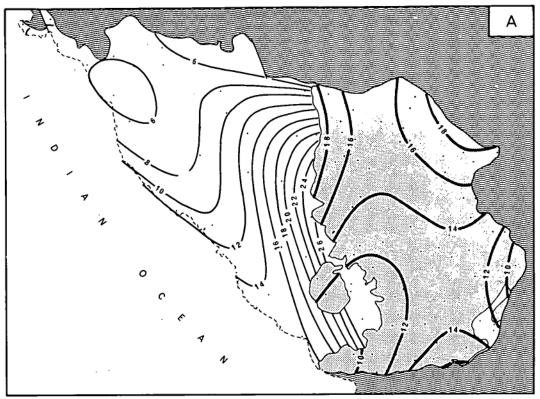the trend surfaces of the red granite 23.4 and
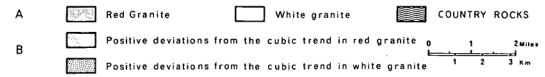the white granite 50.5.

| A | Red Granite | White granite | COUNTRY ROCKS |

Positive deviations from the cubic trend in red granite

Positive deviations from the cubic trend in white granite

B

0   1   2 Miles

1   2   3 Km

70/7/059

The higher Sn content in the red granite (type R2 and R1) could be related to the accessory sphene and magnetite, which is abundant mainly in the type R1 and in the upper part of the type R2.

Fluorine

The trend surface analysis for F is shown in figure 26. The general shape of the surface for the red granite is quite similar to that of Sr and Ba. The surface consists of a flat ridge trending north - south and a parallel complementary trough of low F content on the bottom of the red granite layer. The surface for the white granite is more complex.
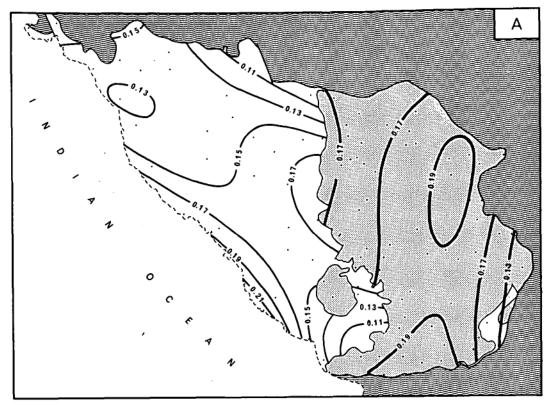
Positive deviations of fluorine for the white granite consist of two parallel belts trending E - W which correspond to the elevations of the white granite underneath the red granite (Mt. Heemskirk and Mt. Agnew antiforms in figure 4).

Lead
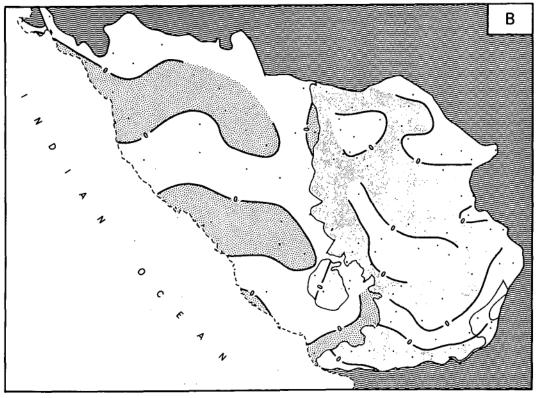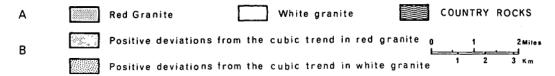
The trend surface analysis for Pb is shown in figure 27. The surface for the white granite is remarkably similar to that of Rb showing the ridge-like shape with NW-SE trend. Low Pb content mostly coincides with the distribution of types R2 and R1 respectively.

Figure 26

A - trend surface analysis (third degree) and
B - positive deviations for F in rocks of
the Heemskirk granite massif (values in %).
Per cent of squares accounted for by the trend
surfaces of the red granite 16.1 and the white
granite 38.5.

A   Red Granite   White granite   COUNTRY ROCKS

B   Positive deviations from the cubic trend in red granite

Positive deviations from the cubic trend in white granite

0   1   2 Miles

0   1   2   3 Km

Figure 27

A - trend surface analysis (third degree) and
B - positive deviations for Pb in rocks of
the Heemskirk granite massif (values in ppm).
Per cent of squares accounted for by the trend
surfaces of the red granite 6.2 and the white
granite 41.0.

A

B

Red Granite   White granite   COUNTRY ROCKS

Positive deviations from the cubic trend in red granite

Positive deviations from the cubic trend in white granite

0   1   2 Miles

1   2   3 Km

The positive deviations for the red granite are mostly concentrated in the type R3 and in the lower parts of the type R2. The positive deviations for the white granite cover most of the type W2 area. The greatest anomaly coincides with the topmost part of the white granite.

7.1.4. Regional trends of elements and their positive deviations in biotites
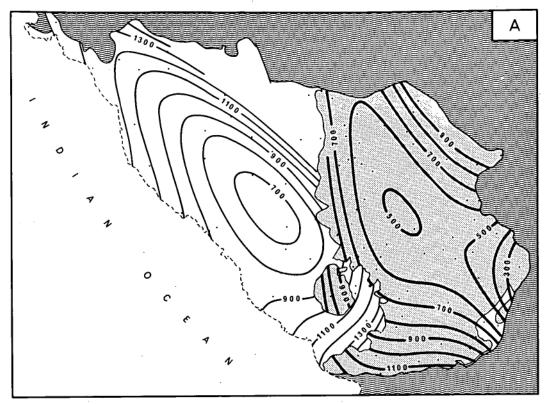
The third order surfaces (linear + quadratic + cubic trends) were considered for Rb, Sc, Ni, Cr, F, Cl, Zn, Nb and Sn in biotites of the red white granite (biotite R and biotite W).
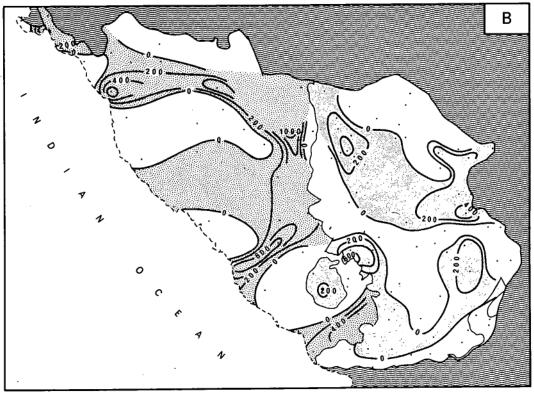
Rubidium, chlorine and fluorine
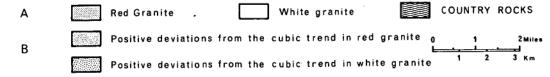
The trend surface analysis for Rb, Cl and F is shown in figures 28, 29, 30. General features of the trend surfaces for these elements are quite similar (except the surface of F for the biotite R). The Rb, Cl and F contents in all cases decreases towards the highest parts of the white granite structure. The high F content in the coincides with the type R3 and the low F content with the type R2.

The Rb anomalies partly correspond to the spread of the tin deposits. The greatest deviations of Cl coincide with the position of the Rb deviations. In general the ma-

Figure 28
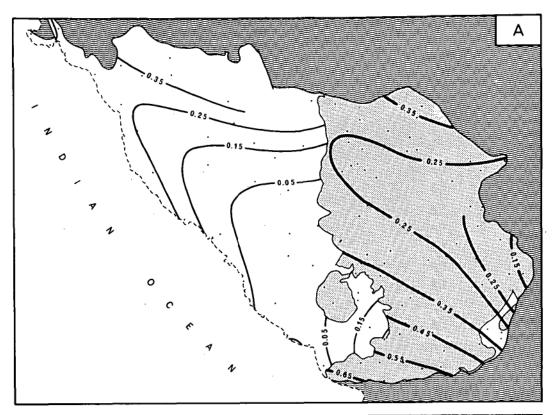
A - trend surface analysis (third degree) and
B - positive deviations for Rb in biotites of
the Heemskirk granite massif (values in ppm).
Per cent of squares accounted for by the trend,
surfaces of the biotites - R 42.2 and biotites
- W 25.0.

A

B

Red Granite

White granite

COUNTRY ROCKS

Positive deviations from the cubic trend in red granite

Positive deviations from the cubic trend in white granite

0   1   2 Miles

1   2   3 Km

Figure 29

A - trend surface analysis (third degree) and
B - positive deviations for Cl in biotites of
the Heemskirk granite massif (values in ppm).
Per cent sum of squares accounted for by the
trend surfaces of the biotites - R 54.4 and
biotites - W 57.9.

A   ▨ Red Granite   □ White granite   ▩ COUNTRY ROCKS

     ▨ Positive deviations from the cubic trend in red granite

B   ▨ Positive deviations from the cubic trend in white granite

0   1   2 Miles

1   2   3 Km

70/7/157

Figure 30

A - trend surface analysis (third degree) and
B - positive deviations for F in biotites of
the Heemskirk granite massif (values in %).
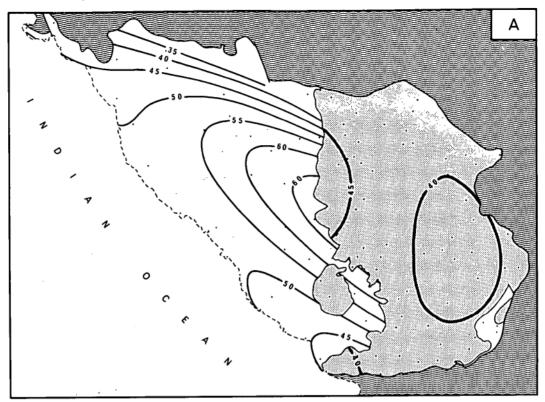Per cent sum of squares accounted for by
the trend surfaces of the biotites - R 19.2
and biotites - W 38.5.

A   ▒▒▒ Red Granite   ☐ White granite   ▓▓▓ COUNTRY ROCKS

B   ░░░ Positive deviations from the cubic trend in red granite

     ▓▓▓ Positive deviations from the cubic trend in white granite

0   1   2 Miles
1   2   3 Km

ximum deviations for the biotite W correspond to the upper part of the intrusion. An important feature is the absence of positive deviations around the red granite plate (xenolith?) in the SE and of the white granite area.
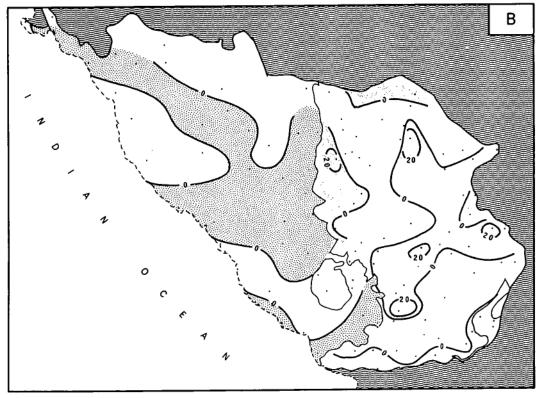
Scandium
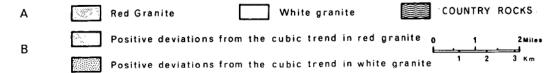
The trend surface analysis of Sc is shown in figure 31. The Sc surface for the biotite R shows a very smooth shape with Sc content increasing toward the west from about 70 ppm to 100 ppm. The high Sc content corresponds mainly with the distribution of the type R3. The trend surface isolines are semi-parallel to the contact in the southern and eastern part of the red granite. The surface for the biotite W shows a cupola-like shape trending east-west. The high Sc content corresponds to the distribution of the type W2.

The distinctive feature of the patterns for Sc in both biotites is the coherence of the trend surface isolines. It indicates the close similarity in the distribution of Sc in both biotites. The Sc contents in the types R3 and W2 are nearly identical and also the Sc contents in the type R2 (R1) and W3 (W1) are very similar. It could be interpreted as a result of the parallel layering within the Heemskirk massif. Literature data (Oftedal,
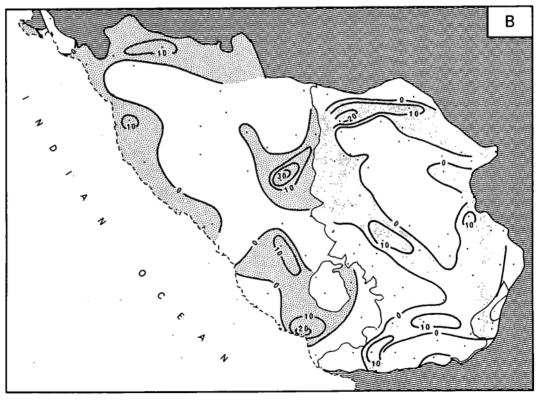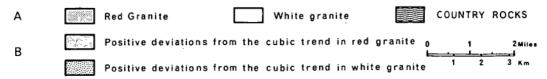
Figure 31

Â - trend surface analysis (third degree) and
B - positive deviations for Sc in biotites of
the Heemskirk granite massif (values in ppm).
Per cent sum of squares accounted for by
the trend surfaces of the biotites - R 40.2
and biotites - W 71.9.

A   ░ Red Granite   ☐ White granite   ▨ COUNTRY ROCKS

    ░ Positive deviations from the cubic trend in red granite

B   ▒ Positive deviations from the cubic trend in white granite

70/7/143

1943; Ingerson, 1955) indicate that the Sc content in bio-
tites increase[s] with decreasing temperature of crystalli-
zation. The more general use of the Sc geothermometer is
limited by the lack of experimental data. Nevertheless
the application of the Sc data for petrological purposes
a semi-quantitative basis is possible. From this point of
view biotite from granite types R3 and W2 crystallized
at relatively lower temperatures than biotite from types
R2 and W3.
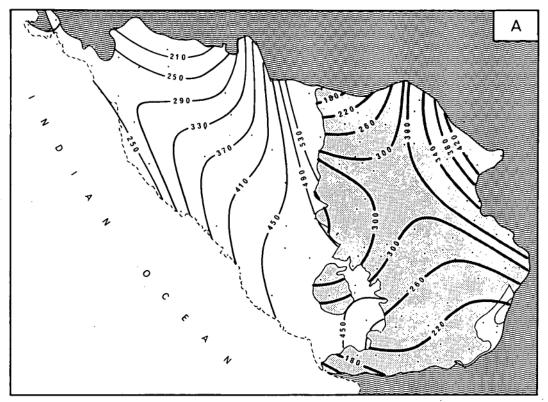
The distribution of the positive deviations for the
biotite R and W corresponds predominantly to the type R3
and W2 with some exception on the southern contact of
the red granite and eastern part of the white granite.
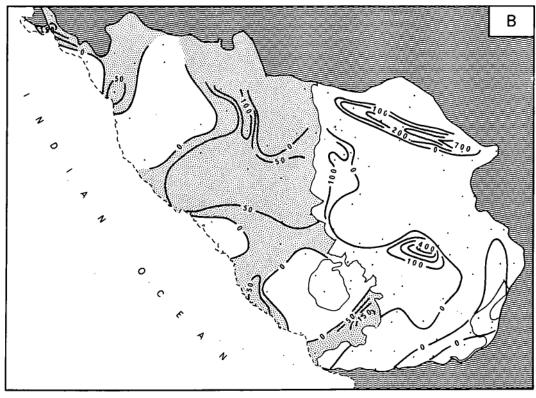
Niobium and nickel
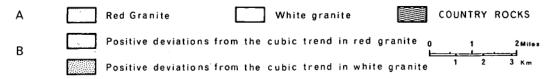
The trend surface analyses of Nb and Ni are shown in
figures 32,33. The content of both elements rises westerly
as well as easterly, with low Nb, Ni concentrations in
the type R1, R2 and high Nb, Ni content in the R3 type.
The surfaces for the biotite W are only slightly similar.
There is a general rise in the Nb, Ni content from the
west to the east.

The distribution of the positive deviations for both
elements in the white granite are very similar. There is
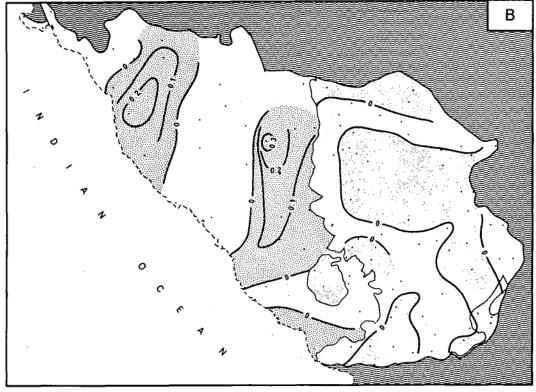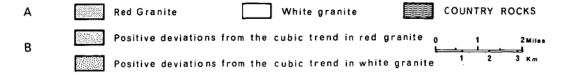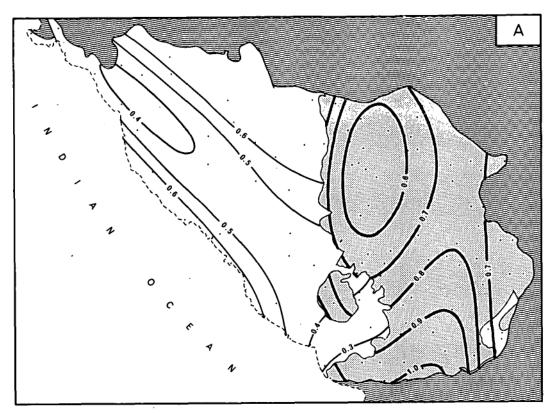a remarkable lack of positive anomalies around the red

Figure 32
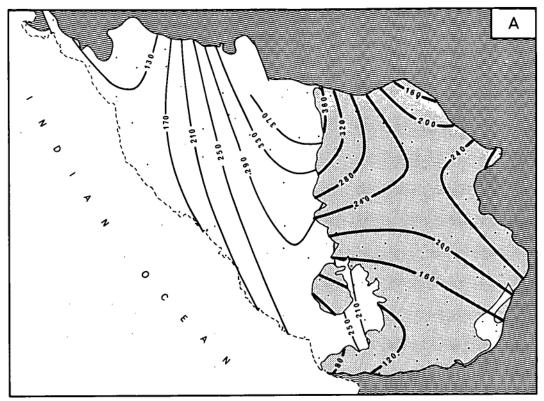
A - trend surface analysis (third degree) and
B - positive deviations for Nb in biotites of
the Heemskirk granite massif (values in ppm).
Per cent sum of squares accounted for by
the trend surfaces of the biotites - R 16.7
and biotites - W 54.4.

A ☐ Red Granite ☐ White granite ▦ COUNTRY ROCKS

☐ Positive deviations from the cubic trend in red granite

B

▨ Positive deviations from the cubic trend in white granite
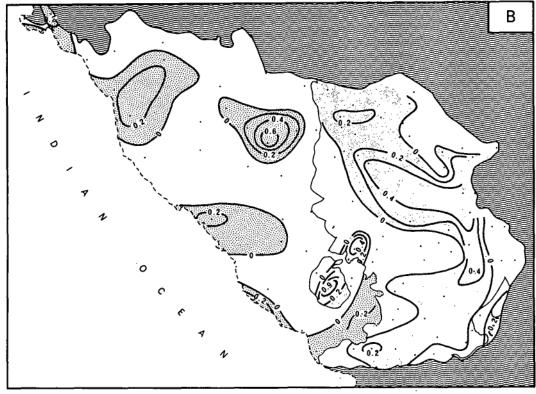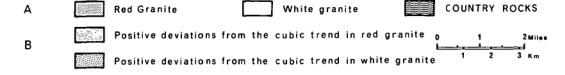
Figure 33

A - trend surface analysis (third degree) and
B - positive deviations for Ni in biotites of
the Heemskirk granite massif (values in ppm).
Per cent sum of squares accounted for by
the trend surfaces of the biotites - R 31.2
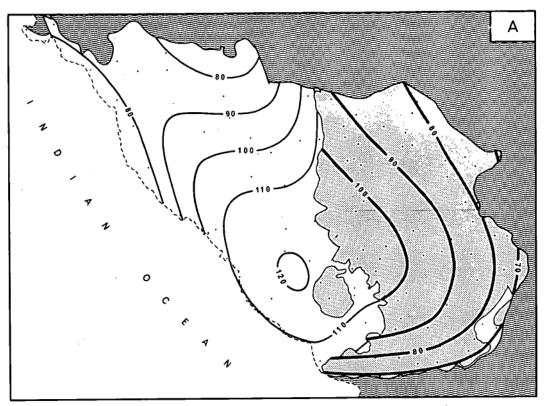and the biotites - W 69.5.

A Red Granite White granite COUNTRY ROCKS

B Positive deviations from the cubic trend in red granite

  Positive deviations from the cubic trend in white granite

0 1 2Miles

1 2 3 Km

70/7/149

granite xenolith in the SE part of the white granite area (similar to Rb).

Chromium
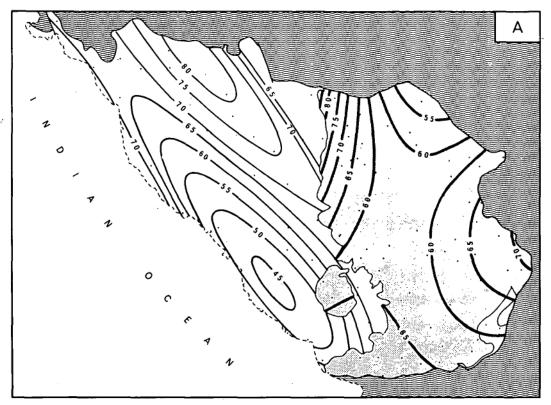
The trend surface analysis of Cr is shown in figure 34. The surface for the biotite W consists of a ridge of high Cr contents trending NW - SE and a complementary trough parallel to the coast line.
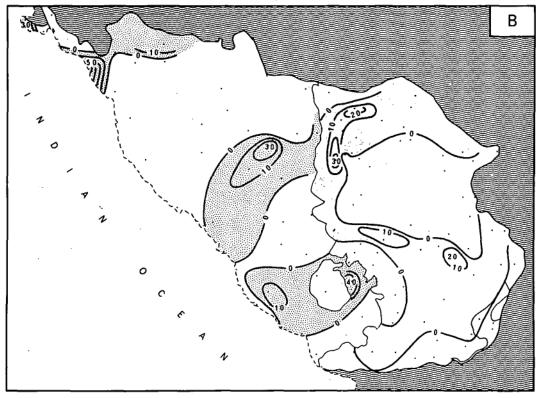
The positive deviations for the biotite W consists of three separate anomalies which partly correspond to the distribution of the W2 type. The positive deviations for the red granite coincides with the outcrops of the type R3. Anomalies within the R2 type indicate the thiner parts of the layer of that type. A significant feature of the deviation pattern within the red granite is the absence of positive anomalies in the central areal between Mt. Heemskirk and Mt. Agnew.
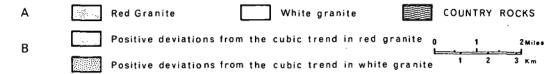
Zinc

The trend surface analysis of Zn is shown in figure 35. The surface for the biotite R shows an identical shape to that of Na_2O in the rocks with low Zn content in the Mt. Agnew antiform area (dominantly the type R2) and high Zn content in the Mt. Heemskirk antiform area (predominantly the type R3). The surface for the biotite W

Figure 34
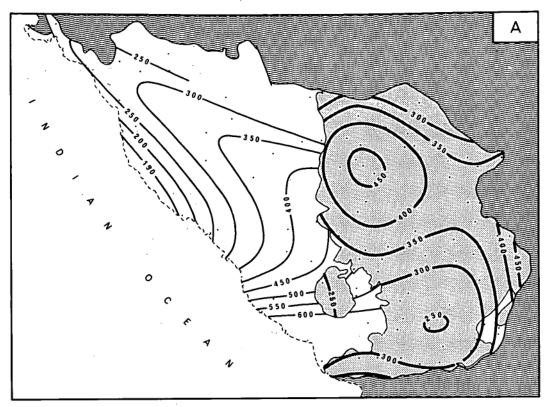
A - trend surface analysis (third degree) and
B - positive deviations for Cr in biotites of
the Heemskirk granite massif (values in ppm).
Per cent sum of squares accounted for by
the trend surfaces of the biotites - R 24.7 and
the biotites - W 25.2.

A — Red Granite — White granite — COUNTRY ROCKS

B — Positive deviations from the cubic trend in red granite

Positive deviations from the cubic trend in white granite

0   1   2 Miles

1   2   3 Km

Figure 35

A - trend surface analysis (third degree) and
B - positive deviations for Zn in biotites of
the Heemskirk granite massif (values in ppm).
Per cent sum of squares accounted for by
the trend surfaces of the biotites - R 17.4 and
the biotites - W 76.5.

A	Red Granite		White granite		COUNTRY ROCKS
B	Positive deviations from the cubic trend in red granite
	Positive deviations from the cubic trend in white granite

0   1   2 Miles
1   2   3 Km

shows a ridge of high Zn content increasing toward the east.
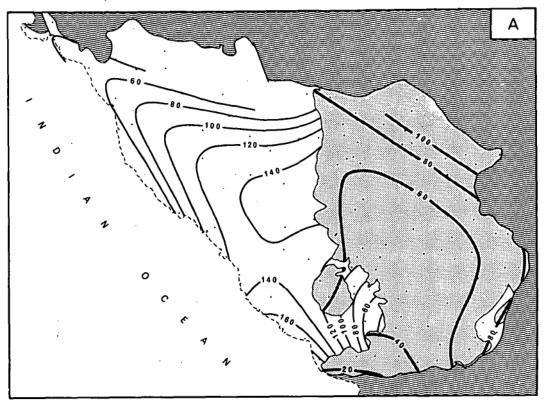
The high positive deviations for the biotite W predominantly cover the type W2 area. The highest Zn anomalies for the biotite R lie in the type R3 area. The general shape of the positive deviations corresponds to the morphology of the white granite contact underneath the red granite. The high Zn content coincides with the Mt. Heemskirk and Mt. Agnew antiforms.

Tin
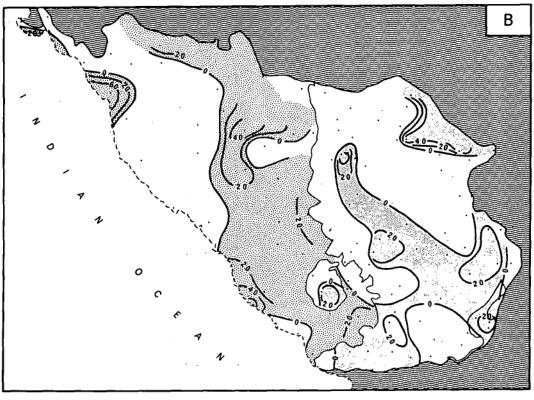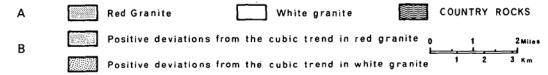
The trend surface analysis of Sn is shown in figure 36. High Sn content corresponds with the type R3 and low Sn content is related to the type R2. In the biotite W the high Sn content coincides with the outcrops of the upper layer of the white granite.

The distribution of the positive deviations for the biotite W completely covers the type W2 and the upper part of type W3. In the red granite the position of the Sn anomalies partially corresponds with the sub-surface elevations of the white granite.

Figure 36

A.- trend surface analysis (third degree) and
B - positive deviations for Sn in biotitites
of the Heemskirk granite massif (values in ppm).
Per cent sum of squares accounted for by
the trend surfaces of the biotites - R 38.6
and biotites - W 47. 5.

A   ▨ Red Granite   □ White granite   ▨ COUNTRY ROCKS

B

▨ Positive deviations from the cubic trend in red granite

▨ Positive deviations from the cubic trend in white granite

0   1   2 Miles

1   2   3 Km

7.1.5. Regional trends of elements and their positive deviations in the potassium feldspars of the red granite

Strontium and barium

The trend surface analysis for Sr and Ba is shown in figures 37, 38. The general shapes of the surfaces are quite similar and suggest a bilateral symmetry with the maximum Sr and Ba lying in the upper part of the red granite layer. A well defined belt of high Sr and Ba contents runs from the southern margin of the granite to its northern contact. The low Sr, Ba content corresponds to the lower part of the red granite (type R3).

Rubidium

The trend surface analysis for Rb is shown in figure 39. The general shape of the surface is quite similar to those of Sr and Ba, but with areas of low Rb corresponding to areas of high Ba and Sr. A well-defined belt of low Rb content runs from the southern margin to the northern contact of the red granite.
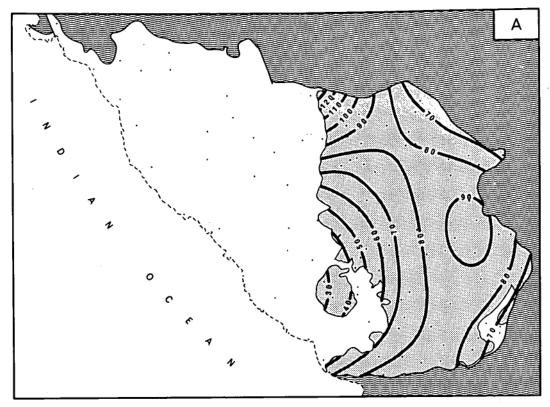
The positive deviations cover quite a large area trending N-S.

Na_2O
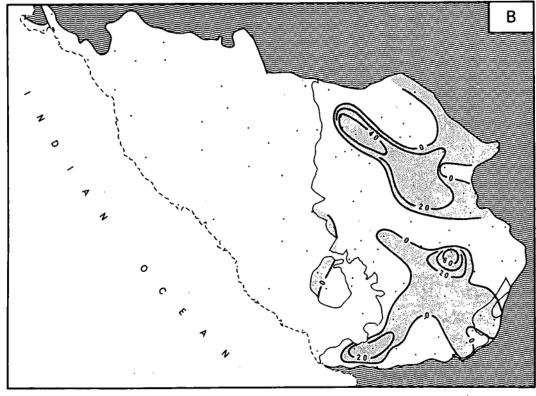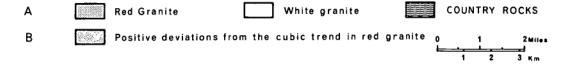
Trend surface analysis of Na_2O is shown in figure 40. The surface of Na_2O for potassium feldspar is very similar to that of Na_2O for the rocks and Zn for the biotites.
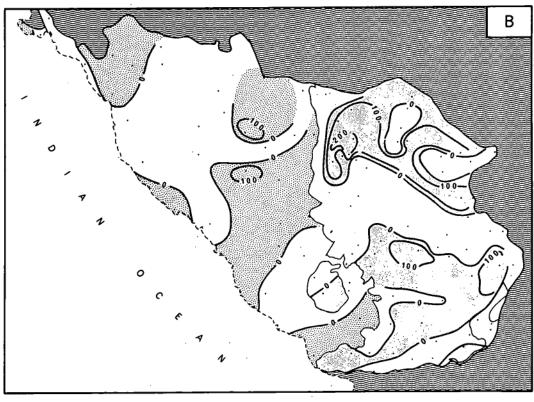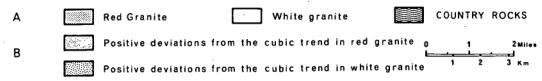
Figure 37

A - trend surface analysis (third degree) and

B - positive deviations for Sr in K-feldspars

of the Heemskirk granite massif (values in ppm).
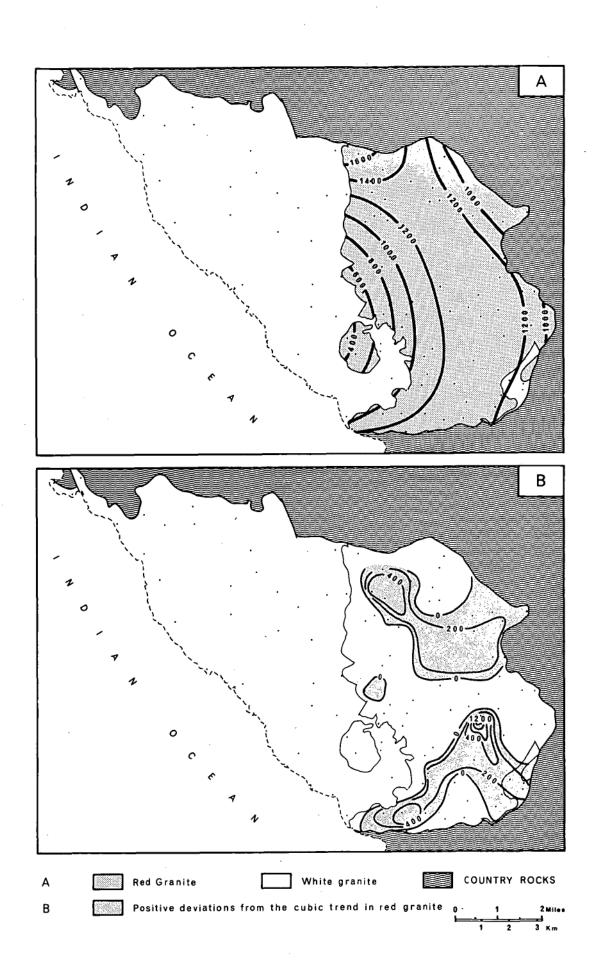
Per cent sum of squares accounted for by

the trend surface of K-feldspars 32.2.

A   ▨ Red Granite   ☐ White granite   ▩ COUNTRY ROCKS

B   ▨ Positive deviations from the cubic trend in red granite

Figure 38

A - trend surface analysis (third degree) and
B - positive deviations for Ba in K-feldspars
of the Heemskirk granite massif (values in ppm).
Per cent sum of squares accounted for by
the trend surface of K - feldspars 35.3.

A	▨ Red Granite	☐ White granite	▩ COUNTRY ROCKS
B	▨ Positive deviations from the cubic trend in red granite		

76/7/162
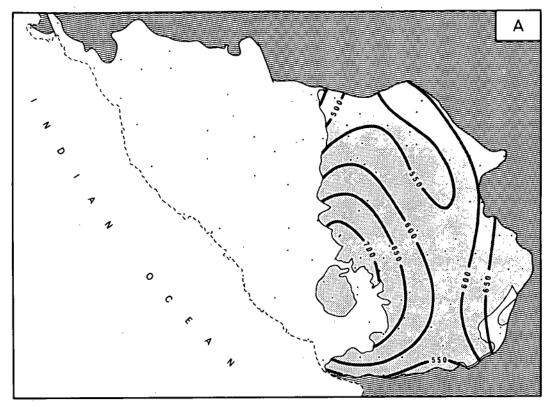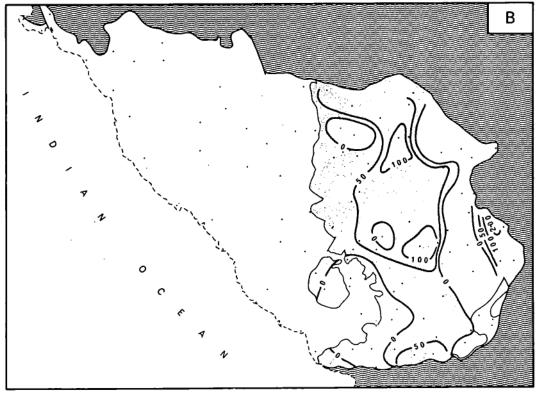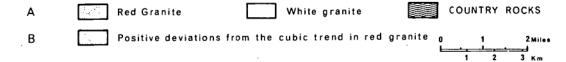
Figure 39

A - trend surface analysis (third degree) and

B - positive deviations for Rb in K-feldspars

of the Heemskirk granite massif (values in ppm).

Per cent sum of squares accounted for by

the trend surface of K-feldspars 35.3.

INDIAN OCEAN

A

INDIAN OCEAN

B

A   Red Granite   White granite   COUNTRY ROCKS

B   Positive deviations from the cubic trend in red granite

0   1   2Miles

1   2   3 Km

Figure 40
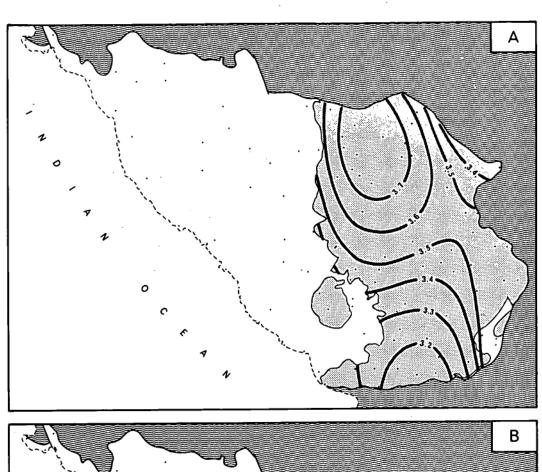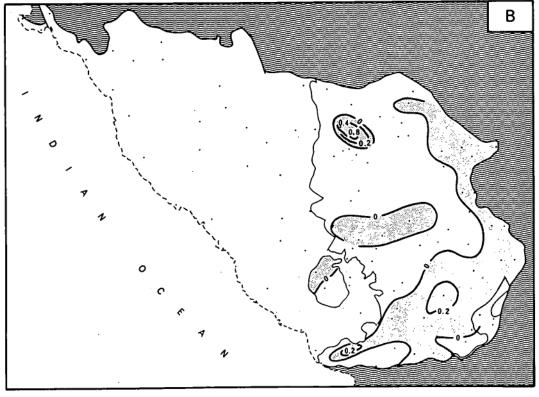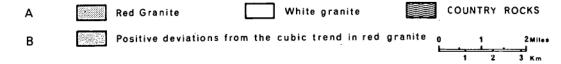
A - trend surface analysis (third degree) and
B - positive deviations for Na_2O in K-feldspars
of the Heemskirk granite massif (values in ppm).
Per cent sum of squares accounted for by the
trend surface of K-feldspars 39.8.

A
:::::: Red Granite □ White granite ▓▓▓ COUNTRY ROCKS

B
▒▒▒ Positive deviations from the cubic trend in red granite

0   1   2 Miles

1   2   3 Km

The positive deviations are mostly concentrated along the eastern contact, predominantly within the types R2 and R1.

Lead

The trend surface analysis of Pb is shown in figure 41. The surface is quite similar to that of Pb for the rocks, with low Pb content on the eastern part and high Pb content in the western area of the red granite.
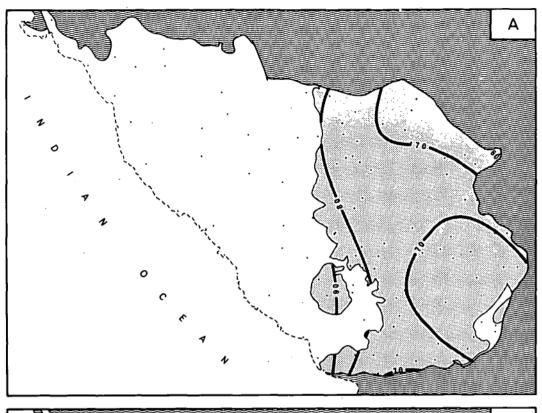
The positive deviations consist of two major anomalies. The larger one occupies the central and northern area and the smaller one lies in the SE marginal zone of the red granite. Both anomalies partly correspond to some parts of the Mt. Heemskirk and Mt. Agnew elevations.
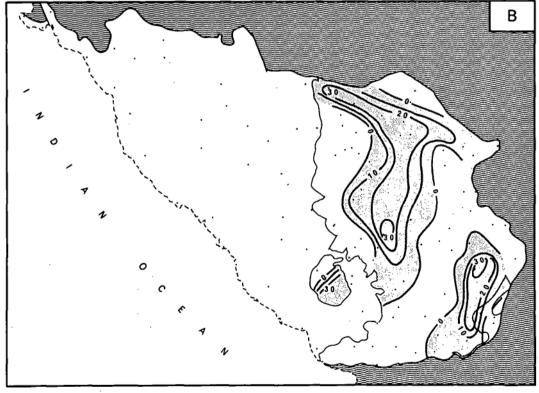
Tin

Trend surface analysis of Sn is shown in figure 42. High Sn content is on the eastern margin and the low Sn content is on the western margin of the red granite.

The highest anomalies are related to the type R2. In the area of the Mt. Agnew elevation the anomalies correspond with the topmost part of that structure, which partly corresponds to the distribution of the tin mineralisation.
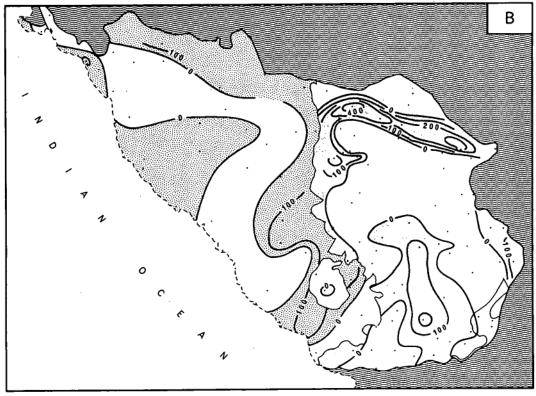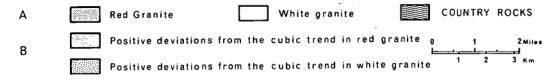
Figure 41

A - trend surface analysis (third degree) and
B - positive deviations for Sn in K-feldspars
of the Heemskirk granite massif (values in ppm).
Per cent sum of squares accounted for by the
trend surface of K - feldspars 33.5.
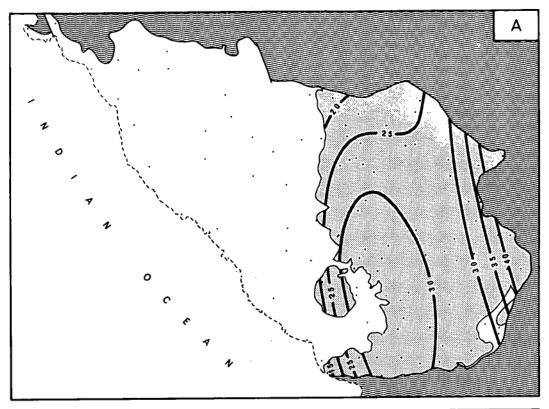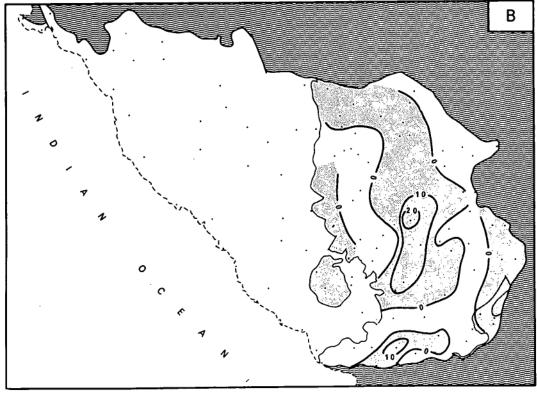
A   Red Granite   White granite   COUNTRY ROCKS

B   Positive deviations from the cubic trend in red granite

0   1   2 Miles
1   2   3 Km

Figure 42
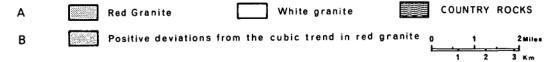
A – trend surface analysis (third degree) and
B – positive deviations for Pb in K-feldspars
of the Heemskirk granite massif (values in ppm).
Per cent sum of squares accounted for by
the trend surface of K-feldspars 11.8.

| A | ▦ Red Granite | ☐ White granite | ▨ COUNTRY ROCKS |
| B | | Positive deviations from the cubic trend in red granite | |
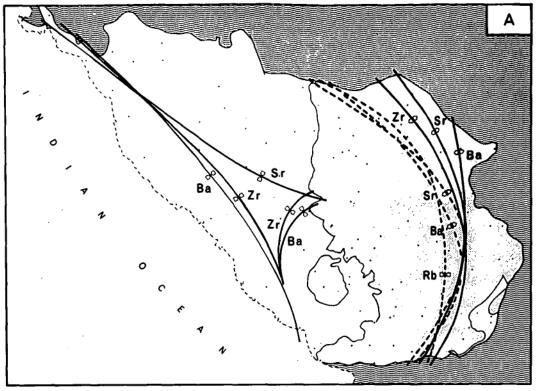
7.1.6. Summary of the trend surface analysis for investigation of the internal structure of the Heemskirk granite massif.

Despite some disadvantages of the trend surface analysis both in the theory and practice, the method was found to be very useful for testing the geological and structural models of the Heemskirk granite. The trends confirm the relationship between the trace elements distribution in the rocks and their minerals and the general structure of the granite body. Due to the marked topography of the Heemskirk massif the distribution patterns of most elements largely emphasize the vertical direction of the regional trend. In this sense we are able to study the granite layer for a thickness of up to 900 m.
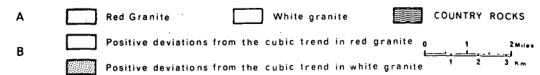
Two-dimensional patterns of trace elements in the red and white granite are characterized by a well marked discontinuity, mainly in absolute values (except Sc). The bilateral symmetry of the cupola-like trend surfaces (mainly in the white granite) indicates the presence of a very flat dome structure, elongated in a WNW - ESE direction. The general higher density of isopleths near the southern and northern margins of the body probably reflects the steeper flanks of the cupola. The trend surfaces are deformed due to the mountainous relief of the Mt.Heemskirk

Figure 43

A - The major ridges and troughs of the trend
surfaces (third degree) for Ba, Sr and Zr of
the rocks (full lines) and Rb, Sr and Ba of
K-feldspars (dashed lines)
B - Complex positive anomalies for Sr, Ba and
Zr of the rocks.

A

B

| A | Red Granite | White granite | COUNTRY ROCKS |

Positive deviations from the cubic trend in red granite

B

Positive deviations from the cubic trend in white granite

0   1   2 Miles
1   2   3 Km

and Mt. Agnew area. The shapes of the Sr, Zr and Ba surfaces for the red granite are very similar to those of Sr and Ba in the feldspars from the same rocks. The axes of the ridges are concentrated in the narrow belt running from the southern to the northern contact of the granite body and curving (probably due to morphology) to the west (Fig. 43). This zone with maximum Zr, Sr and Ba content both in the rocks and their feldspars roughly corresponds to the distribution of the topmost part of the red granite in which there are many areas of contaminated porphyritic granite (Rl type). On the other hand the surfaces of Ba, Sr and Zr for the white granite show depressions very similar in shape and orientation of their axes of symmetry. As is shown in figure 43-A the axes are concentrated in a belt running NW-SE which divides in the southeast part of the white granite area towards the south. The marked region in figure 43-A represents the minimum Zr, Sr and Ba content in the white granite and is mainly occupied by the type W2, i.e. the granite layer underlaing the bottom of the red granite. The zone of the minimum Ba, Sr and Zr content traces the major axis of symmetry of the Heemskirk intrusion in the western part of the granite outcrop, dipping towards the NW.

In general the major axes of the surfaces of the studied elements are oriented in the red granite predominantly in

the N-S direction while those in the white granite are
oriented mainly in the NW-SE direction (Fig. 43-A).

Brooks and Compston (1965) have interpreted very
high values for initial Sr^{87} / Sr^{86} in the Heemskirk gra-
nite massif as due to contamination by radiogenic Sr
from the crustal material during emplacement. The possi-
tion of the granite in dominantly Precambrian rocks rich
in radiogenic Sr favours this hypothesis. Marks of conta-
mination have been found both in upper parts of the white
and red granite which were situated close to the contact
of the granite body and the country rocks. These areas
mostly coincide with the positive anomalies of Sr, Ba
and Zr in both rock types on the present surface of the
intrusion. Figure 43-B illustrates the areas in which the
positive anomalies of Sr, Ba and Zr are overlapping. In
the red granite these multiple positive anomalies correspond
to the spreading of the scattered bodies of porphyritic
granite with abundant hornblende, sphene and zircon. Small
bodies of this granite type have the character of xenoliths-
- relicts of the intensively assimilated sedimentary rocks
with horizons of ultramafic and mafic rocks. Martite -
- hematite patches which occur in the northern part of
the body may also be regarded as relicts of country rocks.
The positive anomalies of Sr, Zr and Ba could be interpret-
ed as ghost structure (Whitten 1959), although a few xeno-

lithic relicts of the country rocks are known from most
of the area involved. The ghost structure of the country
rocks within the Heemskirk granite massif is in good ag-
reement with the fold structure of the country rocks around
the intrusion (see Fig. 8) and explains for example, the
presence of the largest multiple positive geochemical
anomaly as the continuation of the brachysyncline of
the country rocks dipping toward the East (Fig.43-B).
In general the Rb, Na_2O and Nb positive deviations in the
red granite represent a local variability of the lower red
granite layer, in contrast to the Sr, Zr and Ba positive
deviations which reflect the local variability of the up-
per layer of the red granite.

7.2. Multivariate discriminant analysis[1]

Discriminant analysis is a statistical method which
allows one to classify samples into predetermined groups
on the basis of a large number of variables. It is used
to test the significance of the difference in already
established groups of the white and red granite, and also
to assign unknown samples to appropriate groups. An unknown
sample is classified as a red or white granite by substi-

----

[1] The programme of discriminant analysis was prepared
after Davis and Sampson (1966).

tuting the values of K variables for that sample into
the discriminant function. Samples are distinguished ac-
cording to their position relative to the index R_o. It is
apparent that discriminant analysis cannot be used when
the differences between two groups are not statistically
significant or when all the samples belong to one group.
These assumptions of differences between the two groups
must be tested.

Test of statistical significance is derived from Mahala-
nobis' generalised distance function D^2 which is a measure,
of the distance between the multivariate means of the two
clusters of the a priori selected groups of samples. It
is derived by substituting the difference between the va-
riable means $\bar{A}$, $\bar{B}$ .... $\bar{K}$ into the discriminant
function:

$$D = \lambda_a \, \Delta \bar{A} + \lambda_b \, \Delta \bar{B} + \lambda_c \, \Delta \bar{C} + \ldots \ldots \lambda_k \Delta \bar{K}$$

To test the significance of differences between the multi-
variate means the value F can be used.

$$F_{k_1 n_1 + n_2 - K - 1} = \left[\frac{n_1 \, n_2}{(n_1 + n_2) \, (n_1 + n_2 - 2)} \right] \left[\frac{n_1 + n_2 - K - 1}{k} \right] \cdot D^2$$

How each variable contributes to the total distance between
the multivariate means can be expressed as a percentage:

$$\frac{\lambda a \; \Delta \bar{A}}{D^2} = \% \text{ which A contributes to the total distance}$$

$$\frac{\lambda k \; \Delta \bar{K}}{D^2} = \% \text{ which K contributes to the total distance.}$$

The values of the constants (λ) are obtained by solving a series of K simultaneous equations:

$$SS_A \lambda_a + SS_{AB} \lambda_b + SS_{AC} \lambda_c + \ldots \ldots SS_{AK} \lambda_k = \Delta \bar{A}(n_1 + n_2) - 2$$

$$SS_{AK} \lambda_a + SS_{AK} \lambda_b + SS_{BC} \lambda_c + \ldots \ldots SS_K \lambda_k = \Delta \bar{K}(n_1 + n_2) - 2$$

This information makes it possible to determine which of the variables contributes significantly to D^2 and those which contribute only a little. Some authors use this method to eliminate unimportant variables from the set of criteria used for classification. The selection of significant variables is very often complicated due to the fact that the degree of independence of variables amongst themselves is not always known.

Discriminant analysis in the Heemskirk massif was carried out on both bulk rock samples and on the biotites of the red and white granites. The results are tabulated in Tables 16, 17, 18 and graphically represented in figure 44. The F-test proves that there is a significant difference between the red and white granites.

Table 16

Discriminant analysis of the rocks and their biotites from the Heemskirk granite massif

Rocks:

F = 49.2038 with 9 and 86 degrees of freedom
D^2 = (Mahalanobis' generalized distance function) = 21.29
R = (Multivariate mean of the red granite) = 20.91
DI (Discriminant Index) = 12.71
W (Multivariate mean of the white granite) = -0.37

Contribution of each variable to the total distance between the multivariate means:

Variable	Constants	Per cent contribution
Rb	-0.0653	36.76
Sr	-0.3568	-14.58
Na	-7.2569	-1.28
Zr	0.1480	77.08
F	16.6378	1.40
Nb	0.1850	0.68
Pb	-0.0179	0.75
Ba	-0.0088	-2.78
Sn	-0.1172	1.96

Biotites:

F = 18.9178 with 10 and 75 degrees of freedom
D^2 (Mahalanobis' generalized distance function) = 10.54
R (Multivariate mean of the biotite R) = -8.66
DI (Discriminant Index) = -12.59
W (Multivariate mean of the biotite W) = -19.21

Contribution of each variable to the total distance
between the multivariate means:

Variable	Constants	Per cent contribution
Rb	-0.0119	37.30
Sr	-0.0025	-0.01
Sc	-0.0393	3.26
Cr	-0.2136	11.09
Ni	0.0280	0.38
F	1.8783	3.61
Cl	0.0025	38.95
Zn	0.0023	-0.80
Nb	0.0016	-1.27
Sn	-0.0195	7.49

Table 17

Discriminant functions of the red and white granite

R e d   g r a n i t e

2	9.68783	24	30.51791	42	18.05611	71	23.60220
3	31.99419	25	19.99625	43	22.55241	72	21.27080
4	11.96736	26	21.32748	44	23.87022	73	20.69653
5	24.27380	28	19.39032	45	18.64461	74	23.52176
6	18.27957	29	11.89773	47	21.99821	75	20.11189
7	12.59573	31	28.96017	48	20.29381	76	27.87102
8	17.07068	32	15.64680	49	16.53662	77	25.43542
9	26.25710	33	23.97681	52	26.29298	78	25.90749
10	31.50023	34	23.41718	53	21.69179	79	25.49484
11	17.16806	35	19.80666	55	12.17845	80	25.70613
12	14.22705	36	20.46053	56	13.55876	81	24.22385
18	17.12302	37	22.66116	57	17.83751	86	25.00703
19	16.27261	39	26.91579	63	12.62345	104	14.77271
21	20.67850	40	17.94298	69	27.10646	105	22.45276
23	19.58925	41	21.84146	70	21.27196		

W h i t e   g r a n i t e

1	-0.06233	61	-4.96660	84	0.73362	94	1.88539
13	-2.48380	62	-4.39094	85	0.91795	95	-1.21612
14	-2.28089	64	0.34471	87	-0.25633	96	-0.08327
15	-4.22516	65	-0.68650	88	2.11810	98	-1.53340
16	4.31030	66	-3.49304	89	10.86468	99	-1.04329
17	-1.54565	67	-3.31519	90	-0.42605	100	-1.61086
51	-0.06552	68	0.56683	91	-9.92194	101	-0.89732
59	-4.68481	82	1.63041	92	-2.23445	102	5.34336
60	-2.33300	83	-0.14189	93	3.87865	103	4.35451
20	7.52430	27	22.30202	38	8.38787	50	9.53547
22	15.84974	30	15.19966	46	17.80495	54	8.46997
						58	3.54059

Table 18
Discriminant functions of biotites

b i o t i t e s   R

2	-5.93661	21	-4.41404	41	-5.24113	63	-8.23383
3	-8.92048	23	-9.73483	42	-7.05385	69	-2.67290
4	-16.48737	24	-5.01687	43	-7.72998	70	-8.17209
5	-8.96227	25	-11.34528	44	-7.43456	71	-6.63937
6	-4.25255	26	-11.65223	45	-5.00762	72	-8.80446
7	-5.31003	28	-15.16970	47	-10.95767	73	-11.26970
8	-13.46741	29	-10.20250	48	-9.43128	74	-11.50636
9	-8.96611	31	-10.00412	49	-6.98578	76	-6.30645
10	-4.91444	32	-7.15794	52	-5.18178	77	-7.79980
11	-8.84132	34	-7.10593	53	-8.07253	79	-8.14541
12	-8.59643	35	-9.33740	55	-9.37879	80	-9.89852
18	-8.02119	39	-11.60442	56	-13.39357	81	-9.96284
19	-6.67072	40	-7.84783	57	-9.00742	86	-7.87368
						104	-6.71542

b i o t i t e s   W

1	-20.78377	61	-18.08836	84	-27.28688	94	-15.60522
14	-20.84291	62	-18.56442	85	-18.81566	95	-16.20351
15	-15.68567	64	-22.44582	88	-23.23827	96	-23.57463
16	-14.89659	65	-16.93797	89	-20.10789	97	-15.79627
17	-20.31323	66	-14.04277	90	-27.20718	98	-19.25417
51	-22.49286	68	-17.92686	91	-25.87042	99	-19.02760
59	-18.95053	82	-9.94051	92	-13.24689	101	-22.41423
60	-20.54306	83	-16.79366	93	-19.78433	102	-13.82252

20	-9.66895	38	-15.08470	50	-1.93915	58	-10.35175
27	-5.71606	46	-13.53190	54	-9.70393		
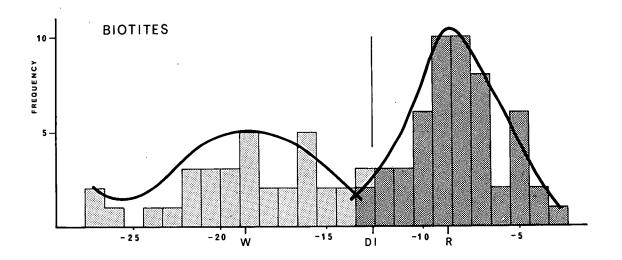
In figure 44 the multivariate mean W for the white granite
and its biotite lies to the left of discriminatory index
DI and is apparently further from the index than the
multivariate mean R for the red granite and biotite R
which lie to the right of the index. Discriminatory function
of the individual samples are grouped in close proximity
to the multivariate means of the red and white granites.
In the white granite group the samples form a distinctly
segregated group having a range from -5 to +5. The red
granite group exhibits a much greater range of discrimina-
tory functions, from +10 to +30. Some of the samples of
the red granite lie on the left side of DI. From the sym-
metrical shape of the graph it is possible to suppose
a normal distribution of the discriminatory functions of
the red and white granites. A marked separation of the red
and white granite proves their geochemical independence
and the range of their degree of geochemical homogeneity.
According to these criteria the white granite is more ho-
mogeneous.

The discriminant functions for biotite show that they
are closer to the discriminant index DI than the values
for rock samples. As can be seen from the diagram (Fig.44)
the range of the discriminatory function of biotite is
the same for both groups and varies between -3 and -13 for
the biotite R and from -14 to -20 for the biotite W.

Figure 44

Histograms showing the variation in discriminant
functions for rocks and their biotites.

W - multivariate mean of the white granite
    (biotite - W)
R - multivariate mean of the red granite
    (biotite - R)
DI - discriminant index

The frequency graph of discriminant functions for the biotite R has the character of a normal distribution. The very close proximity and partial overlap of the biotites R and W indicates a continuous development of the magmatic series the red-white granite. This continuity is characterized by the geochemical similarity between the most acid members of the two granite groups.

Table 16 shows how each individual trace element contributes to the total distance between the multivariate means in both rock groups. In the rock Zr contributes most to the discrimination (77%) between the red and white granite. Zr occurs as zircon in both granites. The generally higher Zr content in the red granite supports the idea that part of the zircon in the red granite was transferred into the granite from assimilated country rocks. This was earlier confirmed by qualitative analyses of heavy minerals (see Plate 20 and 21). Rb and Sr are also important trace elements for the purposes of discrimination. Rb contributes 37% to the discrimination and Sr 14%. The different levels of content of Rb, and Sr in the two granites (higher Rb and lower Sr concentration in the white granite) indicate the difference between the main masses of the red and white granite.

Discrimination of biotites is most significantly shown by Cl (contribution of 39 %) and Rb (contribution of 37%)
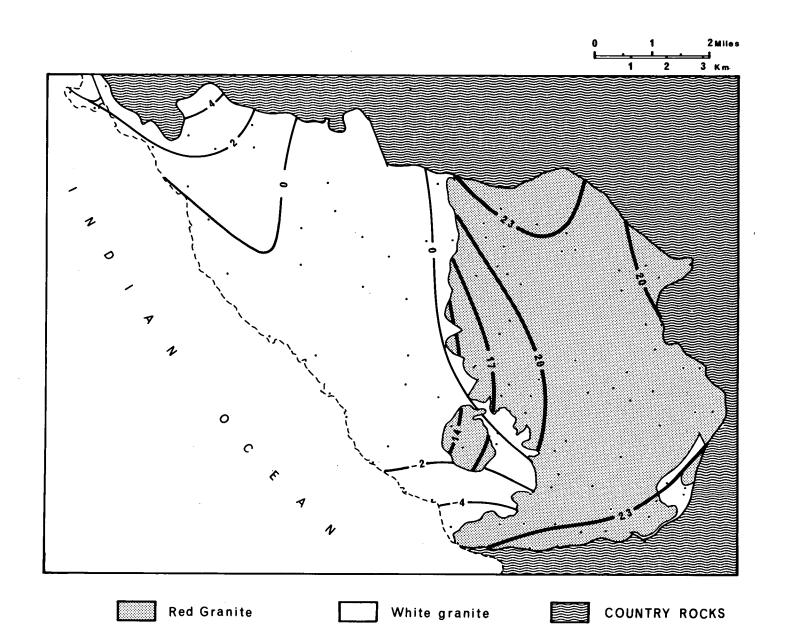
concentration. Cr and Sn show also relatively significant contribution for purposes of biotite discrimination.

The results of discriminatory analysis confirm that the red and white granites are basically two different geochemically defined rock types. A closer look at the distribution of the discriminatory values for biotite shows that there is a marked similarity between the fine grained types of both groups. This similarity indicates the continuity of magmatic differentiation within the granitic body up to the early stages of crystallisation. In the later stages the effects of assimilation markedly influenced the geochemical regime of the red granite (for instance the content of Zr and Sr). These external influences are the bases underlaying the significant discrimination of geochemical characteristics of the red and white granite. The range of the discriminatory functions represents the serious effect of endogenous and exogenous influences during the emplacement, crystallisation and final consolidation of the Heemskirk massif.

Trend surface analysis was used to find distribution patterns of the discriminant functions within the red and white granite and their biotites respectively (Figs. 45 and 46).

The trend surfaces for discriminant functions of the rocks shown in figure 45 reflect the general features of the

Figure 45

Trend surface analysis (third degree) of discri-
minant functions for rocks of the Heemskirk gra-
nite massif. Per cent sum of squares accounted
for by the trend surfaces of the red granite 20.2
and the white granite 25.2.

| Red Granite | White granite | COUNTRY ROCKS |

70/8/16

chemical and mineralogical variation within the both gra-
nite groups. The pattern of the trend surfaces for the
red granite proves the higher mineralogical and chemical
homogeniity of the central mountainous part of the red
granite area between Mt. Heemskirk and Mt. Agnew. This
part of the intrusion corresponds to the upper sequence
of the red granite layer, lying nearly parrallel to
the topography. On the steep slopes of the western side
of the Heemskirk Range there is obvious by a rapid decrease
of the discriminant functions. Low values of the discri-
minant functions correspond to the lower bed of the red
granite (more acid, medium to fine grained granite -
type R3). The highest values of discriminant functions
occur in the vicinity of the northern and southern margins
of the intrusion, and indicate the presence of the more
basic facies of the red granite.

The pattern of the trend surface for the white granite
roughly coincides with the distribution pattern of the
major rock types (Fig.45). The area within the zero iso-
pleths corresponds predominantly to the coarse grained
white granite (type W3). The area east of the zero iso-
pleth (lying close to the red granite contact), and the
southern part of the white granite region with negative
discriminant functions, correspond to the more acid type
of the granite (medium to fine grained granite - type W2).

The positive discriminant functions in the north-western part of the white granite coincide with the outcrops of the marginal type of the granite with abundant remnants of the granitised and assimilated country rocks. The absolute values of the discriminant functions indicate the tendency of that part of the white granite to approach the red granite composition.

The trend surfaces for discriminant functions of the biotites shown in figure 46 reflect similar features of the variation in chemical composition within both rock groups as do the surfaces of the discriminant functions of the rocks.
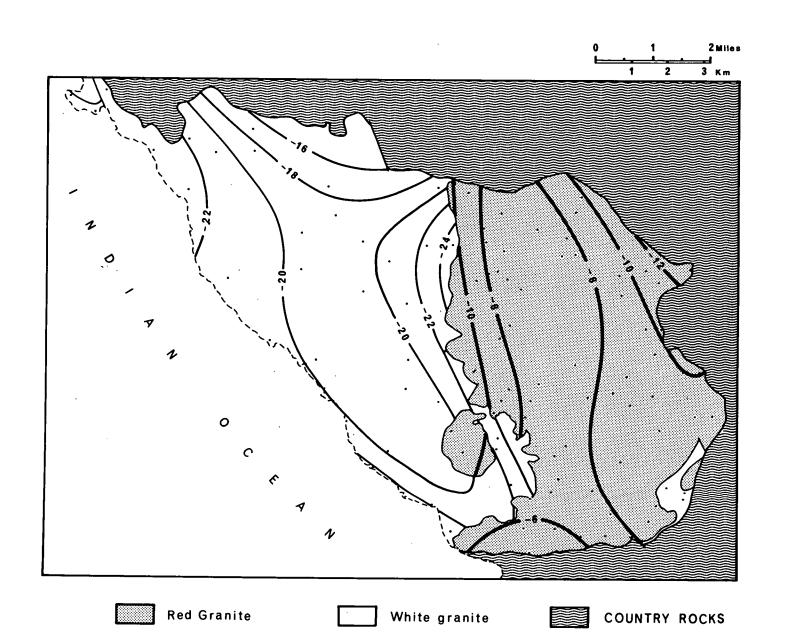
The pattern of the surface for biotite R proves the same tendency of the chemical composition of the red granite layer as was shown in figure 45.

In fig. 46 the stratigraphical bedding of the red granite is represented by the sequence of the discriminant isopleth from -12 to -6, from the bottom to the top of the stratum.

The surface for functions of the biotite W shows a similar pattern to the trend surface for the white granite in figure 45. The sequence of the discriminant isopleths roughly represents the stratigraphy within the white granite. The topmost part of the intrusion, outcropping on the contact with the red granite, corresponds to the values -22

Figure 46

Trend surface analysis (third degree) of discri-
minant functions for biotite of the Heemskirk
granite massif. Per cent sum of squares account-
ed for by the trend surfaces of the biotites -.R
38.8 and the biotites - W 24.7.

Red Granite   White granite   COUNTRY ROCKS

70/4/:74

- -24). The lower part of the intrusion, occupying
the centre of the white granite area is limited by the
isopleths -20. Remarkably higher isopleths (-18, -16)
cover the northern margin of the intrusion where there
are abundant remnants of the assimilated country rocks.
The far west of the white granite is covered by the iso-
pleths -22 and lower. This is in good agreement with
the prevalence of the fine grained granite (type W2) in
these parts of the intrusion. In general the trend surfa-
ce analysis of the discriminant functions of the rocks
and their biotites supports the existence of the layering
and stratigraphy within both rock groups.

7.3. R-mode factor analysis

The distribution of trace elements in granites is
characterized by the occurrence of groups of geochemically
coherent elements, that is, groups of elements that under
given conditions behave in a similar way. Factor analysis
enables one to define geochemically coherent groups of
trace elements and leads to the reduction of observed re-
lationships among many variables to simpler relationships
among fewer variables. By using factor analysis it is pos-
sible to indicate the nature of the basic factors such as
chemical conditions of crystallisation and assimilation
which influence the distribution of the elements. As most

of the trace elements show more lognormal distribution
rather than normal distribution all the data were transform-
ed to logarithm of the concentration of each element to
form the correlation matrix for the factor analysis.

To enable a simpler interpretation of the factor
analysis results, the red granite, white granite, biotite
R, biotite W and the "red" potassium feldspar were facto-
rized separately. Factor matrices of each individual group
are given in Tables 19, 20, 21, 22 and 23. The proportion
of the overall data variability contained in each factor
is expressed as a percentage of variance. The degree of
representation of each element in a coefficient matrix
is measured by the communality, which is the sum of squar-
ed factor loadings for each variable. The communality 1.0
signifies complete representation of variable. Choice of
the number of factors to be used is determined somewhat
subjectively by cutting off the number of eigenvalues
smaller than 0.5. The factors are presented in figure 47.
The horizontal line in each diagram is a zero loading for
the elements. Positive loadings occur above the centre line
and negative loadings occur below. The further a particu-
lar element is from the horizontal line the higher its
loading.

In interpreting the results of factor analysis it is
necessary to emphasize that the loadings on the first

TABLE 19.

Varimax factor matrix of the red granite *

Element	Factor						Communality
	1	2	3	4	5	6	
Rb	0.819				-0.427		0.873
Sr	-0.860				0.290		0.868
Na$_2$O	0.209					-0.960	0.992
Zr	-0.914						0.872
F		0.974					0.997
Nb	0.239				-0.938		0.951
Pb			-0.973				0.996
Ba	-0.843					0.281	0.863
Sn				-0.989			0.998
Percent of variance explained by factor							
	34.5	11.4	11.9	11.23	13.4	11.7	
Cumulative percent of variance							
	34.5	45.8	57.1	68.4	81.7	93.4	

*Loadings < 0,2 omitted

TABLE 20.

Varimax factor matrix of the white granite*

| Element | Factor | | | | | Communality |
	1	2	3	4	5	
Rb	0.587	0.344		-0.524	-0.344	0.857
Sr	-0.848			0.347	0.275	0.935
Na_2O	0.772	-0.267		0.295	-0.304	0.881
Zr	-0.922					0.897
F		0.977				0.964
Nb	0.396				-0.901	0.984
Pb			0.229	-0.926		0.913
Ba	-0.900				0.219	0.886
Sn			0.966			0.973
Percent of variance explained by factor						
	38.7	13.2	11.9	15.5	12.9	
Cumulative percent of variance						
	38.7	51.8	63.7	79.2	92.1	

*Loadings < 0.2 omitted

TABLE 21.

Varimax factor matrix of "red" biotites[*]

Element	Factor 1	2	3	4	5	Communality
Rb	0.875					0.899
Sr		-0.240			-0.910	0.919
Sc			0.957			0.948
Ni	-0.384	-0.757		0.300		0.827
Cr	-0.799	-0.424				0.856
F	0.722		-0.221	-0.343		0.725
Cl	0.749		-0.225	-0.461		0.876
Zn	-0.335			0.874		0.895
Nb		-0.481	0.451	0.644		0.902
Sn		-0.858			-0.269	0.814
Percent of variance explained by factor						
	28.3	18.4	12.6.	16.3	11.0	
Cumulative percent of variance						
	28.3	46.7	59.3	75.6	86.6	

[*]Loadings < 0.2 omitted

TABLE 22.

Varimax factor matrix of "white" biotites*

Element	Factor 1	2	3	4	5	Communality
Rb		0.963				0.975
Sr			0.894		0.223	0.866
Sc	-0.750	-0.287	0.212		0.245	0.768
Ni				-0.941		0.946
Cr	0.858	-0.428			0.915	0.949
F				0.292	0.309	0.897
Cl	0.640	0.549			-0.492	0.911
Zn	-0.356		0.638			0.795
Nb	-0.846			-0.433		0.924
Sn	-0.658			-0.564		0.795
Per-cent of variance explained by factor						
	30.3	16.0	13.4	15.3	13.3	
Cumulative per-cent of variance						
	30.3	46.3	59.7	75.0	88.3	

*Loadings < 0.2 omitted

TABLE 23.
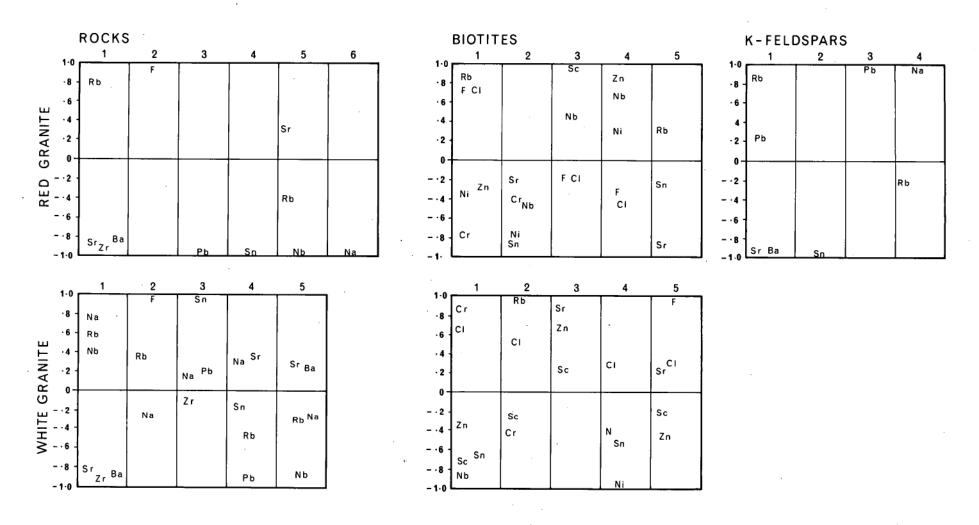
Varimax factor matrix of "red" K-feldspars*

Element	Factor				Communality
	1	2	3	4	
Rb	0.856			-0.267	0.828
Sr	-0.939				0.942
Na_2O				0.962	0.990
Pb	0.239		0.955		0.999
Ba	-0.940				0.911
Sn		-0.996			0.996
Per-cent of variance explained by factor					
	43.2	17.0	16.9	17.5	
Cumulative per-cent of variance					
	43.2	60.1	77.0	94.4	

* Loadings < 0.2 omitted

Figure 47

Composition of factors in rocks, their bioti-
tes and K-feldspars

ROCKS

RED GRANITE

	1	2	3	4	5	6
1·0		F				
·8	Rb					
·6						
·4					Sr	
·2						
0						
-·2						
-·4					Rb	
-·6						
-·8	Sr Ba					
-1·0	Sr Zr		Pb	Sn	Nb	Na

WHITE GRANITE

	1	2	3	4	5
1·0		F	Sn		
·8	Na				
·6	Rb				
·4	Nb	Rb		Na Sr	Sr Ba
·2			Na Pb		
0					
-·2		Na	Zr	Sn	Rb Na
-·4				Rb	
-·6					
-·8	Sr Zr Ba			Pb	Nb
-1·0					

BIOTITES

	1	2	3	4	5
1·0			Sc	Zn	
·8	Rb			Nb	
·6	F Cl				
·4			Nb	Ni	Rb
·2					
0					
-·2	Ni Zn	Sr	F Cl	F	Sn
-·4		Cr Nb		Cl	
-·6					
-·8	Cr	Ni Sn			Sr
-1·					

	1	2	3	4	5
1·0	Cr	Rb	Sr		F
·8	Cl		Zn		
·6		Cl			
·4				Cl	Sr Cl
·2			Sc		
0					
-·2	Zn	Sc		N Sn	Sc
-·4		Cr			Zn
-·6					
-·8	Sc Sn Nb			Ni	
-1·0					

K-FELDSPARS

	1	2	3	4
1·0			Pb	Na
·8	Rb			
·6				
4				
·2	Pb			
0				
-·2				Rb
-·4				
-·6				
-·8	Sr Ba	Sn		
-1·0				
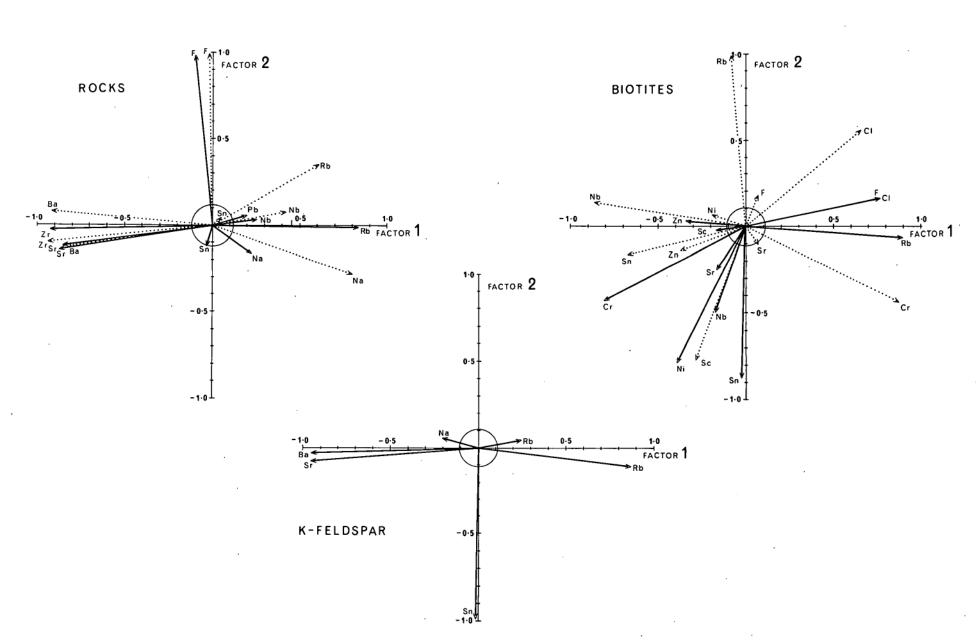
factor delineate the most general pattern of relationship,
in the correlation matrix and in turn, in the original
data. The loadings on the second factor delineate the
next most general pattern and so on. Where an element
is confined to a simple factor it is likely that its
occurrence within granites, biotites and potassium feld-
spars can be explained by a simple process, but where a
complex factor pattern is observed for an element then
several independent or partially independent processes
-probably contribute to its distribution.

Relationships between the variables can be expressed by
factor axes which are at right angles to each other (Fig.
48). Vectors represent factor loadings between variables.
Variables that are closely correlated will be clustered
together, whereas uncorrelated variables will be at right
angles to each other. Antipathetic related variables will
be opposed to each other at about 180° in the direction
of the vectors.

Factor scores for each sample are important to the
interpretation of the data, for they are a reduced set of
new uncorrelated variables that carry almost the same
information content as the original data. Factor scores
can be used as a data for the trend surface analysis.
This trend surface analysis is very similar to cannonical
correlation. It is a partial summation of areal variation

Figure 48

Plots of varimax loadings for factor 1 and 2 of
the rocks, biotites and K - feldspars. Full lines
- loadings for the red granite; dotted lines -
loadings for the white granite. Circles - limits
of the statistical significance of the loadings.

of trace elements within a particular factor. In appendix
II Tables 6, 7, 8, 9 and 10 record the factor scores of
the Heemskirk massif. Figure 49, 50, 51, 52 shows the
areal variation of the factor scores of selected factors
within the studied area.
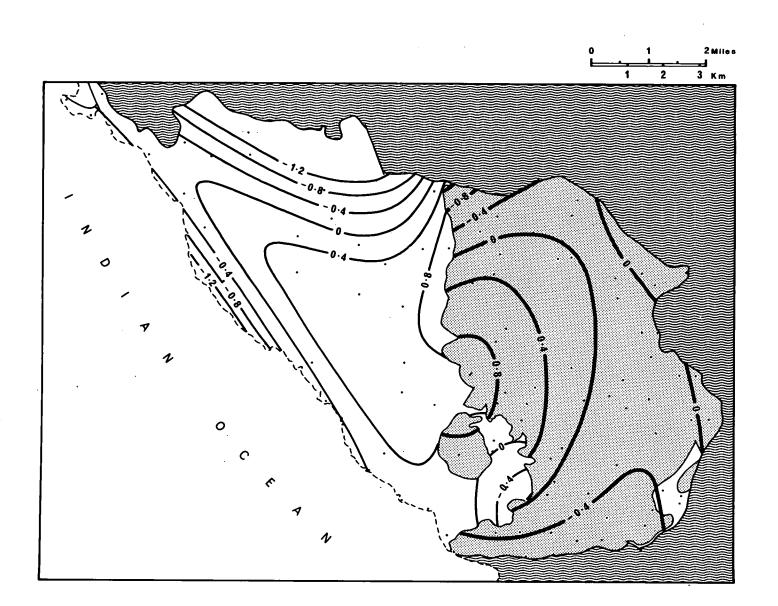
The following description of factors is based on the rota-
ted varimax factor matrix as well as on the total cubic
trend surfaces of factor scores.

The results of factor analysis indicate that the
mentioned trace elements are grouped into six independent
factors in the red granite, five in the white granite
and biotites and four factors in potassium feldspar.
In general the distribution of trace elements is controlled
by the bulk chemical composition of rocks and their rock-
-forming minerals and reflects the chemical conditions
of differentiating crystallization and contamination.
Discussion which follows uses the factor loadings of the
elements and the influences of the factors at different
parts of the granite body (factor surfaces) to investi-
gate this significance. Figure 47 shows that the overall
difference in composition of factors and their sequence
in the white and red granites is very similar. Significant
differences were found in composition of factors for
biotites from the same groups of rocks.

7.3.1. Interpretation of factors in the rocks

The most important factor in both red and white granite is a bipolar factor including two groups of elements. Sr-Ba and Zr is opposed by Rb. Na_2O has a major loading with Rb in the white granite but occurs on a different factor (factor 5) in the red granite. Rb-Ba-Sr-Zr in the most important factor in both granites (as shown by discriminant analysis) indicating that the concentration of these elements determines the classification of samples into the red or the white granite. In both cases factor 1 characterizes the group of potassium feldspars as a major component of both granites as well as the accessory mineral - zircon.

The trend surface for this feldspar-zircon factor is shown in figure 49. Total cubic trend surface for factor 1 may be compared with the equivalent trend surfaces of the individual elements Zr, Sr, Ba and Rb. Despite the differences for Rb the surfaces for these elements are quite similar to each other and to the surface for factor 1. There is a better fit between the percentage sum of the squares of factor 1 in the white granite than in the red. This indicates a higher degree of similarity in the distribution of the above mentioned elements in the white granite.

INDIAN OCEAN

0   1   2 Miles
1   2   3 Km

7019/180

Figure 49

Trend surface analysis (third degree) of factor
scores – factor 1 for rocks. Per cent sum of
squares accounted for by the trend surfaces
of the red granite 34.0 and the white granite
20.1.

Most monocomponent factors - 2, 3, 4, 5 (6 for
the red granite) are essentially related to one of the rock
forming minerals.

Factor 2 accounts for almost all the variation of fluorine
in both rock types. The main source of F is biotite, even
though some F is contained in irregularly disseminated
tourmaline and accessory fluorite and apatite. Factor Pb
is essentially related to feldspars. Factor Sn represents
firstly the isomorphically bound Sn in biotite and free
accessory cassiterite. Factor 5 of both granites involves
significant loadings of Nb as well as Sr and Rb. The geo-
chemical coherence of Nb and Rb is dependent mainly on
the occurrence and chemical composition of biotite. Factor
6 in the red granite is related exclusively to the distri-
bution of Na - essentially albite. These factors (2-5 and
6 for the red granite) do not present any additional
information to that provided by the raw F, Sn, Pb, Na data.

Figure 48 shows the inter-relationship of variables
between the two most important factors. Variables are
clustered into two groups. Most trace elements are grouped
closely to factor axis no. 1 and confirms the complex cha-
racter of factor 1. A second group of vectors is represented
by fluorine in both rock types. This is one of the most
important volatiles in the magma and apparently cannot be
significantly correlated with other trace elements.

7.3.2. Description of factors in the biotites

Significant differences in the composition of individual factors for biotite (Fig.47) indicates crystallisation under different physical and chemical conditions. The most important factor in the biotites of both granites is obviously bipolar.

In the biotites-R Rb-F and Cl are opposed by Cr. In addition to these major loadings Ni and Zr are consistently loaded with Cr. The Rb group represents anions and interlayer cations and the Cr group are the cations of the octahedral sheet. In the white granite factor 1 consists of the group Cr-Cl which is opposed by Nb-Sc-Sn and Zr coherent group.

Factor No. 2 in the biotite R is represented by most cations of octahedral sheet in relatively high negative loadings (Sn-Ni-Nb-Cr).

Factor 4 in both groups of biotites is characterized by the bipolar position of the groups of anions (Cl, F) and cations in the octahedral sheet. The antipathetic character of the loadings of these elements in the biotite R and W emphasizes the difference in the structure of both biotites.

Factor 5 for the biotite W represents a high loading of F.

The position of F in the last factor of the biotite W is in contrast to the position of F of the biotite R in factor 1.

The total cubic trend surface for factor 1 has a better fit than any other factor. The essential form of the trend surface, shown in figure 50, reflects common features in the distribution patterns of the above mentioned elements involved in factor 1 of both biotites. A decrease of scores represents a decrease in the content of elements with negative loadings. The relatively smooth decrease of factor scores along the structural axis of the white granite contrasts with the more complicated pattern for the biotite R. This is partly explained by the different composition of the above mentioned factors. A better fit of the percentage of squares for the trend surface of factor 1 for the biotite W indicates a higher degree of similarity in the distribution of the above mentioned trace elements in this type of biotite.

The total cubic trend surface for factor 2 reflects Sn, Ni, Cr, Nb and Sr regional distribution in the biotite R and Rb, Cl, Se, Cr in the biotite W. Fit of the percentage of squares for this surface of Factor 2 is again better for the biotite W. The pattern of the trend surface shown in figure 51 is very similar to the partial trend surface for original data of trace elements presented in factor 2
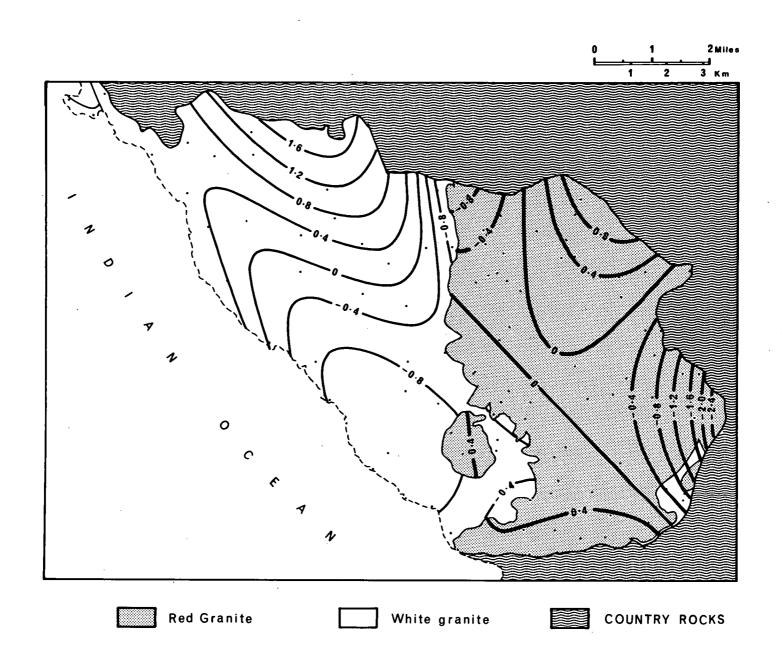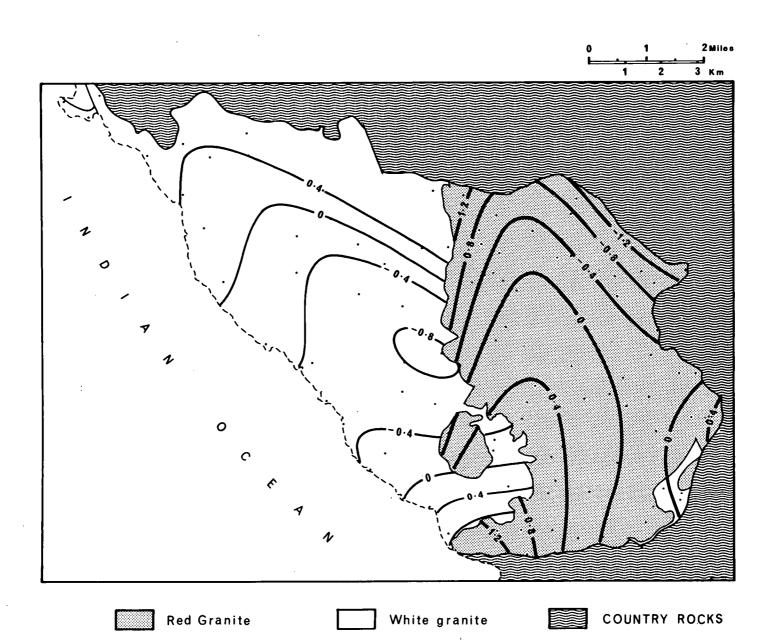
Figure 50

Trend surface analysis (third degree) of factor
scores - factor 1 for biotites. Per cent sum of
squares accounted for by the trend surfaces of
the biotites - R 36.4 and biotites - W 60.9.

| Red Granite | White granite | COUNTRY ROCKS |

INDIAN

OCEAN

1.6
1.2
0.8
0.4
0
-0.4
-0.8

0.8
0.4
0
-0.4
-0.8
-1.2
-1.6
-2.0
-2.4

-0.4

-0.4

0
-0.4
-0.8
-1.2
-1.6
-2.0
-2.4

0 1 2 Miles

1 2 3 Km

Figure 51

Trend surface analysis (third degree) of factor
scores - factor 2 for biotites. Per cent sum of
squares accounted for by the trend surfaces of
the biotites - R 31.7 and biotites W 21.4.

Red Granite   White granite   COUNTRY ROCKS

70/9/178

as well as to the trend surface for factor 1.
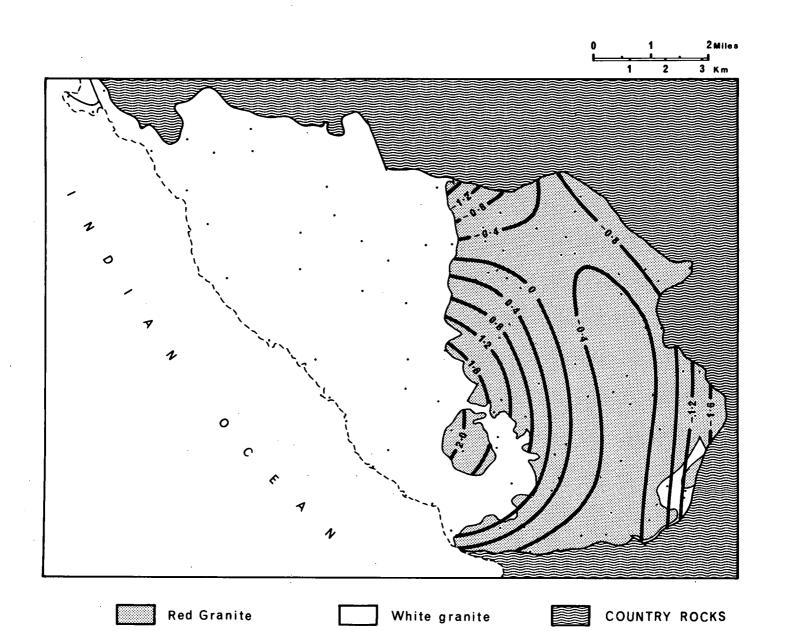
Fig. 48 shows a plot of the distribution of all ten elements in the plane formed by factor 1 and 2. Trace elements are clustered into two groups. The major group of variables can be seen to project into the axis of factor 1 and consists of Cl, F, Rb, Cr, Sc and Zn for red biotite and Ni, Nb, Sn, Zn for the biotite W. At right angles to the main vectors there is Rb, Sc of the biotite W and the Sn, Nb and Ni for the biotite R. A marked difference in the distribution of the vectors of both biotites R and W indicates the different physico-chemical environment during their crystallisation.

7.3.3. Description and Interpretation of Factors in
Potassium Feldspar

The six trace elements analysed form a coherent group Sr-Ba vs. Rb, Pb in factor 1 (Fig.47). Sr shows coherence to Ba and the Ba/Sr ratio decreases with increasing fractionation of the granite magma. This behaviour is interpreted by Heier and Taylor (1959) as due to the less ionic character of the SrO bond, which leads to the preferential acceptance of Ba^{2+}. Rb and Pb exhibit a mutual coherence due to substitution for K but the existence of

Figure 52

Trend surface analysis (third degree) of factor
scores for K-feldspars of the Heemskirk granite
massif. Per cent sum of squares accounted for by
the trend surface of K-feldspars 51.3.

| | Red Granite | | White granite | | COUNTRY ROCKS |

high positive loadings in factor 3 indicates a more compli-
cated bonding of Pb in K-feldspar. The trend surface for
factor 1 shown in figure 52 represents a distribution
pattern which is very similar in form to the trend surface
for individual elements (Rb, Ba, Pb and Sr).

Factor 2 is related exclusively to the Sn distribution
within the K-feldspar. It is believed that Sn occurs as
very fine disseminated Sn mineral or, according to Borchert
and Dybek (1960), in a possible substitution of SnO_4^{4-} com-
plexes for SiO_4^{-4} tetrahedra in silicate and alumosilicate
rock forming minerals.

Factor 5 is essentially a Na factor. The independence of
Na shows that it is present in feldspars only as albite
(perthite).

Figure 48 represents a plot of varimax loadings for
factors 1 and 2. There is a similarity between Ba, Sr, Na
and Rb data. No statistically important relationship exists
between these elements and Sn.

8. Use of the geochemical data for locationg hidden (blind) tin mineralisation in the Heemskirk massif

Throughout the world, tin deposits have ranked among
the earliest discoveries of mineral resources and the ma-
jority of deposits which can be located easily from

a superficial examination of the earth's surface have been
discovered. The current emphasis is, therefore, on methods
of exploration for ore bodies which do not outcrop
(Saukov, 1959; Barsukov & Volosov, 1967; Bradshaw & Stoyel,
1968).

One of the main methods of investigation of this
problems involves the use of regional geochemistry in con-
nection with detailed geological mapping. The chemical and
geological models of the massif were used to contour the
contact between the white and red granites. These models
are compared with the spatial distribution of known Sn de-
posits and their mineralogy in discussing the locality of
hidden (blind) mineralisation within the Heemskirk massif.

8.1. The relief of the white granite surface

A series of geological profiles and geochemical maps
of selected trace elements were used to determine the va-
riation of the elements vertically between the white/red
granite contact and the top of the granite dome (i.e. the
group surface or the contact of the red granite with country
rocks, fig. 54). Variation factors for the content of trace
elements against thickness of the red granite cover are
shown in table 24. These show a direct variation of element
content with thickness.

Table 24

An increase or a decrease of the trace element content
with increasing of the thickness òf the red granite cover
by 100 ft.

	Rocks (ppm)	biotite (ppm)	An increase of the thickness (in ft.) of the red granite about
Zr	3 (Increase)		100
Ba	25 (Increase)		100
Sc		5 (Decrease)	100

Figure 53

Idealised cross-section through the Heemskirk
granite massif.

C - is the altitude of the basement of the red
    granite at particular point on the map

A - is the altitude of the ground at the parti-
    cular point on the map

x - is the content of trace element on the
    present surface in the red granite

y - the content of trace element in the red gra-
    nite at the red/white granite contact, in
    a W - E direction parallel to the axis of
    the major structure of the Heemskirk massif.

W

A

E

x

y

Red
granite

C

White granite
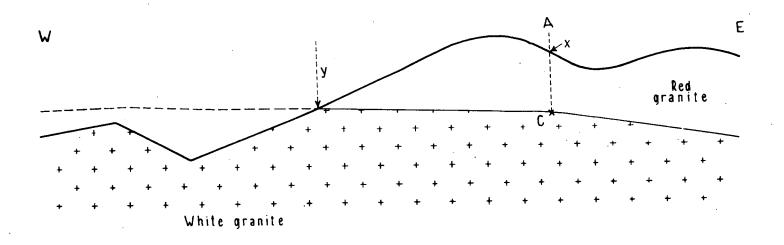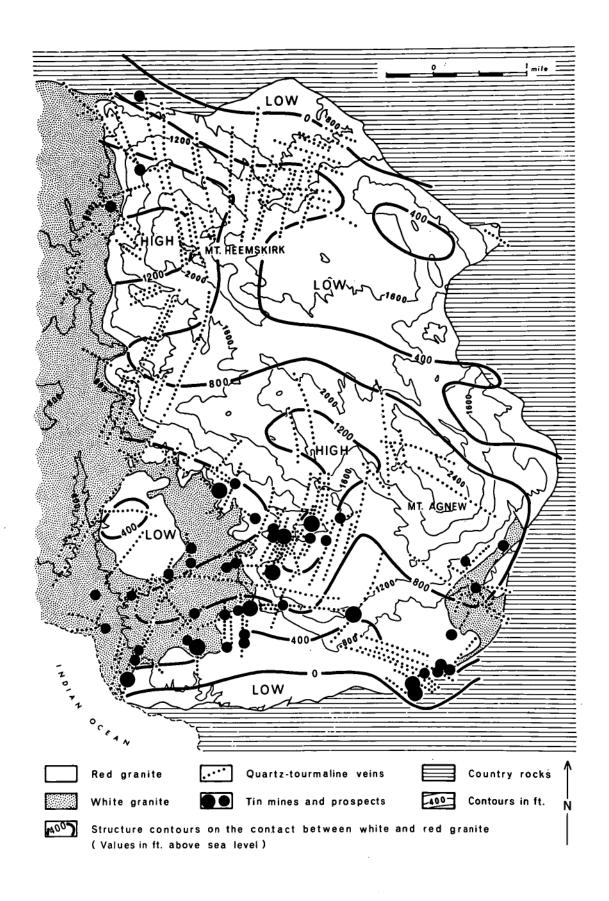
Figure 54

Structural map of the eastern part of the Heemskirk
granite massif.

	Red granite		Quartz-tourmaline veins		Country rocks
	White granite		Tin mines and prospects	400	Contours in ft.

400 Structure contours on the contact between white and red granite
(Values in ft. above sea level)

LOW

1200

HIGH

MT. HEEMSKIRK

1200 2000

1600

800

400

LOW

1600

400

2000

1200

HIGH

1600

MT. AGNEW

2400

400

LOW

1200 800

400 800

800

0

LOW

INDIAN OCEAN

0 1 mile

N

70/11/19

The altitude (C) of the base of the red granite at a particular point on the map (see figure 53) was calculated from the equation:

$$C = A - \frac{(x-y)}{z} \cdot 100$$

where A - is the altitude of the ground at the particular
point on the map

    x - is the content of trace element on the present
surface in the red granite

    y - the content of trace element in the red granite
at the nearest red/white granite contact in
a W-E direction parallel to the axis of the
major structure of the Heemskirk massif

    z - an increase (+) or a decrease (-) of the content
in ppm with increasing altitude by loo feet.

Figure 54 shows structure contours on the contact between the red and white granite and illustrates the form of the white granite surface beneath the red granite. The basic shape is a flat cupola with minor elevations and depressions. Particularly well developed is the Mt Agnew antiform which bifurcates towards the west. The Mt Agnew and Mt Heemskirk antiforms are separated by a brachisyn- clinal depression. The antiformal axes are approximately parallel in an E-W direction. At the eastern end the structu-

res curve towards the south. Their amplitudes are approximately the same but the apex of the Mt Agnew antiform is further east. The axes of both structures plunge gently to the east. The majority of quartz-tourmaline veins and greisen zones, often tin bearing, are concentrated in the apical parts of the Mt Agnew and Mt Heemskirk antiforms (Fig. 54). This is confirmed by the presence of economic tin mineralisation in these antiformal structures (see position of tin mines and prospects, figure 54).

8.2. Discussion

Almost all the studied trace elements exhibit a discontinuity in their regional pattern between the red and white granite. This discontinuity is illustrated by the form of the isopleths, and absolute values.

Distribution patterns of selected elements in the white granite, especially in the contact zone with the red granite, reflect the general features of the structure of the base of the red granite. Towards the west the structure of the white granite has a flat cupola-like character, elongated in a WNW direction. The discordance of the isopleths at the contact indicates the continuation of this structure beneath the red granite further east.

In general the internal structure of the intrusion

is stratiform with the boundaries between the granite layers sub-parallel. Variation studies throughout the area proved that cryptic layering within the individual rock groups follows a similar pattern. This sub-parallel layering shows a diminishing influence of the structure of the country rocks with depth.

The established patterns of trace-element concentration in rocks and their minerals reflects the physico--chemical conditions of crystallisation and consolidation of the granite body. The isotherms of crystallisation within the intrusion would have been generally parallel to the isopleths of the content of the trace elements. According to the calculations of Larsen (1945) and Van Moort(1966) these isotherms seem to be sub-parallel during cooling and crystallisation of granite magma, and cross the boundaries of the granite bodies at low angles. The same can be said of the trace-element isopleths.

Garnett (1966), who studied the distribution of cassiterite in vein tin deposits in Cornwall, concluded that the Sn zone was probably related to the regional isotherms of the granite mass as a whole. The results of work at Heemskirk indicate that the zone of economic tin concentration crosses the red-white granite contact at a small angle and dips away more gently than the peripheral granite

boundary. According to Bauman (1970) one of the most essential prerequisites for the deposition of commercially important tin deposits in Erzgebirge (centra Europe) is the development of tectonic structures during intrusion and consolidation of tin-bearing granites, the residual solutions being concentrated in the upper parts of granite cupolas. Internal layering within the granite cupolas is flatter than the granite dome and the lower boundary of the tin zone is parallel to the internal layering of the granite.

Similar relationships between the internal structure of the granite and the distribtuion of tin mineralisation have been found in the Heemskirk massif. Economically important accumulations of Sn in the red granite area are commonly located in close proximity to the contact with the white granite. The abundance of Sn concentrations at the present surface is dependent on the thickness of the preserved layer of the red granite i.e. on the depth of the contact below the present ground level. In the Mt Agnew and Mt Heemskirk antiforms indications of mineralisation are relatively close to the present surface. These areas are the most promising regions for detailed geological prospecting. The main factor which limits subsurface investigation is the thickness of the preserved red granite layer. Where this exceeds 600 feet any economically impor-

tant tin accumulations have been uncovered at the surface. The red granite in the area of the Mt Heemskirk antiform is generally thicker than 600 feet. This suggests that the occurrences of mineralisation at the surface in this area are in the topmost parts of the ore zone. On the other hand to the west of the Mt Heemskirk and Mt Agnew antiforms disseminated occurrences of cassiterite indicate the lower boundary of the same ore zone.

In general the ore zone approximately corresponds to the upper surface of the white granite. Within the Heemskirk and Mt Agnew antiforms the mineralisation overlies the red- -white granite contact surface in the form of ore aureoles. The lower boundary of the ore zone is parallel to the cryptic layering within the granite body. The upper boundary forms a much more pronounced dome than the white granite surface. This observation is in agreement with the work of Garnett (1966) and Bauman (1970).

One of the most important factors controlling mineral zonation around the ore-bearing granites is temperature. The isograds of crystallisation of the granite are probably conformable with the cryptic layering, consequently the mineral zonation within the ore zone itself may be parallel to the cryptic layering in the granite. Further experimental evidence is needed to clarify the above conclusions.

8.3. Summary

The Heemskirk massif, particularly its eastern part,
is a good example of a granite terrain where the distri-
bution of tin mineralisation can be investigated in three
dimensions. The tin deposits, which are closely related
both spatially and genetically to the white granite, are
strictly controlled by the form of its upper surface.
The red granite forms the country rock. The results of
this study show that in monotonous granite areas it is
possible to use detailed geological mapping to demonstrate
a precise pattern of internal anisotropy. This anisotropy
is characterised by cryptic layering which is shown to
persist to depth in the exposed part of the intrusion, and
which may have a marked effect on the distribution of tin
mineralisation within the granite.

9. Petrogenesis

The petrogenesis of the Heemskirk granite massif is discussed in terms of some major problems which are specific for that intrusion. Problems considered to be most important are:

1) Relationship between the white and red granite
2) The origin of the tourmaline nodules
3) The sequence of crystallization of the mineral components
4) Estimation of the physical conditions during emplacement and crystallization of the Heemskirk massif
5) Genesis of the Heemskirk intrusion.

9.1. Relationship between the white and red granite

The problem of the relationship between the white and red granite has been discussed all geologists who have studied the Heemskirk intrusion. Brooks and Compston (1965) found the contact between the pink and white granites to be commonly obcured, but where exposed, it is a zone of irregular and diffuse mixing. Green (1966) did not observe the actual contact between pink and white granites because of poor outcrops. According to him exposures on the shore-

line reveal that an intervening porphyritic aplite occurs
between the two granites and the writer agrees with this
observation. There are two types of contacts between the
red and white granites:

In the first type the coarse grained red granite is
in sharp contact with the fine grained nodular aplitic
granite which belongs to the white granite group.

In the second type, the fine grained red granite
(sometimes aplitic and/or nodular) is in sharp contact
with the medium to fine grained variety of the white gra-
nite which is distinctly nodular and shows gradational
contacts with the coarse grained white granite.
In both cases the fine grained facies of the red and white
granites represents the zone of discontinuity in the deve-
lopment of the upper and lower parts of the intrusion.

According to Green (1965) the later white granite
magma had a high volatile content. The volatiles tended
to accumulate near the roof of the body and formed the
tourmaline nodular aplite when the mass cooled and this
opinion is in full agreement with results of this study.
The magma giving rise to the red and white granites had
a uniform composition during the act of intrusion.
The red and white granites differed in the content of vo-
latiles, the oxygen fugacity and the PT conditions, pro-
ducing during crystallization a different mineral

assemblages in each granite. The presence of abundant ultramafic and mafic rocks in contact with the red granite, and the lack of such country rocks against the white granite may be also one of the causes of the existing difference between the two types. Differences between the granite types have been developed gradually during and after emplacement of the magma. The red granite occupies the topmost part of the intrusion and towards the west is laterally replaced by the white granite. The red granite functions as country rock, being consolidated earlier than most of the white granite. The characteristic mineral assemblage of the red granite (haematite-magnetite-allanite) corresponds to the higher oxygen fugacity in the granite.

9.2. Origin of the tourmaline nodules

The replacement of other minerals by tourmaline, whether before or after consolidation of the granites, involves considerable chemical changes. Many writers have noted a reciprocal relation between biotite and tourmaline (e.g. Brammall and Harwood 1925).

Three models of nodule formation are considered plausible:

1) Volatile segregations in the early stage of crystallization

2) Metasomatic replacement of the surrounding rock in

the late stage of consolidation

3) Replacement of biotite by tourmaline in basic segre-
gations at a fairly early stage in consolidation.

The trace element and normative bulk composition studies
presented in this investigation are most easily interpret-
ed in terms of the first origin.

1) The distribution of "primary" tourmaline in the
Heemskirk granite is indicated schematically in   map I.
In the chronological order of granite types and varieties,
it is apparent that there is a tendency for the amount of
tourmaline to increase with time. This increase tends to
be accompanied by an increases in fluorite and points to
an increase in volatile content in the later stages of
emplacement (B, F). These volatiles tended to accumulated
near the roof of the body and formed the tourmaline nodules
in the white granite when the mass cooled. This would ex-
plain   the maximum concentration of nodules and apparent
gradational decrease in their amount toward the deeper parts
of the intrusion. Nodules differ in composition (different
content of quartz) from the rest of the magma and crystal-
lize from their centres outward.

The origin of tourmaline nodules as volatile segre-
gations in the early stage in crystallization is supported
by the absence of biotite in the narrow rim of country

rock around the nodules. Biotite could not exist or was dissolved in the vicinity of the volatile segregations in the granite magma. Because the tourmaline is mostly schorl, the Fe^{+2} content was exhausted in the vicinity of tourmaline nodules and no iron remained to build the biotite structure.

2) The origin of the tourmaline nodules could be also explained by metasomatic replacement of the surrounding rock in the late stage of consolidation. During the consolidation of the granite the concentrations of volatiles in the rock matrix were starting points for crystallization of tourmaline. However, the replacement of other minerals by tourmaline, whether before or after consolidation of the granite, involves considerable chemical changes in the white granite and these were not suggested by the present study.

3) Nockolds (1931), Koide (1951) and others attributed nodule formation in granites to reactions between magma and xenoliths. This alternative origin of the tourmaline nodules probably has only minor importance in the case of the white granite because there are rare biotite-rich xenoliths and mafic xenoliths in which however there is no evidence of metasomatic replacement by tourmaline.

9.3. The sequence of crystallization of mineral components

The succession of mineral components shown in figure 55 is based on the microscopic study of textural relationships in the major rock types and their varietis.

In general terms the sequence of crystallization is in agreement with the reaction series of Bowen (1928). The main period of magmatic crystallization can be separated from late or postmagmatic textural rearrangements and recrystallization recognizable first of all in the fine grained varieties of both granites. The reaction phenomena between biotite, tourmaline and felsic minerals which correspond to the appearence and disappearence of the minerals during the emplacement and magmatic crystallization of the granite are partially hidden by post-magmatic crystallization. These autometamorphic effects are very common in the majority of tin-bearing granites from different parts of the world (Sattran and Klomínský 1970).

9.4. Estimation of physical conditions during emplacement
and crystallization of the Heemskirk massif

Proper interpretation of field and laboratory data, and the reconstruction of former processes are often only possible through the information gained from experimental

Figure 55

Sequence of crystallization of the major

mineral components of the Heemskirk granite

CRYSTALLIZATION	MAGMATIC	POST-MAGMATIC
PLAGIOCLASE	————————	myrmekite ———— albite
BIOTITE	————————	chlorite
TOURMALINE	nodules ? ——————— —	— — — — — —
QUARTZ	phenocrysts ———	———————
K-FELDSPAR	——————— —	

———⟶ T I M E

work on synthetic systems.

In this section an attempt is made to estimate some of the physical conditions which prevailed during some stages of the crystallization history of the Heemskirk granite massif.
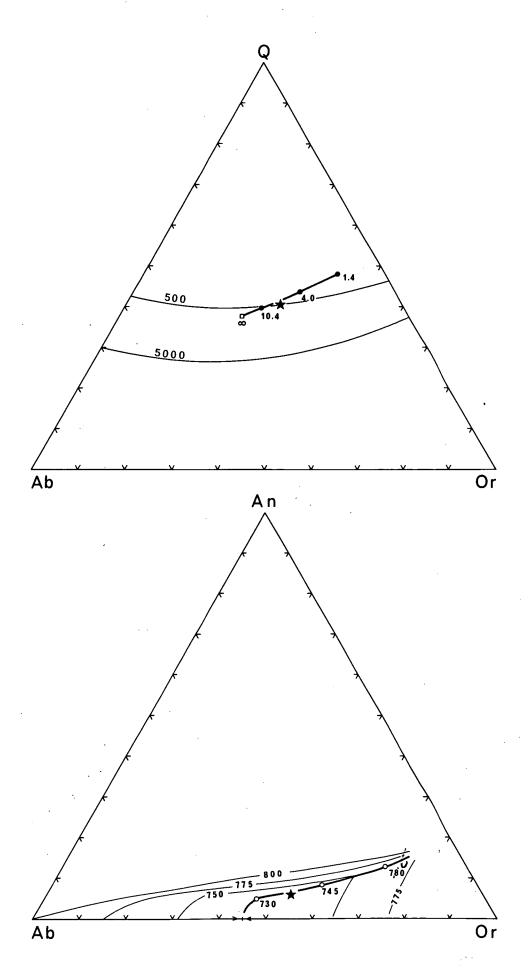
9.4.1. P_{H_2O} and the depth of intrusion

Shown in figure 56A are piercing points for system Ab - Or - An - Q - H_2O at 1000 bars (after James and Hamilton, 1969) and cotectics in the system Q - Ab - Or - H_2O at 500 and 5000 bars P_{H_2O} (after Tuttle and Bowen 1958, Luth et al. 1964). Average normative compositions (catanorm) of the samples from the Heemskirk granite massif is projected on the Q - Ab - Or plane (black star in figure 56A). The normative composition of the granite massif interpreted in the light of experimental data in the system Ab - An - Or - Q - H_2O suggests that most of it crystallized at a P_{H_2O} of approximately 500 bars. Such a low P_{H_2O} in turn suggests that the Heemskirk massif was emplaced at rather shallow depth in the crust. P_{H_2O} = 500 bars suggests that the final crystallization of most of the granite massif occured at low water pressures.

Figure 56

A) Piercing points for the system Ab-Or-An-Q-H_2O
(after James and Hamilton 1969). Numerals indi-
cate the Ab/An ratios - value of ∞ is for
the minimum compositions in the granite system.
Full lines are the cotectics in system Q-Ab-Or-
-H_2O at 500 and 5000 bars P_{H_2O} (after Tuttle
and Bowen 1958, Luth and others, 1964).

B) The liquidus surface for a portion of the quartz
- saturated ternary feldspar system at 1000 bars
P_{H_2O} after James and Hamilton (1969). Black star
- average composition of the average composition
of the average composition of the Heemskirk gra-
nite.

70/9/82

9.4.2. Temperature during intrusion and magmatic

crystallization

A temperature corresponding to the close of magmatic
crystallization and the intrusion of granites can be esti-
mated by comparison with the temperatures of liquidus
minima in the quartz saturated ternary feldspar system at
1000 bars P_{H_2O} after James and Hamilton (1969), figure 56B.
The average normative composition of the Heemskirk granite
massif falls in the low-temperature through of the
Ab - Or- An - SiO_2 system and corresponds to 735 - 740° C.
This temperature can be cited as a probable lower limit for
the Heemskirk intrusion. Marked depression of liquidus
temperatures occurs with small amoutns of fluorine
(Wyllie and Tuttle 1961) and with 5 weight percent HF in
the volatile fraction, the "granite" liquidus lies near
650°C. Considering the proportion of fluorine in the bioti-
te and or tourmaline of both granites, and the accessory
fluorite, the presence of at least 5 weight percent HF in
the volatile fraction appears very reasonable. Larger
amounts of HF do not produce much additional depression of
the liquidus, and thus a temperature of 650°C is estimated
for the last stages of magmatic crystallization of the
Heemskirk massif. This estimation of temperature is in

good agreement with Barth's two-feldspar thermometer, for the red granite it is 650° C (see the chapter on mineralogy of feldspars).

10. Genesis of the Heemskirk intrusion

Heier and Brooks (1965) have suggested that the parent magma intruded to form the red granite which came in contact with and was contaminated by the already formed white granites and the surrounding sediments. Although Heier and Brooks (1965) suppose formation of the white granite from the reaction between the magmatic vapour phase and earlier crystallized granite, their graphic interpretation of the emplacement of the Heemskirk massif clearly shows the proposed mechanism of formation to be in two stages. The first magmatic activity corresponds to the intrusion of highly differentiated parent magma - the top portion of which is the white granite. The second activity consists of intrusion of parent magma into the white granite to form the red granite. This interpretation of the formation of the Heemskirk massif and of the relationship between the white and red granite does not agree with results of this study. Brooks and Compston (1965) report that the use of Sr^{87}/Sr^{86} ratio in granite rock as an index of anatectic

origin, reflecting the age and Rb/Sr ratio of its source region has not been convincingly demonstrated. According to the present field investigations the red granite forms a comparatively thin layer, while the white granite represents the major part of the Heemskirk intrusion at depth. There is probably no difference in the time of emplacement of the white and red granites, although the red granite may be older in the sequence of crystallization and consolidation of the Heemskirk granites. The major element composition of the rock indicate that there is very small variation in their chemistry and the white granites are almost identical to some of the red varieties.

Two modes of origin for the Heemskirk granite are considered plausible:

1) Fractional crystallization of the acid magma and

2) partial melting of surrounding rocks.

Although an origin by partial melting of surrounding rocks is possible for the upper part of the Heemskirk granite massif, an origin for whole granite body by fractional crystallization of an acid magma, derived partial melting of part of the lower crust, is favoured by the author. Such a magma would have to undergo extensive fractionation on a calc-alkaline trend before emplacement.

The relicts of the country rock structures in the massif

indicate a passive mode of the emplacement, the magma
digesting the Precambrian quartzites, modstones and part
of the Cambrian ultramafic and mafic rocks. This process
of partial melting affected the composition of both gra-
nites. Traces of contamination of granite magma by country
rocks were mainly found in granite types W1 and R1.

11. The age of the Heemskirk massif and its relationship to the granites of western Tasmania

Twelvetrees (1901), Ward (1909) and Waterhouse (1916)
suggested a Devonian age for the Heemskirk massif according
to geological and stratigraphical evidence. Evernden and
Richards (1961) report a biotite K - Ar age of 338 m.y.,
for the Heemskirk granite. According to McDougall and
Leggo (1965) biotite and muscovite from the Heemskirk mas-
sif yield K - Ar data ranging from 326 to 345 m.y. Most
of the results are in good agreement at 340 ± 5 m.y., and
this can be taken as a reliable minimum age for the time
of emplacement of the Heemskirk granite (i.e. Early to
Middle Carboniferous). According to Brooks and Compston
(1965) the ages of the red and white A granite by the
Rb-Sr method of whole rock samples are indistinquishable
at 354 m.y., but the white B granite (contaminated white
granite) could be several million years older. They report

the maximum age for the emplacement of the granite to be
400 m.y. or less, and the lower limit to the age of a hy-
pothetical metamorphism which is given by the biotite data
at about 354 m.y.

The spatial distribution of granitic intrusions in
Tasmania has a zonal character reflecting the general struc-
ture of the island. The out_er zone of the alaskite grani-
tes is most marked and coincides spatially and genetically
with Sn-W mineralization. These types of granites have
penetrated (northeast part of island) into the zone of re-
latively older granodiorites which coincide spatially with
Au mineralization.

The Heemskirk granite massif lies in the outher zone of
the alaskite granites with the Hampshire, Meredith and
Pieman Heads granite massifs (Hall and Solomon 1962).
The zone borders Precambrian rocks of the Rocky Cape ge-
anticline (Fig.1). The close relationship between tin de-
posits and those granite massifs seem to be significant in
indicating subsurface connections of individual outcrops
of granites. The distribution of tin mineralization indi-
cates that the Heemskirk and Meredith massifs and
Mt.Bischoff and Renison Bell complexes and probably also
Pieman Heads massif may be interconnected at depth (Hall
and Solomon, 1962 and Groves, 1967). The massifs in the
vicinity of the Heemskirk granite (Pieman Heads and

Meredith massifs) also show significant similarity in chemical and mineralogical composition (Groves 1967).

12. The problem of metallogenesis and relationship of the Heemskirk granite massif to the Pb-Zn mineral field

The problem of metallogenesis of the Heemskirk grani-te massif and its relationship to the Zeehan Pb-Zn mineral field[+] has been summarized by Both and Williams (1968). Twelvetrees and Ward (1910) suggested that the ore depo-sits in the Heemskirk and Zeehan field have a zonal re-lationship to the Heemskirk granite massif. This opinion is accepted by most later authors.

Twelvetrees and Ward (1910) modified Waller's observations (1904) on the zonal distribution of ores and divided those ore deposits spatially related to the Heemskirk granite massif into the following zones:

1) The granite zone consisting of ore-bodies in which cassiterite is associated with pyrite and minor wolfra-

---

[+]Zeehan mineral field is a large groups of Pb-Zn-Ag ore deposits in the vicinity of Zeehan township, 4 miles to east from the outcrop of the Heemskirk granite massif (see Fig. 58).

mite, Bi-ores and arsenopyrite.

2) The contact metamorphic zone including the magnetite lences close to the eastern outcrop boundary of the Heemskirk granite massif.

3) The transmetamorphic zone which consists of the pyritic belt (pyrite-sphalerite-galena or pyrite-galena) and the sideritic belt (siderite-galena).

Magnetite deposits within the contact metamorphic zone (Twelvetrees and Ward 1910) are apparently genetically related to Cambrian intrusives.
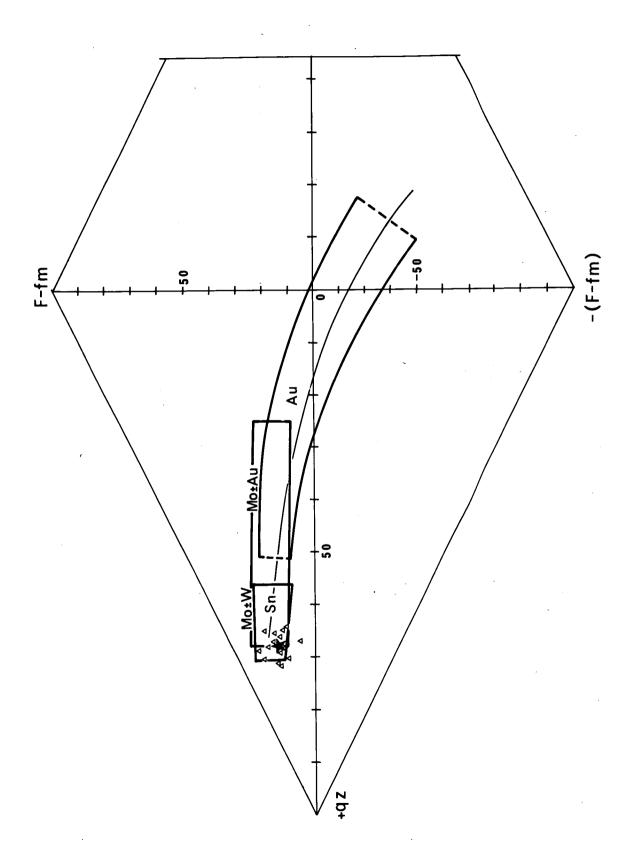
12.1. Relationship between the Heemskirk granite massif and tin mineralization

Tin deposits in or immediately adjacent to the Heemskirk granite massif show a relationship to the intrusion. This opinion is accepted by most geologists who have worked in that region. The problem was also discussed by Klomínský and Groves (1970). Tin mineralization is spatially related to the white granite being concentrated in both white and red granites. The majority of the ore deposits were found on the white/red granite contact. This observation is in agreement with the investigations of Heier and Brooks (1966) but disagree with interpretations given by Both and Williams (1968).

According to Sattran and Klomínský (1970) the classi-
fication of magmatogenic ore deposits on the basis of
petrometallogenic series is one of the ways of showing
the relationship between phenomena such as magma - igneous
rocks - magmatogenic ore deposits. The most varied range
of ores appears in connection with the differentiation of
the calc-alkaline series (Fig.57). The acid pole of the
calc-alkaline group partly coincides with the composition
of the tin-bearing granites of the different tin provinces
of the world (see Sattran and Klomínský 1970). This Sn
series of granites is characterised by a trend in chemi-
cal composition towards alkaline granites and by intensive
deuteric processes of alkalisation and greisenisation.

Sattran and Klomínský (1970) and others have suggest-
ed that the K/Na atomic ratio of the tin-bearing granitic
rocks aproaches 1.0 with K and Na (in atomic proportions
x 1000) both equal to about 100. These rocks have a cha-
racteristically low Mg and Fe content (Mg content in ato-
mic proportion x 1000 is less than 20 and generally below
10). Rattigan (1960) suggested that australian tin-bearing
granites have characteristically high K+Na/Ca+Mg ratios.
The K/Na atomic ratio 1.05 (111:106) and Mg content equal
to 6 in atomic proportions for the Heemskirk granite mas-
sif indicate that the intrusion is similar to typical tin-
bearing granites.

Figure 57

Diagram after Köhler and Raaz (1951) the mean dif-
ferentiation tendencies of the calc - alkaline
group of the petrometallogenic series of igneous
rocks and magmatogenic ore deposits (modified
after Sattran and Klomínský, 1970). The individual
series are designated by symbols (Sn, Mo±W, Mo±Au,
Au). Open triangles - individual samples of the
Heemskirk granite, black star - the average compo-
sition of the Heemskirk granite massif.

70/9/187

12.2. Relationship between the Heemskirk granite and the

Zeehan mineral field

The major features of the Zeehan Pb-Zn-Ag/Sn deposits
are summarised in Table 25, after Both and Williams (1968).
The zonal relationship originally postulated by Waller
(1904) and Twelvetrees & Ward (1910) was improved by Both
and Williams (1968) after detailed geochemical and minera-
logical investigations. They recognised a Cassiterite zone,
Pyritic zone, Intermediate (sidero-pyritic) zone and Si-
deritic zone (Fig. 58).
Both FeS and MnS contents in the sphalerite show a syste-
matic decline from west to east. These geochemical data
were treated by trend surface analysis. The third degree
trend surface for Fe in sphalerites is shown in figure 58.
Figure 58 shows the similarity between the trend surface
pattern of iron content in sphalerite and the distribution
of the individual mineral zones. The iron content above
10% corresponds with Pyritic zone. The Intermediate zone
covers the area between isolines 10% and 5% of the iron
content. Sideritic zone coincides with the iron content
lower than 5%.
From comparison of the figures 54 and 58 it is clear that
the distribution of the pyritic zone does not strictly

Figure 58

Schematic map of the Zeehan mineral field

1 - The Heemskirk granite massif

2 - Pyritic zone

3 - Intermediate zone (sidero-pyritic zone)

4 - Sideritic zone

    (Zonation according to Both and Williams 1968)

5 - Centre of hypothetic elevation of granite

    (the white granite)

6 - Aplites and porphyries

7 - Old Pb-Zn-Ag mines

8 - Major faults

9 - Major folds (synclines and anticlines)

10 - Isolines of trend surface of the Fe content

    in sphalerites (%) (third degree).

11 - Major roads and tracks

M. N.

1	
2	
3	
4	
5	
6	C
7	•
8	
9	
10	
11	

1 MILE
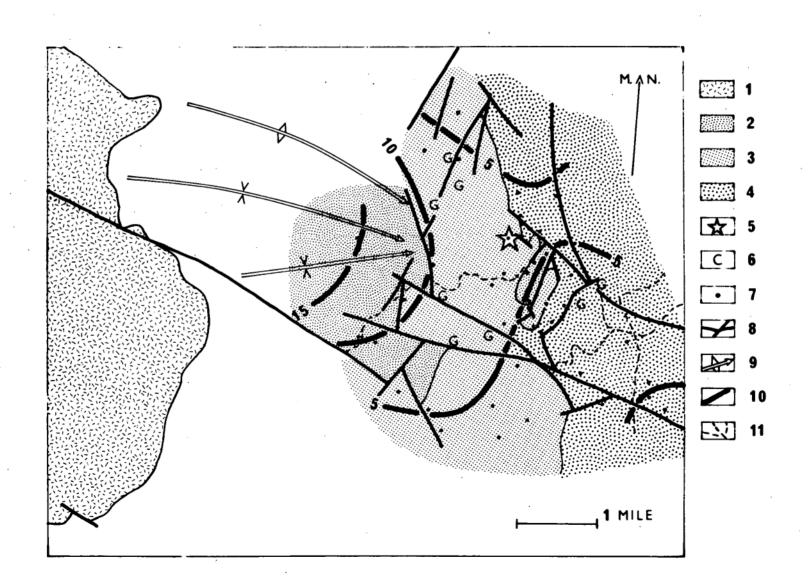
Table 25

General characteristics of the Zeehan mineral field

Geological position of ore bodies	Fissure veins located within rocks ranging in age from late Proterozoic to Early Devonian. Quartzites, silt-stones, shales to the north and west of Zeehan, similar rocks contain ba-saltic lavas and tuffs and beds of do-lomitic limestone (Solomon 1965) of Early Cambrian age.
Strike and dip	Major sets of veins NNW, others N - NNE dip mostly steep (60° or more).
Shape of ore bodies	Lenticular or highly irregular and apparently pinched out at depths of about 100 m. Width 0,01-5 meters. Strike length rarely exceeded one hundred meters.
Mineralogical zoning	Transitional nature of mineralogical zoning in horizontal plane.
Geochemical zoning	Gradual change of content of Iron and Mn in sphalerite.
Occurence of Stannite	The distribution of stannite in Queen Hill area represents one of the major anomalies in the zonal schemes of Waller (1904) and Twelvetrees & Ward (1910).

Emplacement of granite	Occurence of dykes of the granitic rocks in the middle of Zeehan field as the evidence of presence of granite body under Zeehan field (Both et al., 1969).
Superimposed zoning	Occurence of a separate intrusion beneath the Queen Hill.
Queen Hill area	The cupola was related to a second intrusive or mineralisation phase, emplaced in this area some time after a broad regional zoning had been established around the main body of the Heemskirk granite then simple explanation can be found for all the anomalous features.
Sulphur isotopes	Sulphide minerals from the Heemskirk granite and the adjacent Zeehan lead-zinc veins show a considerable range in sulphur isotopic composition. The range for the sulphides in the granite is simmilar to that of the lead-zinc ores and both groups show a overall enrichment in S^{34} with respect to meteoritic sulphur. Early minerals have consistently higher S^{34} values than those formed later in the sequence.

conform to the model proposed for the granite structure
of the eastern part of the Heemskirk granite massif.
The Pyritic zone and high iron content in sphalerites is
situated above the brachysynclinal closure between the
Mt. Agnew and Mt. Heemskirk antiforms. The hypothetic ele-
vation beneath the Oonah and Queen Hill may be a part of
that structure. According to Both and Williams (1968)
the blind granite stockwork in the centre of the Zeehan
mineral field complicates the relatively simple zonal
distribution of the ore minerals, and is genetically re-
lated to the tin mineralization (stannite and cassiterite)
occuring within the intermediate zone.
Both and Williams (1968) explain the presence of abundant
stannite in the middle of the Zeehan mineral field by
a reaction between tin-bearing fluids and pre-existing
sulphides. If the tin mineralization is related genetically
(sensu stricto) to the Heemskirk granite massif they admit
the emplacement of the sulphide mineralization in the
Zeehan field before crystallization and consolidation of
the Heemskirk granite massif. This is in agreement with
the unusual position of stannite and cassiterite in
the sequence of crystallization of the ore minerals in
the ore deposits. Tin minerals are considered to be one of
the youngest ore minerals in the mineral association of
the Zeehan field. The sulphur isotope study of Both,

Rafter, Solomon and Jensen (1969) of sulphides from the both Heemskirk and Zeehan field also indicate that the Zeehan ores were derived from two sources of ore fluids. According to Both and Williams (1968) each zone has a characteristic mineral association. They explain the anomalies as being due to the effect of faulting or granite structure underneath of the mineral field. The occurence of abundant Sb minerals (jamesonite) is association of sphalerite, cassiterite and fluorite in the granite - in the middle of cassiterite zone - is not explained.

12.3. Summary

1) Tin mineralization is spatially and genetically related to the Heemskirk granite massif (the white granite). Geochemical characteristics of the Heemskirk massif indicate that the intrusion is similar to other tin-bearing granites (in sense of Sattran and Klomínský 1970).

2) Pb-Zn-Ag mineralization in the Zeehan mineral field is characterized by a geochemical and mineralogical zonal structure.
   Zonation is probably controlled by:
   a) the distribution of the pre-existing stratiform ore deposits of Cambrian age (Rosebery type)

b) the lithology of the country rocks (carbonates)

c) the relief of the granite intrusion beneath
   the Zeehan mineral field (white granite).

The relationship between the Zeehan mineral field and the Heemskirk granite is probably a pseudogenetical[+] one. The emplacement of the ore deposits and the zonal distribution of the ore minerals could be controlled by the intrusion of the Heemskirk massif. From this point of view the Zeehan mineral field (Pb-Zn ores) may represent a type of regenerated ore deposit (in the sense of Schneiderhöhn's theory).

[+] Pseudogenetical relationship - genetic relationship between mineralization and igneous rocks sensu lato - the source of metals is outside of the intrusion, and hydrothermal fluids from intrusion provide the redistribution of the metals with zonal pattern around the intrusion.

13. Conclusions

The Heemskirk granite massif is an epizonal body intruded into extensively folded Proterozoic to Cambrian rocks (mainly sediments). The intrusion consists of the red and white granite, the bulk chemical compositions of which are very similar. However, discriminant analysis of rocks and minerals by trace element data proved significant differences in composition of the red and white granites with the white granite showing a higher degree of geochemical homogeneity than the red granite. Zr, Sr and Rb contributes most to the discrimination between the red and white granites.

The intrusion has a generally stratiform character, with the sequence from the bottom to the top: coarse-grained white granite $\longrightarrow$ medium- to fine-grained white granite $\longrightarrow$ medium- to fine-grained red granite $\longrightarrow$ coarse-grained red granite. All rock types are granites according to the classification of Hietanen (1963).

A characteristic mineral component of the granites is tourmaline (schorl) and the roof zone of the white granite is enriched by the tourmaline nodules. They are proto, single-shell orbicules with granular and/or radial cores dissimilar to matrix. The origin of tourmaline nodules as

volatile segregations in crystallizing magma is favoured in this study.

The upper part of the Heemskirk body has a flat cupola-like structure and the surface of the body reflects on a subdued scale the anticlinorial structure of the original sedimentary cover. The structure of the country rocks has the form of a brachyanticlinorium. The existence of the ghost structure of the country rocks in the roof of the intrusion is also indicated by the distribution of the contaminates and positive anomalies of some trace elements, particularly within the red granite.

Trend surface analysis demonstrates the existence of very strong and consistent gradients for each trace element examined within the Heemskirk massif. Major axes of the trend surfaces are parallel and superimposed and virtually identical trends were found for large number of trace element patterns. In general the major axes of the surfaces are orientated in the red granite predominantly in N-W direction while in the white granite mainly in the NW-SE direction.

13.1. Internal structure and tectonics

Almost all the studied trace elements exhibit a discontinuity in their regional patterns between the red and

white granite. The discordance of the isopleths at
the contact indicates the continuation of the flat cupola-
-like structure beneath the red granite further east.
Particularly well developed is the Mt.Agnew antiform which
bifurcates towards the west. The Mt. Agnew and Mt.Heems-
kirk antiforms are separated by a brachysynclinal depres-
sion. The antiformal axes are approximately parallel in
an E-W direction. The majority of quartz-tourmaline veins
and greisen zones, commonly tin-bearing, are concentrated
in the apical part of both antiforms. Economically im-
portant accumulations of Sn in the red granite area are
commonly located in close proximity to the contact with
the white granite. The distribution of Sn concentrations
at the present surface is related to the thickness of the
preserved layer of the red granite i.e. on the depth of
the contact below the present ground level. Where the
thickness of the preserved red granite layer exceeds
600 feet any economically important tin mineralization will
not crop out. The greatest thickness of the red granite
exceeding 1000 feet is probably in the depresion east of
Mt.Heemskirk. The red/white granite contact is expected to
be less than 600 feet below the present surface in the
broad area in the southern and western parts of the
Mt.Agnew antiform and in narrow belt west of Mt.Heemskirk,
and this area may therefore warrant exploration.

The Heemskirk granite massif is characterised by very regular fracture systems. Cross joints are the system of long joints which strike NNE predominantly showing very shallow doming with fan-like structure to the dip. Extensive greisenisation and hydrothermal alteration follow the croww joints. The filling of the fissures is quartz, tourmaline and frequently cassiterite.

13.2. Petrogenesis

The normative composition of the granite massif interpreted in light of experimental data suggest that most of it crystallised at a P_{H_2O} of approximately 500 bars, suggesting that the massif was emplaced at a rather shallow depth. A temperature of $650^{\circ}C$ is estimated for the last stages of magmatic crystallization. It is suggested that the body formed by fractional crystallization of an acid magma, derived by partial melting of lower part of crust and local digestion. The relic_s of the country rock structures in the massif indicate passive mode of the emplacement, the magma digesting the Precambrian quartzites, mudstones and part of the Cambrian ultramafic and mafic rocks.

The Pieman Heads and Meredith massifs in the close vicinity of the Heemskirk massif show significant sim_ila-

rity in chemical and mineralogical composition. The distri-
bution of tin mineralization indicates that the Heemskirk
and Meredith massifs and Mt.Bischoff and Renison Bell
complexes may be interconected at depth.

The difference between the red and white granites is
in the different content of volatiles and different oxygen
fugacity producing during crystallization different mi-
neral assemblages in the granites. The characteristic mi-
neral assemblage of the red granite (heamatite-magnetite-
-allanite) corresponds to the higher oxygen fugacity in
the granite. The red and white granites are probably two
magmatic phases of rocks represented by the several rock
types all belonging to magma. Differences between the red
and white granites developed gradually during and after
emplacement. The red granite occupies the topmost part of
the intrusion and toward the west is lateraly replaced by
the white granite. The red granite was consolidated
earlier than the white granite.

13.3. Metallogenesis

Occurences of columbite, lepidolite, Ag-tetrahedrite
and jamesonite are described from the Heemskirk granite
massif for the first time. The most interesting oc-
curence of columbite is in the vicinity of Allison's

Workings and could have economic importance.

The relationship between the Heemskirk massif and tin mineralization in and immediately adjacent to the granite has a genetic nature sensu stricto, while the relationship between the Zeehan Pb-Zn mineral field and the Heemskirk granite massif could be classified as a genetic relationship sensu lato (pseudogenetic relationship).

APPENDICES

APPENDIX I

Regional Geochemistry and Relationship of Granitic Rocks
to Ore Deposits in the Tasman Orogenic Zone (Eastern
Australia)

I-1. Introduction

The results of Lindgren (1915), Buddington (1927)
and more recently Viewing (1968) and Hall (1969), indicate
the existence of systematic variations in the compositions
of granitic rocks within the orogenic zones and show
the possibility of the quantitatively defining the rela-
tionship between granitic rocks and ore deposits on the
basis of their chemical composition. These authors suggest-
ed that the granitic rocks with the relatively higher K
content are concentrated in the periphery of the orogenic
zones or cratons.

Sattran and Klomínský (1970) postulated on an empiri-
cal basis   characteristic atomic Na/K and Mg/K (Na)
ratios for typical tin bearing and gold-bearing granitic
rocks in the Bohemian massif (Central Europe). These authors
found the atomic amounts of Mg as 10-15 and Na/K ratios of
1.0 for typical tin-bearing granites and Mg 50 and Na/K
ratio 2.0 for characteristic gold-bearing granitic rocks.

Similar contrasts in the composition of granitic rocks spatially related to tin and gold ore deposits was indicated by Klomínský and Groves (1970) in Tasmania.

For the purposes of this study regional geochemistry was used both to determine the distribution of granite rock-types in the Eastern Australia and as a measure of the relationship of these granitic rocks to mineralisation (chiefly Au and Sn). Trend surface analysis has been used to measure regional variation in the composition of .the eastern Australian granitic rocks. The variation in Na/K ratio and Mg in atomic amounts x 1000 are illustrated also in hand contoured geochemical maps.

I-2. Analytical Data

Data for the study of regional geochemical variations in granitic rocks in Eastern Australia is based mainly on the work of Joplin (1963), Branch (1966), Crowder (1968), Kryser and Lucas (1969), Rattigan (1968), Groves (1968), and Shaw, Phillips, Lawrence and Nickinson in Packham (1969). From figure 59, 60 it can be seen that the distribution of data is not uniform in the scattered outcrops of granitic intrusions and also in that there is a lack of sufficient analytical data for Queensland.

A study of the systematic regional variation in the compositions of granitic intrusions is hence restricted to

Victoria, New South Wales and parts of Tasmania and
N.E.Queensland.

The 270 available samples are marked as points on
the maps (Fig. 59, 60, 61, 62). Numerous examples are
means of several analyses from a single locality or within
distance which are negligible on this scale. All analyses
of minor intrusive phases or obviously unrepresentative
material were excluded (microgranite, porphyry, aplite,
pegmatite and altered rocks). Incomplete analyses and those
published before 1930 were also excluded as being chemical-
ly unreliable. The analyses range between granite and
granodiorite.

The constituents of the rocks whose variation was
considered to be of most interest were Na, K and Mg.

I-2.1. Trend surface analysis

Trend surface analysis was carried out for the Na/K
ratio and Mg. Because of the heterogeneity of the eastern
region of Australia and the non-uniform distribution of
analyses, trend surface analysis was carried out for three
separate regions (Region A - Tasmania, Victoria and south-
ern part of New South Wales; Region B - New England; and
Region C - Herberton area in Queensland).

The results of the trend surface analysis represented

by linear and quadratic and cubic surfaces are illustrated
in figures 59, 60, 61, 62. Measure of variability for gi-
ven trend surfaces is based on the percentage of the total
sum squares.
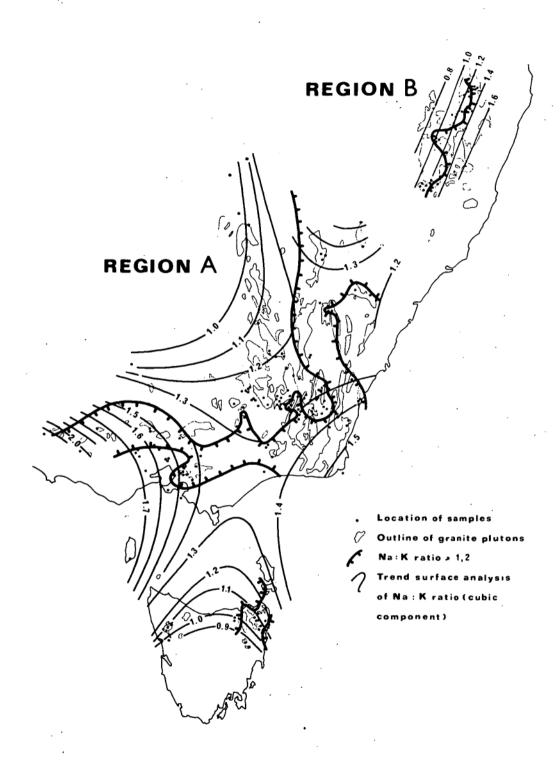
I-3. Results

I-3.1. Na/K Ratio

The existence of regional variations for Na/K can be
seen from figures 59, 60 in which hand made contours
arbitrarily chosen as 1.2 are illustrated. Ratios smaller
than 1.2. represent a prevalence or granites (s.s.) and
ratios greater than 1.2. indicates a tendency towards
granodiorites.

In the Tasmanian area the Na/K ratio is less than 1.2.
Higher values are very localised and occur in the North
East around Scottsdale and the south west part of Flinders
Island. The distribution of Na/K values in the Victoria
and south west New South Wales is bilaterally symmetrical.
The maximum Na/ K ratios lie in an L-shaped zone. In
Victoria this zone trends E-W and in New South Wales in
a NNW direction. On both sides of the zone and mainly on
the inside Na/K ratio is considerably smaller than 1.2 and
tends to decrease towards the peripheries of the zone.

241

Figure 59

The trend surface analysis (third degree) and hand
contours for Na:K ratio (computed as atomic amounts
x 1000) in granites of south-eastern Australia
(region A and B). The percentage of the variation
explained by the cubic component in the Na:K surfa-
ce is 28 % for region A and 39 % for region B.

REGION B

REGION A

- Location of samples
- Outline of granite plutons
- Na : K ratio ⩾ 1,2
- Trend surface analysis
  of Na : K ratio (cubic
  component)

Distribution of Na/K ratio in New England (Region B) is considerably simpler. Isoline 1.2 divides the granite batholith into two parts in the NE-SW direction. In general on the west the values are less than 1.2 while on the east the values are higher than 1.2.
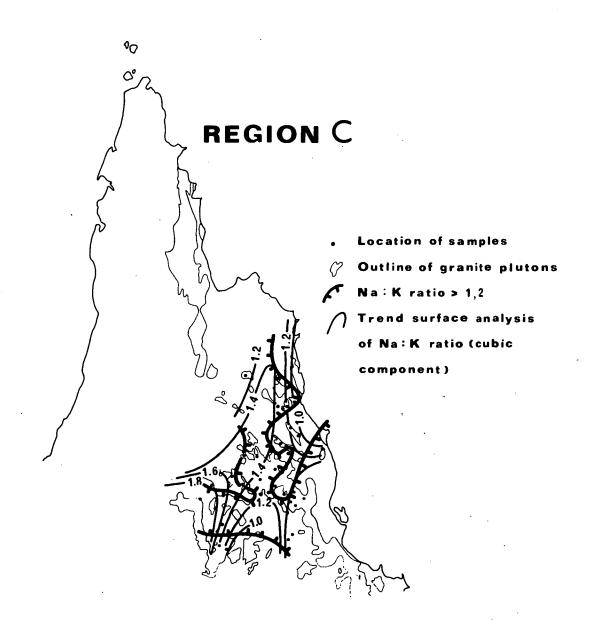
In the Herberton area (NE Queensland) the Na/K ratio distribution is more complex (Fig. 60). A limited number of analyses and their complete absence from the northern and southern areas seriously restricts the possibility of characterizing the granites in this region of the Eastern Australian orogen.

All the values greater than 1.2 are in zones firstly trending in a N-S direction and secondly trending E-W. On the periphery of these zones there are granites of lower Na/K values. The distribution pattern of the Na/K ratio in this area is basically similar to the pattern of the Victorian and south west New South Wales area. The existence of the systematic regional variation of Na/K ratio in the granitic rocks within the East Australian orogenic belt is further proved by results of the trend surface analysis. In region A which covers Tasmania, Victoria and southern part of New South Wales (Fig.59) the some features of distribution of Na/K ratio which were described above can be seen. The area of

Figure 60

The trend surface analysis (third degree) and hand
contours for Na:K ratio (computed as atomic amounts
x 1000) in granites of the Georgetown area (region C)
in Queensland. The percentage of the variation ex-
plained by the cubic component in the Na:K surface
is 26 %.

REGION C

Location of samples
Outline of granite plutons
Na : K ratio > 1,2
Trend surface analysis
of Na : K ratio (cubic
component)

western Victoria is occupied by maximal values of Na/K
ratio. On the other hand the lowest values are in Tasmania
and in the south west area of New South Wales. The eastern
Victoria and southern New South Wales area is transitional,
with Na/K value 1.3 to 1.4 with a tendency for the ratio
to increase in both south and east directions. The shape
of those trend surface suggests some features of bilateral
symetry. In general the periphery is occupied by relatively
low Na/K ratios, where as the areas around the axis of
symetry are higher or maximal.
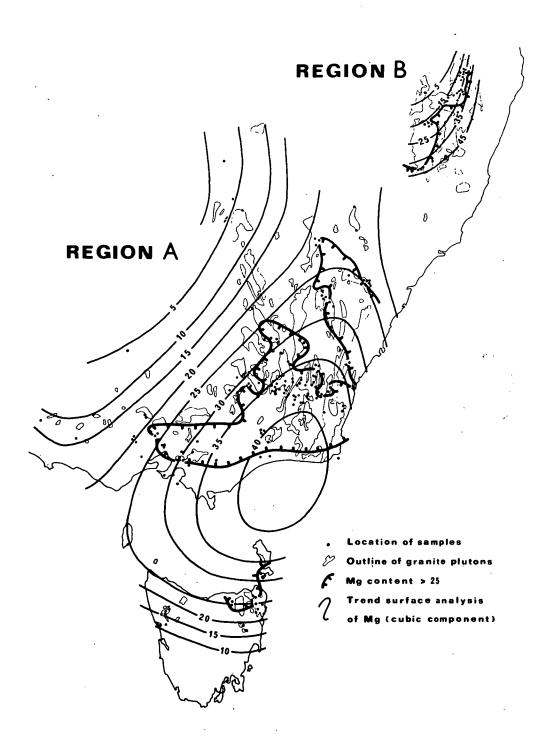
In region B which predominately covers the isolated
New England block linear trend surface illustrates a gene-
rally decreasing tendency of Na/K ratios from SE to NW.

In region C the shape of the trend surface suggests
a bilateral symetry with the maximum Na/K ratios along
an axis orientated NE-SW. Lowest values of Na/K are predo-
minantly on the peripheral areas which corresponds approxi-
mately to the spread of Sn mineralisation.

I-3.2. Magnesium

The existence of regional variation of Mg in granitic
rocks of the East Australian orogenic belt can be seen in
figures 61, 62. Values higher than 25 (in atomic amount
of Mg x 1000) indicate prevalence of rocks of adamelite –

Figure 61

Trend surface analysis (third degree) and hand
contours for Mg content (computed as atomic amounts
x 1000) in granites of south-eastern Australia
(region A and B). The percentage of the variation
explained by the cubic component in the Mg surface
is 13% for region A, and 34% for region B.

REGION B

REGION A

Location of samples
Outline of granite plutons
Mg content > 25
Trend surface analysis
of Mg (cubic component)

- granodiorite composition.
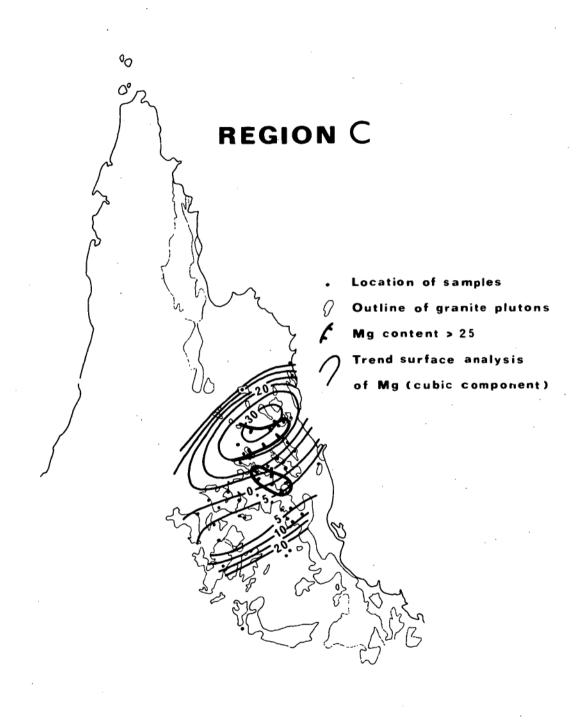
In the area of Tasmania there is a prevalence of values less than 25 and areas of higher values are approximately the same as areas with maximal Na/K values (Fig.6).

Distribution of Mg in Victoria and southern New South Wales shows a slightly different pattern than Na/K ratio. In general the shape of contours delimiting the higher Mg values reflects also the L-shaped structure of the granitic intrusives namely in the Victoria and southern part of New South Wales area. The majority of the lowest values of Mg lie on the periphery of this sharp reverse L-shaped zone. In the New England region the Mg isoline 25 approximately copies the Na/K isoline 1.2.

Region C is characterised by generally low Mg values (Fig. 62). Only a few values deviate from this pattern and those granitic rocks occupy a fairly limited area approximately in the centre of this region.

The existence of systematic variations in Mg content in granitic rocks of the East Australian orogenic belt was further proved by the trend surface analysis. In region A the shape of the trend surface suggests also a bilateral symmetry with maximum values of Mg in the centre of orogenic belt. A marked feature illustrated in figure 61 is the decrease of Mg in both NW and S directions towards the older stable blocks (Murry and Tasmania blocks). This

Figure 62

Trend surface analysis (third degree) and hand
contours for Mg content (computed as atomic
amounts x 1000) in granites of the Georgetown
area (region C) in Queensland. The percentage of
the variation explained by the cubic component
in the Mg surface is 18%.

REGION C

Location of samples

Outline of granite plutons

Mg content > 25

Trend surface analysis

of Mg (cubic component)

feature corresponds roughly to the distribution of Na/K
ratios in the region and is important in relation to
the problem of the geometry of the orogenic belt (symmetry
or asymmetry). In region B trend surface analysis of Mg
shows a very simple pattern with a decreasing tendency of
Mg content towards the NW.

In region C the shape of the trend surface has the sa-
me orientation as the trend surface pattern of Na/K ratio.
All isopleths lie below an arbitrarily selected value of
25 (atomic amount of Mg x 1000). In general the trend surfa-
ce of Mg in this region is bipolar as in Regions A and B.

I-4. Discussion

Hand contoured maps and the trend surface analysis
indicates that there is a remarkable regional variation in
the composition of East Australian granites. In region A
the pattern is defined by a ridge of high Na/K ratios and
the Mg content. The shape of this L shaped structure indi-
cates a bilateral symmetry. In region B the pattern of
systematic geochemical variations is defined by a substan-
tial decrease of Na/K ratio and Mg towards the west.

In region C, the general shape of trend surfaces of
Na/K ratio and Mg are very similar and show signs of bila-
teral symmetry as in region A (Fig. 6o, 62).

Mg trend surface does not show such a steep gradient as in region A and B. In all the regions substantial regional variation probably reflects basic features of crustal structure beneath the folded sediments of the Tasman Geosyncline.

A characteristic feature of the granitic rocks in the studied part of Australia is a markedly higher content of potassium and complementary lower content of Mg on the western side of the orogenic zone which is adjacent to the older Precambrian cratonic blocks. That is, the higher content of potassium and lower Mg content in granites are closely associated with the edges of older cratonic blocks. This was also found by Lindgren (1915), Buddington (1927), Hall (1969), Viewing (1968) and Engel (1968), in various part of the world.

In the east australian orogenic belt a central zone of granitic rocks is usually situated in the area of most intensive metamorphic and tectonic activity, in places of the deepest sinking of geosynclinal sediments into relatively thin crustal material. This granodiorite-adamellite suite can be derived from mixed material from the transitional zone between the crust and upper mantle. Towards the periphery of the orogenic zone there is an increase in granites derived from continental crust. The granite-adamellite suite is richer in alkalies (Na,K) and relatively

deficient in Mg. A major feature is the geometry of the geochemical variations of the granites of the Tasman geosynclinal zone. The bilateral symmetry in some parts of the orogen supports the idea of the distribution and thickness of stable cratonic blocks on both sides of the orogenic belt. Where there is an obvious asymmetry (New England block) it can be expected that part of the orogenic zone together with the stable basement is missing due to continental drift.

I-4.1. Relationship of granitic rocks to the endogenous ore deposits

A discussion of the genetic relationship of the granitic rocks to the endogenous ore deposits is based on Niggli's idea that the metallogenesis is essentially a continuation of petrogenesis and tries to answer Bateman's (1951) question "Why ore is where it is?" The relationship of the composition of granitic rocks to endogenous mineralisation is discussed on the basis of the principles of substitution of elements according to Goldschmidt (1937) and Vendel (1956).

The possibilities of the accumulation of a certain element increases when the diadochically bonded cations of a certain element exceed the saturation limit of the major

elements of crystallising magma, which are suitable for substitution according to atomic properties (size of atoms, electronegativity etc.). For example Sn for Fe, Mg; Au indirectly for K. For the accumulation of Sn granitic magma which has a low content of Fe, Mg is the most suitable; for Au concentrations magmatic associations with a prevalence of Na over K. Similar results were obtained by H.Schneiderhohn (1925), Spurr (1923.), Vogt (1898), Buddington (1933), Gallagher (1940), Rattigan (1963), Sattran and Klomínský (1970) et al.

I-4.2. Geochemical patterns in relation to ore deposits

From a comparison of the geochemical maps with the distribution of ore deposits it is evident that the potassium rich and Mg poor granites occur in the vicinity of the tin deposits and granitic rocks with prevalence Na and rich in Mg are situated in the vicinity of the Au deposits. Atomic amount of Mg for tin-bearing granites in East Australian orogenic belt is not higher than 30.

Mg/K ratios for Au metallogenic provinces indicate a remarkably larger spread with an increase of Mg content and decrease in K content. The characteristic average for Mg/K ratio is 40:60 (in atomic amounts x 1000). Limit of the spread of data of Au provinces lies around the Mg 25 (atomic amount x 1000).

I-5. Summary

As can be seen from the above description, granitic rocks spatially related to endogenous Sn and Au deposits are characterised by very specific and markedly different chemical composition. The determined ratios of Na/K in this study are consistent with the values published by Sattran and Klomínský (1964, 1970) for Central Europe and major Sn, Au provinces throughout the world and with results of Rattigan (1963) for Sn-bearing granites of Australia.

From this comparison it can be concluded that the spatial relationship of the granitic rocks to Sn and Au mineralisation in the considered areas of the East Australian orogenic belt is also a genetic one. The distribution of Sn ore deposits within the Australian orogenic belt is controlled by the distribution of granites with a low Mg content and an average Na/K ratio around 1.0. On the other hand endogenous Au mineralisation shows a close spatial and apparently also genetic relationship to the rocks of tonalitic composition with a remarkably high Mg content and Na/K ratio varying from 1.3 to 2.0.

APPENDIX II

Analytical procedures

II-1. XRF - Analytical methods

All analyses of trace elements were performed with
a Philips vacuum X - ray spectrograph (P.W. 1540)
(results see Tab. A-1, A-2, A-3, A-4 and A-5). Samples
were prepared as pressed powder pellets with boric acid
backs and edges according to the method given in Norrish
and Hutton (1964) A minimum of 2 gm of rock and mineral
powder respectively was used in the X - ray analysis to
ensure an "infinitely thick" sample. The conditions of
analysis are given in Table A-11.

Standards were prepared by diluting a pure compound
of the element to be analysed with powdered kaolin to
obtain varying concentrations and thoroughly mixing the
resultant powder in a Siebtechnik vibratory grinding mill.
Kaolin was chosen as a dilument as its chemical composi-
tion is essentially constant and its mass-absorption is
fairly close to the mass absorption of granites. However,
the kaolin used contained some of the trace elements to
be analysed and to overcome this kaolin blanks were pre-
pared along with the standards. Measurments of these

blanks revealed the original trace elements content of the kaolin thus the trace element concentration of the standards was known. A blank of pure SiO_2 was prepared by crushing clear quartz crystals, boiling the resulting powder with aqua regia and washing it with deionized water. The powder was then permanently mounted in a Philips specimen holder and used to determine contamination from the X-ray tube, fittings in the vacuum chamber, and chemicals used in preparative procedures. The accuracy of the results was tested by analysing the standard rocks G1, G2, T1, S1, AGV1, BR, DTS1, and biotite standards and comparing the results with the recommended values and with results obtained by Thomas Kempe (1963), Fleisher Stevens (1962) and Leake and others (1669). The comparisons show that most results fall within the range of values obtained by other analysts for the standard rocks and that many results are close to the recommended values.

Machine conditions for analysis were adjusted to give maximum sensitivity in as short a counting time as possible while keeping the counting error to a reasonably low level (Table A-11).

The matrix corrections were applied to the determination of most trace elements using the "Compton Scattering" technique of Reynolds (1963). The range of elements that may be studied is limited by the absorption edge of Fe in

the long wave-length direction and by capability of the
equipment to excite and measure the K_α spectra of
the heavier elements in the short wave-length direction.
For elements such as Ba, mass-absorption of the sample has
been calculated from the mean chemical analysis of the red
and white granite respectively. For biotites the mean che-
mical composition of the biotites from the tin-bearing
granites was chosen.

Duplicates of the rock samples (slabs and powders) are
stored in the Geology department of the University of
Tasmania.

II-2. Precision and accuracy of analyses

Table A-12 records the means and standard deviations
of repeat determinations on a single sample of the rock
and biotite. The number of repeat determinations is given
in the third column and the coefficient of variation in
per cent, for each element, in the fourth column, where:

$$C = \frac{100 \times \text{standard deviation}}{\text{mean}}$$

The accuracy of the data may be noted from table A-13
which shows respectively the author's analyses of standards
G-1, G-2, T-1 and W-1.

Table A-1

N	U	V	W	Rb ppm	Sr ppm	Na %	Zr ppm	F %	Nb ppm	Pb ppm	Ba ppm	Sn ppm
2	663	1689	2450	564.	1	3.48	131	0.120	20	49	41	19
3	435	1607	1600	339	27	2.97	282	0.157	13	40	195	18
4	734	1367	1450	469	10	3.52	118	0.174	17	40	7	18
5	736	1371	1450	356	22	3.05	212	0.201	13	43	128	17
6	1016	1434	2400	506	3	3.60	154	0.100	27	42	10	20
7	1009	1409	2200	459	11	3.59	127	0.192	4	49	14	11
8	987	1379	2100	490	4	3.34	161	0.179	17	53	19	22
9	485	1782	1550	344	24	3.01	238	0.216	7	39	132	24
10	400	1703	1400	338	22	3.15	254	0.216	12	51	167	21
11	573	1892	2770	342	34	3.06	202	0.233	4	40	217	21
12	652	1807	2500	351	49	3.02	244	0.107	4	33	299	23
18	698	1551	1950	410	17	3.54	155	0.120	14	61	6	18
19	650	1526	1400	433	6	3.22	147	0.115	14	34	25	18
21	852	1852	2450	410	38	3.34	237	0.209	17	32	255.	18
23	613	2037	1400	378	8	3.33	161	0.088	3	33	61	15
24	610	1989	1450	389	13	3.24	230	0.125	22	44	68	15
25	787	1875	2350	345	35	3.14	214	0.178	12	50	251	13
26	736	1954	1350	423	29	3.31	233	0.188	16	44	166	26
28	988	1887	1950	349	35	3.12	224	0.178	9	40	226	26
29	1012	1852	1950	621	1	3.96	120	0.165	35	43	17	17
31	1063	1648	1500	474	1	3.49	213	0.144	26	32	19	26
32	1060	1615	1350	349	25	3.15	165	0.225	9	36	173	27
33	1108	1624	1050	513	13	3.72	214	0.278	26	44	45	41
34	1180	1649	1000	344	20	3.20	196	0.200	15	54	148	26
35	1176	1442	1450	443	10	3.74	155	0.177	23	63	38	30
36	1094	1401	2150	203	91	3.79	295	0.138	1	30	467	24
37	1135	1396	1850	454	4	3.38	154	0.156	48	48	38	33
39	354	1878	650	372	24	3.12	247	0.127	19	43	154	25
40	291	1509	550	338	32	3.14	196	0.195	13	56	223	26
41	265	1666	650	331	28	3.02	203	0.224	17	41	169	27
42	311	1860	650	321	27	3.14	168	0.174	17	40	185	23
43	328	1753	700	315	27	3.11	206	0.172	12	33	185	27
44	270	1741	600	312	29	3.15	204	0.205	12	43	151	17
45	289	1600	550	300	32	3.18	182	0.209	6	28	199	23
47	362	1955	650	408	22	3.14	227	0.138	14	48	179	20
48	377	1525	600	327	34	3.10	204	0.187	14	37	249	15
49	397	1586	1000	322	35	3.17	190	0.124	14	42	219	26
52	290	1442	450	300	32	3.12	231	0.185	10	31	217	17
53	685	1466	1500	389	20	3.30	189	0.208	14	31	109	19
55	617	1426	800	400	7	3.09	130	0.200	4	47	79	29
56	566	1307	400	413	22	3.00	166	0.132	24	44	100	25
57	500	1592	1250	408	14	2.67	183	0.231	22	39	131	26
63	509	1342	600	383	8	3.04	133	0.185	4	44	101	29
69	219	1525	400	339	25	3.13	238	0.196	7	51	162	17
70	232	1324	10	317	41	3.11	233	0.168	9	34	236	19
71	752	1652	2300	361	20	3.00	203	0.250	16	38	155	22
72	723	1800	2500	382	18	3.00	192	0.250	14	33	115	23
73	668	1871	2750	345	32	3.32	212	0.203	7	45	227	23
74	677	1759	2300	375	24	3.03	227	0.132	17	29	156	21
75	1133	1544	1350	474	6	3.85	161	0.118	13	36	60	15
76	963	1502	2150	352	21	3.31	224	0.178	14	32	139	22
77	993	1462	2450	369	25	3.38	230	0.187	10	52	165	23
78	1068	1452	2300	212	85	3.96	300	0.125	9	39	454	18
79	1007	1775	1500	304	39	3.29	248	0.145	14	36	352	22
80	949	1783	1450	378	22	3.27	230	0.217	13	49	171	27
81	1228	1665	800	352	41	3.35	271	0.140	6	36	158	34
86	1233	1351	850	320	39	3.02	255	0.187	10	36	259	16
104	860	1470	1650	361	18	3.30	145	0.158	9	49	88	28
105	807	1407	1250	385	20	3.06	226	0.161	9	51	162	25

Table A-1

Table A-2

ROCKS - White Granite

#	U	V	W	Rb ppm	Sr ppm	Na %	Zr ppm	P %	Nb ppm	Th ppm	Ba ppm	Sn ppm
1	1496	234	10	501	32	2.60	185	0.128	4	50	312	12
13	919	1180	1300	595	1	3.73	62	0.142	19	95	7	31
14	952	1058	1000	599	3	3.67	71	0.100	19	54	19	28
15	1093	1057	1350	567	1	3.47	41	0.201	17	61	37	27
16	1164	979	950	513	6	3.40	100	0.165	14	37	64	31
17	1245	958	800	530	10	3.35	87	0.165	6	47	46	27
20	603	1510	1050	507	1	3.25	113	0.095	16	43	45	23
22	851	1892	2350	625	1	3.63	157	0.171	45	50	35	21
27	732	2000	1150	521	11	3.58	155	0.197	63	46	23	22
30	1020	1971	1900	498	14	3.66	161	0.120	30	51	50	33
38	408	1909	700	642	1	3.65	127	0.106	43	50	18	28
46	392	1962	650	490	7	2.94	200	0.138	13	33	59	19
50	514	1435	600	369	1	2.91	71	0.132	22	58	6	24
51	418	1475	600	618	1	3.32	66	0.116	42	42	6	18
54	651	1443	1150	480	8	3.29	120	0.211	14	58	45	31
58	531	1621	1650	514	1	3.44	83	0.110	14	41	35	27
59	506	1129	400	557	3	3.26	69	0.169	6	44	43	33
60	461	1091	10	564	6	3.21	65	0.253	23	48	55	29
61	380	1180	10	550	3	3.20	58	0.196	7	39	28	29
62	354	1253	10	562	1	3.37	72	0.114	14	68	37	46
64	548	1434	650	469	27	3.29	118	0.143	17	62	159	32
65	682	1176	650	557	4	3.45	76	0.211	14	67	10	34
66	642	1271	550	602	1	3.36	66	0.166	20	53	37	27
67	278	1309	200	535	10	2.99	79	0.174	19	42	119	24
68	764	924	200	524	7	3.29	79	0.215	16	53	54	29
82	1140	626	200	331	42	2.61	142	0.156	3	61	217	16
83	989	682	200	408	27	2.96	110	0.135	4	52	152	20
84	1089	1234	800	619	1	3.63	90	0.137	16	48	8	21
85	1083	1306	900	577	1	3.45	71	0.181	23	61	8	23
87	1246	1264	750	222	81	4.24	83	0.080	9	22	46	18
88	1450	303	10	572	1	3.53	65	0.152	17	37	8	3
89	1515	332	100	408	15	3.23	113	0.233	10	31	55	17
90	1236	567	150	473	10	3.18	79	0.172	1	48	53	21
91	1344	465	10	378	66	2.79	147	0.143	1	49	305	23
92	1403	748	500	298	78	2.55	206	0.129	4	52	390	21
93	1012	881	400	524	4	3.75	79	0.129	14	50	60	23
94	1112	882	650	515	3	3.55	80	0.095	10	43	45	28
95	1038	1132	1350	406	36	2.97	120	0.180	6	59	200	21
96	589	1012	10	537	8	3.21	83	0.145	23	51	51	26
97	655	965	100	515	6	3.34	92	0.224	9	44	77	25
98	813	795	10	503	14	3.16	93	0.201	16	63	80	43
99	789	1290	900	621	1	3.75	61	0.141	32	59	8	30
100	762	1187	1000	535	1	3.35	62	0.183	12	57	34	32
101	1378	568	250	439	17	3.23	89	0.090	9	52	103	35
102	1341	750	450	356	35	3.07	140	0.140	7	44	181	27
103	1339	643	350	378	7	3.49	55	0.088	3	38	12	27

U V - COORDINATES, W - ALTITUDE

Table A-3

Biotite   Red granite

N	U	V	W	Rb ppm	Sr ppm	Sc ppm	Ni ppm	Cr ppm	F %	Cl ppm	Zn ppm	Nb ppm	Sn ppm
2	663	1689	2450	85	‹3	123	375	66	0.09	350	440	752	64
3	435	1607	1600	891	‹3	135	198	55	0.47	5050	200	251	60
4	734	1367	1450	356	6	149	229	69	0.42	310	370	487	64
5	736	1371	1450	281	9	104	226	66	0.40	2080	350	251	46
6	1016	1434	2400	1169	‹3	86	561	66	0.63	4210	380	441	95
7	1009	1409	2200	921	21	79	403	64	0.61	4280	470	367	119
8	987	1379	2100	196	‹3	130	536	107	0.01	210	730	424	55
9	485	1782	1550	613	3	78	186	61	1.07	2890	350	233	61
10	400	1703	1400	695	‹3	76	251	61	1.03	3830	450	233	29
11	573	1892	2770	782	‹3	83	326	70	1.20	3320	220	219	95
12	652	1807	2500	529	‹3	83	285	83	0.51	3860	260	194	41
18	698	1551	1950	121	12	88	316	73	0.41	1150	410	268	70
19	650	1526	1400	861	6	106	291	54	0.21	4510	180	399	81
21	852	1852	2450	1000	3	89	468	56	1.20	3160	220	273	64
23	613	2037	1400	30	‹3	65	195	66	0.02	150	620	282	24
24	610	1989	1450	139	24	74	456	71	0.16	1000	300	350	105
25	787	1875	2350	991	‹3	66	214	60	1.35	2970	330	202	60
26	736	1954	1350	45	18	99	267	77	0.32	560	460	316	91
28	988	1887	1950	1129	6	79	220	58	1.07	2580	220	191	85
29	1012	1852	1950	797	9	64	465	66	0.12	1030	660	1147	167
31	1063	1648	1500	571	12	116	422	52	0.19	220	660	549	135
32	1060	1615	1350	637	3	76	189	52	0.68	3120	290	216	44
34	1180	1649	1000	707	3	73	180	52	0.79	3660	150	191	53
35	1176	1442	1450	368	3	89	499	86	0.60	250	870	421	76
36	1094	1401	2150	-	-	-	-	-	0.86	760	270	6	--
39	354	1878	650	680	3	80	152	62	0.32	3270	340	222	66
40	291	1509	550	1220	3	83	143	59	1.15	6470	250	194	35
41	265	1666	650	1066	3	73	143	50	1.08	6070	260	216	59
42	311	1860	650	885	3	69	189	57	0.93	4680	260	177	64
43	328	1753	700	954	3	75	164	53	1.00	4390	310	191	29
44	270	1741	600	858	3	80	161	53	0.87	4190	350	208	26
45	289	1600	550	1090	3	73	174	57	1.08	6370	280	179	38
47	362	1955	650	1033	3	71	149	54	0.94	4400	250	236	114
48	377	1526	600	912	3	79	127	59	0.82	4760	270	199	41
49	397	1586	1000	855	3	79	143	52	0.82	4890	330	214	75
52	290	1442	450	997	3	76	167	52	1.05	5480	330	188	32
53	685	1466	1500	719	3	103	133	52	1.08	3640	320	231	16
55	617	1426	800	1413	3	100	171	46	1.02	5300	370	356	9
56	566	1307	400	1356	3	94	136	56	0.60	5330	270	276	47
57	500	1592	1250	628	3	105	149	53	0.85	2840	330	305	10
63	509	1342	600	1293	3	95	140	52	1.80	6320	240	296	109
69	219	1526	400	1061	3	80	143	52	1.02	7280	230	168	24
70	232	1324	10	1187	3	75	118	51	0.71	5690	370	177	10
71	752	1652	2300	640	3	81	140	48	0.99	3390	370	242	55
72	723	1800	2500	338	3	96	171	58	0.86	1950	190	270	39
73	668	1871	2750	695	3	96	146	58	1.06	2750	320	199	43
74	677	1759	2300	193	27	95	177	68	0.57	1130	380	265	53
76	963	1502	2150	556	3	90	167	55	1.03	3300	330	233	20
77	993	1462	2450	794	3	84	149	50	0.78	3820	620	219	68
79	1007	1775	1500	1030	3	58	177	49	0.90	3910	360	174	34
80	949	1783	1450	462	3	84	164	56	0.61	2340	360	228	98
81	1228	1665	800	749	3	98	220	54	0.56	4070	120	302	195
86	1233	1351	850	882	15	86	208	54	0.77	4440	90	165	65
104	860	1470	1650	673	18	103	180	43	0.61	3260	370	322	58
105	807	1407	1250	571	18	110	195	52	0.40	3320	150	245	64

Table A-4

Biotite   White granite

N	U	V	W	Rb ppm	Sr ppm	Sc ppm	Ni ppm	Cr ppm	F %	Cl ppm	Zn ppm	Nb ppm	Sn ppm
1	1496	234	10	773	<3	64	363	122	0.49	2180	250	159	20
14	952	1058	1000	855	3	109	406	76	0.03	200	320	490	184
15	1093	1057	1350	743	33	105	443	74	0.81	430	390	490	180
16	1164	979	950	507	3	98	279	68	0.76	620	150	344	111
17	1245	958	800	1607	3	80	276	64	0.52	2440	300	427	28
20	603	1510	1050	281	<3	125	490	64	0.03	280	230	530	184
27	732	2000	1150	9	<3	135	837	67	0.31	330	920	871	149
38	408	1909	700	317	<3	131	465	90	0.01	330	100	626	104
46	392	1962	650	151	<3	95	208	70	0.12	330	80	376	36
50	514	1435	600	432	<3	121	186	37	0.03	4220	250	393	59
51	418	1475	600	1791	<3	114	236	39	0.54	1550	490	578	98
54	651	1443	1150	208	<3	93	282	62	0.84	860	300	436	171
58	531	1621	1650	97	<3	110	226	58	0.15	560	120	461	77
59	506	1129	400	604	<3	114	233	60	0.33	150	360	379	175
60	461	1091	10	945	6	111	214	48	0.82	110	570	499	235
61	380	1180	10	728	24	121	177	53	0.58	240	880	470	139
62	354	1253	10	1105	<3	100	304	50	0.15	240	1000	393	160
64	548	1434	650	217	<3	103	171	107	0.33	320	660	307	60
65	682	1176	650	1129	6	121	291	48	1.06	980	550	467	158
66	642	1271	550	522	<3	128	248	47	0.22	360	450	464	143
68	764	924	200	577	<3	118	121	56	0.92	470	240	367	87
82	1140	626	200	1024	<3	70	118	62	0.73	5170	230	171	8
83	989	682	200	1105	<3	76	124	67	0.53	3420	240	228	14
84	1089	1234	800	2627	<3	110	360	50	0.97	3350	300	504	143
85	1083	1306	900	1187	<3	111	409	60	0.53	310	360	649	133
88	1450	303	10	1969	<3	84	226	45	0.68	2460	190	447	92
89	1515	332	100	1797	<3	71	146	45	0.96	2930	210	353	20
90	1236	567	150	1860	<3	60	161	52	0.62	2870	240	324	283
91	1344	465	10	610	18	81	146	122	0.34	2150	380	154	28
92	1403	748	500	914	6	79	149	97	0.48	6250	370	120	14
93	1012	881	400	909	<3	94	208	56	0.22	440	420	458	120
94	1112	882	650	341	3	104	167	62	0.08	350	420	293	69
95	1038	1132	1350	794	3	76	208	107	1.26	4350	330	214	55
96	589	1012	10	1558	3	98	220	50	0.48	1710	340	438	170
97	655	965	100	586	3	103	223	54	0.70	170	300	356	127
98	813	795	10	1111	9	96	180	53	0.66	1120	220	356	55
99	789	1290	900	1117	<3	125	299	39	0.09	160	580	535	184
101	1379	568	250	1280	<3	106	161	67	0.16	2250	210	302	5
102	1341	750	450	1205	<3	83	127	75	0.74	5600	270	174	2
103	1339	643	350	378	-	-	-	-	0.01	240	190	441	-

Table A-5

K-feldspars   Red granite

N	U	V	W	Rb ppm	Sr ppm	Na %	Pb ppm	Ba ppm	Sn ppm
3	435	1607	1600	582	85	3.29	73	1420	33
5	736	1371	1450	722	43	3.45	77	630	35
9	485	1782	1550	597	91	3.57	77	1560	32
10	400	1703	1400	618	73	3.40	50	1110	19
11	573	1892	2770	603	84	3.59	120	950	25
12	652	1807	2500	386	167	3.47	75	2620	31
18	698	1551	1950	644	73	3.57	114	990	19
21	852	1852	2450	561	108	3.57	66	1450	36
25	787	1875	2350	594	96	3.42	73	1230	30
26	736	1954	1350	897	48	3.67	79	550	41
28	988	1887	1950	591	89	3.43	75	1150	33
32	1060	1615	1350	680	60	3.48	94	900	29
34	1180	1649	1000	621	60	3.78	67	1000	27
36	1094	1401	2150	413	144	4.18	14	1880	27
39	354	1878	650	623	71	3.42	109	1270	26
40	291	1509	550	552	111	3.23	53	1660	26
41	265	1666	650	641	72	3.17	59	940	21
42	311	1860	650	579	78	3.25	90	1220	24
43	328	1753	700	609	81	3.18	83	1240	30
44	270	1741	600	609	65	3.19	81	880	31
45	289	1600	550	603	73	2.85	55	1410	51
47	362	1955	650	639	79	3.54	62	1430	36
48	377	1526	600	647	55	3.22	74	980	30
49	397	1586	1000	567	87	3.41	71	1110	23
52	290	1442	450	539	94	3.54	60	1370	25
53	685	1466	1500	758	45	3.51	74	760	31
56	566	1307	400	758	39	3.38	84	310	21
57	500	1592	1250	684	68	3.24	84	1020	44
63	509	1342	600	719	22	3.23	126	300	27
69	219	1526	400	527	84	3.17	127	1240	41
70	232	1324	10	573	55	3.46	93	1090	2
71	752	1652	2300	590	66	3.67	87	1160	56
73	668	1871	2750	582	84	3.44	87	1140	26
74	677	1759	2300	70I	52	3.11	69	780	24
76	963	1502	2150	636	58	3.55	73	890	27
77	993	1462	2450	624	71	3.48	71	1180	23
78	1068	1452	2300	386	135	4.59	63	1770	20
79	1007	1775	1500	357	101	3.63	67	1190	28
80	949	1783	1450	608	71	3.52	69	1450	27
81	1228	1665	800	606	68	3.49	62	1030	22
86	1233	1351	850	548	86	3.17	109	1400	20
104	860	1470	1650	725	30	3.18	86	470	29
105	807	1407	1250	725	36	3.40	94	690	22

Table A-6

LIST OF VARIMAX ROTATED FACTOR SCORES—**RED GRANITE**

	1	2	3	4	5	6
2	2.015957	-1.245678	-0.441120	0.230109	-0.567117	-0.084031
3	-1.033569	-0.570772	-0.060197	0.802562	-0.784889	0.977313
4	1.964479	0.630504	0.295099	0.828233	0.223479	-0.792512
5	-0.266394	0.650220	-0.328426	1.129708	-0.304312	0.706839
6	1.507265	-1.915166	0.144106	0.107177	-1.039004	-0.831676
7	1.782107	1.187223	-0.928661	2.769028	2.019750	-1.029567
8	1.366524	0.243661	-1.028823	-0.013321	-0.383098	-0.183008
9	-0.278362	0.764890	0.228566	-0.319535	0.468854	0.644600
10	-0.853130	0.766850	-1.191130	0.304941	-0.377106	0.078757
11	-0.082104	1.255969	0.013213	0.195507	1.522906	0.570774
12	-0.644197	-2.083436	0.762012	-0.516732	1.140516	1.096949
18	0.850084	-1.217436	-2.253821	0.814966	0.282798	-0.848864
19	1.453314	-1.398686	1.072312	0.546174	0.030991	0.581766
21	-0.697802	1.113824	1.310574	0.846778	-1.076493	-0.602680
23	1.080944	-2.426372	0.986966	1.002130	2.085357	0.264509
24	-0.360708	-1.234458	-0.459406	1.471247	-1.304140	0.166162
25	-0.809710	0.264492	-1.308223	2.197188	-0.222071	0.501699
26	-0.561719	0.352592	-0.348323	-0.648980	-0.807221	-0.391634
28	-0.563996	0.021849	0.010407	-0.720604	0.239223	0.394559
29	2.308425	0.542472	0.465689	0.834448	-1.294187	-2.032010
31	1.265153	-0.668169	1.960621	-0.964061	-1.605233	-0.970514
32	0.322362	1.173183	0.722309	-0.838427	0.775157	0.326486
33	0.246781	2.090844	0.124770	-2.367560	-1.371579	-2.246139
34	-0.357357	0.464887	-1.458320	-0.601538	-0.159946	0.132177
35	0.528545	0.268709	-2.033603	-1.241021	-3.470836	-1.669785
36	-1.893108	-0.676429	1.178418	-0.771540	3.343875	-2.558824
37	0.960979	-0.458291	-0.430870	-1.705954	-1.622954	-0.237603
39	-0.782889	-1.470536	-0.382969	-0.618538	-1.050409	0.571193
40	-0.586480	0.325802	-1.766518	-0.594895	0.072907	0.431034
41	-0.366742	0.918926	-0.011023	-0.706902	-0.405805	0.721555
42	-0.155353	0.081946	0.028309	-0.194985	-0.083245	0.551157
43	-0.354181	-0.068932	1.077511	-0.913778	0.054987	0.432466
44	-0.505959	0.804544	-0.393573	1.132103	0.027819	0.242110
45	0.029498	0.995405	1.943041	-0.279008	1.228817	0.064882
47	-0.511812	-1.002486	-0.961862	0.301437	-0.616303	0.613202
48	-0.589099	0.515169	0.359148	1.582546	-0.327616	0.572433
49	-0.569956	-1.444578	-0.371930	-0.834503	0.018501	0.552468
52	-0.698209	0.426824	1.317058	1.005995	0.008123	0.274115
53	0.205631	1.109938	1.564050	0.582062	-0.324429	-0.343328
55	1.643506	0.550410	-0.547118	-1.278948	2.248687	0.943569
56	0.281803	-1.206849	-0.474976	-0.575869	-0.746016	1.432627
57	0.540254	0.878186	0.387617	-0.530609	-0.864327	2.536179
63	1.487527	0.200423	-0.255914	-1.318311	2.230504	1.184846
69	-0.639801	0.473095	-1.309718	1.092176	0.443686	0.306705
70	-0.771799	-0.051957	0.767204	0.531462	0.147400	0.405722
71	-0.064841	1.490776	0.480703	0.138633	-0.505514	0.784857
72	0.348838	1.562275	1.280405	-0.084874	-0.286014	0.790924
73	-0.529295	0.728820	-0.574308	-0.196578	0.697320	-0.445803
74	-0.315132	-1.089349	1.722442	0.028084	-0.895151	0.950238
75	0.835561	-0.888013	0.865036	1.194558	-0.191358	-1.757605
76	-0.376385	0.284425	1.336729	-0.075108	-0.488869	-0.457121
77	-0.676639	0.324913	-1.300275	-0.172766	0.016016	-0.661814
78	-2.708794	-0.990752	-0.185671	0.615197	0.163468	-2.961326
79	-1.293217	-0.690766	0.484469	-0.123066	-0.505397	-0.282864
80	-0.549988	0.836572	-0.877520	-0.757229	-0.359775	-0.333139
81	-0.857677	-0.987675	0.546385	-1.970396	0.544766	-0.669159
86	-0.962169	0.352309	0.465721	1.315845	-0.222687	0.700927
104	0.579336	-0.323706	-0.979891	-1.092258	1.080263	0.078775
105	-0.336304	-0.542429	-1.236256	-0.572395	0.146934	0.806422

Table A-7

LIST OF VARIMAX ROTATED FACTOR SCORES — **WHITE GRANITE**

	1	2	3	4	5
1	-1.900109	-0.346855	-1.937948	-1.076998	0.120903
13	1.181507	-0.851003	0.418374	-2.089541	-0.108019
14	0.656191	-1.453390	0.202193	-0.555443	-0.703637
15	1.219707	1.042661	0.482292	-0.377892	0.282209
16	-0.233721	0.473843	0.510224	0.998161	-0.803140
17	0.161666	0.373024	0.274173	0.186561	0.577618
51	0.865404	-0.698960	-1.161287	-0.131118	-1.458602
59	0.653093	0.697976	0.578912	0.203352	0.935343
60	0.013397	1.919649	0.524084	0.465664	-0.801785
61	0.923143	1.323810	0.334117	0.717371	0.983630
62	0.480678	-1.043124	1.123383	-1.439158	-0.090532
64	-1.271397	-0.468470	0.789128	-0.480232	-1.264985
65	0.596150	0.756737	0.649032	-0.708183	-0.025820
66	0.570589	0.430043	0.079387	-0.450090	-0.554375
67	-0.596092	0.874414	-0.027386	0.417245	-0.925413
68	-0.123249	1.153161	0.508229	0.099300	-0.527065
82	-1.637856	-0.066411	-0.881870	-0.827076	1.132550
83	-0.871921	-0.361618	-0.320957	-0.284355	0.844738
84	0.901888	-0.459796	-0.721641	-0.349868	-0.562805
85	0.865012	0.344903	-0.375414	-0.770346	-0.577038
87	0.054026	-2.311001	0.458947	4.103517	-0.269792
88	1.328846	0.119614	-4.604635	0.472604	-0.380679
89	-0.511010	1.574637	-0.607928	1.959303	-0.423843
90	0.729249	0.620731	-0.206067	-0.016890	3.185054
91	-1.228880	-0.080380	-0.053563	-0.212306	2.309128
92	-2.529788	-0.692917	-0.400774	-0.393167	0.197500
93	0.288379	-0.636562	0.112506	0.117980	-0.549591
94	0.430313	-1.420547	0.249296	0.127545	-0.074170
95	-1.276243	0.414229	-0.096875	-0.356841	0.224365
96	-0.354997	-0.083067	0.094976	-0.186876	-1.137517
97	-0.094586	1.401986	0.186314	0.625541	-0.032404
98	-0.672823	0.946605	1.298428	0.078710	-0.749610
99	1.132236	-0.448194	0.306718	-0.601257	-0.991873
100	0.775961	0.659019	0.552926	-0.457319	0.319868
101	-0.525210	-1.704696	0.873134	-0.307300	-0.063373
102	-1.404582	-0.350788	0.389371	0.590515	-0.236212
103	1.405026	-1.649266	0.400201	0.908886	2.199373

Table A-9

LIST OF VARIMAX ROTATED FACTOR SCORES **— BIOTITE—W**

	1	2	3	4	5
1	2.579817	-0.332853	-0.490947	-1.710877	-0.061751
14	0.363518	-0.282873	-0.835711	-1.925479	-2.415826
15	0.272478	-0.348051	2.397505	-2.001767	1.225359
16	0.046972	-1.591691	-1.500089	-0.990390	1.595809
17	0.550778	1.147626	-0.349695	-0.667076	-0.052312
51	-1.201244	1.410487	0.164488	0.258804	-0.231999
59	-0.712015	-1.249448	-0.544030	-0.219330	-0.044776
60	-1.383483	-0.391679	0.876287	0.136749	0.551302
61	-1.077680	-0.174852	3.004104	0.820112	0.067577
62	-0.467503	0.684522	0.737918	-0.367312	-2.081492
64	0.345332	-2.482073	0.173687	0.451477	-0.589564
65	-0.908309	0.456050	1.069500	-0.327877	0.624032
66	-1.097923	-0.816904	-0.339530	0.120941	-0.636658
68	-1.130041	-1.442161	-0.844009	1.344091	1.221053
82	0.910199	0.435203	-0.523481	1.639545	0.389363
83	0.684103	0.375151	-0.535706	1.276574	0.156974
84	-0.411054	1.651823	-0.210270	-1.224659	0.695672
85	-0.541564	0.071230	-0.394597	-1.609148	0.190429
88	-0.326443	1.188595	-0.941325	-0.325948	0.902202
89	-0.069048	1.266818	-0.739157	0.983418	0.793505
90	0.211147	1.112194	-0.702628	-0.109016	0.813915
91	1.878210	-0.606514	2.002237	0.452875	-0.152391
92	1.827085	0.247337	0.944414	0.880035	-0.355494
93	-0.440282	-0.015470	-0.300237	-0.002411	-0.727925
94	-0.144597	-1.418604	-0.506109	0.828526	-1.604143
95	1.415074	-0.411718	-0.097855	-0.471193	0.930218
96	-0.521773	0.854897	-0.288374	-0.163805	0.129490
97	-0.767845	-1.314691	-0.727951	-0.037984	0.841098
98	-0.243660	0.182579	0.417261	0.370404	1.027997
99	-1.290213	0.479507	-0.049844	-0.233769	-1.938967
101	0.495455	0.633391	-0.724440	1.045163	-1.141497
102	1.154510	0.682150	-0.141414	1.779326	-0.121199

Table A-1O

LIST OF VARIMAX ROTATED FACTOR SCORES — **K—FELDSPAR**

	1	2	3	4
3	-0.603216	-0.422636	-0.044692	-0.705310
5	1.362077	-0.586604	-0.165586	0.352861
9	-0.603256	-0.475559	0.272409	0.340644
10	0.134912	0.755515	-1.380493	-0.415179
11	-0.213886	-0.020000	1.608474	0.814801
12	-2.608312	-0.261429	0.665466	-0.160782
18	0.021420	0.558974	1.320198	0.627876
21	-0.745717	-0.696680	-0.133561	0.345141
25	-0.477209	-0.294277	0.002839	-0.156992
26	1.905512	-1.117114	-0.130462	1.157500
28	-0.350418	-0.484194	0.092016	-0.040829
32	0.474031	-0.263315	0.615481	0.326089
34	0.491574	-0.099108	-0.246038	1.280258
36	-0.889790	0.089054	-4.544188	1.756584
39	-0.309584	-0.026457	1.186919	-0.013972
40	-1.011782	0.122658	-1.034043	-1.220860
41	0.190769	0.576193	-1.012465	-1.204114
42	-0.502275	0.243733	0.540719	-0.749102
43	-0.452043	-0.222310	0.233579	-1.076929
44	0.127377	-0.248530	0.091407	-0.834793
45	-0.476262	-1.135864	-1.221705	-2.673452
47	-0.152887	-0.689841	-0.518688	0.182247
48	0.361337	-0.177564	-0.257556	-0.818488
49	-0.364070	0.312041	-0.114401	-0.166381
52	-0.605004	0.136379	-0.499567	0.192933
53	1.269245	-0.378694	-0.292767	0.416873
56	2.176732	0.487025	-0.120203	0.362528
57	0.176403	-1.072903	0.205846	-0.690263
63	2.412351	0.076321	1.079376	0.097132
69	-0.969502	-0.869326	1.771226	-0.803200
70	-0.021891	5.447608	0.373993	-0.246756
71	-0.010177	-1.628001	0.713351	1.071184
73	-0.384174	0.007880	0.547272	0.037957
74	0.770806	0.305346	-0.677870	-1.280368
76	0.541198	-0.054082	-0.122533	0.521273
77	-0.002814	0.277791	-0.188888	0.050939
78	-1.456839	0.439560	0.480336	3.679052
79	-1.342608	0.059720	0.269436	0.892413
80	-0.223213	-0.052853	-0.195915	0.133315
81	0.187504	0.412615	-0.622927	0.114719
86	-0.980491	0.631749	1.167704	-1.089757
104	1.826978	-0.062189	-0.078946	-0.537233
105	1.327194	0.399370	0.365454	0.130445

Table A-11

Conditions of XRF analysis

Element	Tube	Crystal	Collimator	Tube voltage KV	Tube current mA
Rb	Mo	LiF 220	fine	48	20
Sr	Mo	LiF 220	fine	48	20
Na_2O	Cr	KAP	coarse	46	22
Zr	Au	LiF 220	fine	48	20
F	Cr	KAP	coarse	46	22
Cl	Cr	KAP	coarse	46	22
Nb	W	LiF 220	fine	40	20
Pb	Mo	LiF 220	fine	40	20
Ba	W	LiF 220	coarse	48	20
Sn	W	LiF 200	fine	48	20
Sc	Cr	LiF 200	fine	48	20
Ni	Au	LiF 200	coarse	48	20
Cr	Au	LiF 200	coarse	48	20
Zn	Au	LiF 200	fine	44	22

Table A-12

Reproducibility data

Ele-ment	Rocks				Biotites			
	mean	s.d.	No.of repeats	Coef.of var.in%	mean	s.d.	No.of repeats	Coef.of var.%
Ba	154	8.0	10	5.19	-	-	-	-
Rb	450	6.7	10	1.49	571	10	12	1.75
Sr	40	1.2	10	3.0	12	2.1	12	17.5
Cr	-	-	-	-	52	2	12	3.8
Ni	-	-	-	-	422	16	12	3.8
Sc	-	-	-	-	116	8	12	6.9
F	0.22%	0.04	10	18.2	0.19	0.04	12	21.0
Cl	-	-	-	-	220	12.2	12	5.5
Sn	35	10.3	10	29.4	135	8.5	12	6.3
Zr	160	6.5	10	4.1	-	-	-	-
Nb	19	1.9	10	10	549	10.3	12	1.9
Zn	-	-	-	-	660	10.8	12	1.6
Pb	43	3.9	10	9.1	-	-	-	-
Na_2O	3.12%	0.14	10	4.48	-	-	-	-

Table A-13

Comparison of author's analysis of selected rock standards with recommended values of Leake at all (1969).

	G-1		G-2		T-1		W-1	
	this work	recommended	this work	recommended	this work	recommended	this work	recommended
Ba^{+}	1250	1124	2250	2134	629	641	369	352
Rb	260	245	190	195	31	34	36	27
Sr	250	271	490	515	412	408	220	201
Cr	49	56	70	65	58	62	77	81
Ni	–	2	9	5	18	16	119	101
Sc	5	3	5	3	6	3		n.d.
Cl	120	97	126	144	330	342	425	409
Sn	n.d.	2		n.d.	64	76	10	4
Zr	195	247	353	348	133	140		82
Na_2O	3.18%	3.32%	3.95%	4.10%	4.45%	4.32%	2.21%	2.07%
Zn	78	62	108	99	208	222	83	94
Pb	50	76	55	54	65	63	14	17
Nb	25	18	14	10	16	12	5	5

n.d. = not detected

[+] values in ppm (except Na_2O)

APPENDIX III

List of mines and prospects in and immediately adjacent
to the Heemskirk granite massif
(Complementary explanations to map III)

Federation mine

    1 . Long tunel

    2 . Air shaft

    3 . Munro's shaft   Central workings

    4 . 220 ft. level

    5 . Black Face

    6 . Eastern workings

    7 . ?

    8 . No.4 Adit

    9 . No.3 Adit

   10 . Yates' level

   11 . No.2 level

   12 . Tributers' adit

   13 . No.1 Adit

   14 . 30 ft. Shaft

   15 . Old Prince George Mine

   16 . Old Montagu Mine (Bullen's Mine)

17 Old Montagu Extended Mine

18 Old Empress Victoria Mine

19 White Face Workings

20 Old Cornwall Mine

21 Old Cliff Mine

22 Spencer Brothers' Workings

23 Wooding's Workings

24 Old Wakefield Mine

25 Sweeney's Mine

26 Old Orient Mine

27 Mayne's Mine

28 Old Kelvin Mine

29 Healey and McIvor's Mine

30 Old Globe Mine (Agnew Mine)

31 Allison's Workings

32 Peripatetic Mine

33 St. Dizier Mine

34 Whelan's Section

35 Fischer and Smith Section

36 Persic Mine

37 Long's Iron Blow

38 Iron ore in the St.Dizier Creek

39 Iron ore in the Twelve Mile Creek

References

Abdullaev, Kh.M., 1960: O petrometallogenicheskikh ryadakh
         magmaticheskikh porod in endogennykh mestorozhdenii.
         Sov. Geol., 3, 5, 3-13, Moscow.

Balk, R., 1937: Structural behaviour of igneous rocks.
         Geol. Soc. America Memoir 5, 177 p.

Barsukov, V.J., 1957: Zur Geochemie des Zinns. Geochemija,
         Hf. 1.

Barsukov V.J. and Voloscv A.G., 1967: A geochemical method
         for estimating depth of sulfide-cassiterite minerali-
         zation and discovery of blind ore bodies. Translation
         from Geokhimiya No 11, pp. 1370-1380.

Bateman, A.M., 1951: The formation of mineral deposits.
         New York.

Barth, T.F.W., 1959: Principles of classification and norm
         calculations of metamorphic rocks. Jour. Geology,
         67, pp. 135-152.

Barth, T.F.W., 1962: The feldspar geologic thermometers.
         Norsk. Geol. Tidsskr., 42, pp. 330-339.

Baumann,L., 1970: Tin deposits of the Erzgebirge. Institu-
         tion of Min. & Metallurgy, Transactions section B,
         Bull. No. 762.

Blissett, A.H., 1962: Geology of the Zeehan sheet (One-mile
         geological map series). Geol. Surv. Tasm. Explan.
         Rept.

Borisenko, L.F., and Radionov, D.A., 1961: Distribution
        of scandium in intrusive rocks. Geochemistry,
        No. 9, pp. 840-847.

Borisenko, L.F., 1961: Skandiy (Scandium). Acad. Sci.
        USSR Press, Moscow.

Borchert, A. and Dybek, J., 1960: Zur Geochemie des Zinns.
        Chemie d. Erde, 20, pp. 137-154, Jena.

Both, R.A. and Williams, K.L., 1968: Mineralogical zoning
        in the lead-zinc ores of the Zeehan field, Tasmania.
        Part 1: Introduction and review. Jour. Geol. Soc.
        Aust., 15 (1), pp. 121-137.

Both, R.A., Rafter, T.A., Solomon, M., and Jensen, M.L.,
        1969: Sulfur isotopes and zoning of the Zeehan
        mineral field, Tasmania. Economic Geology, 64,
        No. 6, pp. 618-628.

Bowen, N.L., 1928: The evolution of igneous rocks.
        Princeton.

Bradshaw, P.M.D., 1969: Distribution of selected elements
        in feldspar, biotite and muscovite from British gra-
        nites in relation to mineralization. Inst. of Min.
        & Met., Trans., Sec. B, 76, Bull. 743, pp. 137-148.

Bradshaw, P.M.D., Stoyel, A.J., 1968: Exploration for blind
        ore bodies in southwest England by the use of geo-
        chemistry and fluid inclusions. Inst. of Min. &
        Met., Trans., Sec. B, 77, Bull. 744, pp. 144-152.

Brammall, A. and Harwood, H.F., 1925: Tourmalinization in
        the Dartmoor granite. Miner. Mag., 20, pp. 319-330.

Branch, C.D., 1966: Volcanic Cauldrons, Ring Complexes, and Associated granites of the Georgetown Inlier, Queensland. Dept. Nat. Dev., Bur. Min. Res., Geol. and Geophys., Bull. 76, p. 158.

Bräuer, H., 1967: Geochemische Gliederung granitischer Gesteine des Thüringer Waldes und Erzgebirges und ihre lagerstätten genetische Bedeutung. Freiberger Forschungs_hefte C 209, Min-Lagerstättenlehre, pp. 154-168.

Brooks, C., 1965: The geology and geochronology of the Heemskirk granite, Western Tasmania. Thesis for Ph.D. (A.N.U.) Camberra.

Brooks, C. and Compston, W., 1965: The age and initial Sr^{87}/Sr^{86} of the Heemskirk granite, Western Tasmania. Jour. of Geophys. Res., 70, No. 24, pp. 6249-6263.

Brooks, C., 1968: Relationship between feldspar alteration and the precise post-crystallization movement of rubidium and strontium isotopes in a granite. Jour. of Geophys. Res., 73, No. 14, pp. 4751-4757.

Buddington, A.F., 1927: Coast range intrusives of south-eastern Alaska. Jour. Geol., 35, pp. 224-246.

Buddington, A.F., 1933: Correlation of kinds of igneous rocks with kinds of mineralisation. Ore deposits of Western States. Lindgren Volume, pp. 350-385, New York.

Carey, S.W., 1953: Geological structure of Tasmania in relation to mineralization. 5th Emp. Min. Metall. Congr., 1, pp. 1108-1128.

Chayes, F., and Suzuki, Y., 1963: Geological contours and trend surfaces (A discussion). Jour. Pet., 4, pp. 307-312.

Coleman, R.,1968: Thesis. The University of Tasmania, Hobart, Tasmania.

Crowder, D.F., 1968: Geology of a part of North Victoria Land, Antarctica. U.S. Geol. Surv. Prof. Pap. 600-D, pp. 95-107.

Davis, J.C. and Sampson, R.J., 1966: Fortran II program for multivariate discriminant analyses using an IBM 1620 computer. Comp. Contr., 5, Geol. Surv. Lavrence.

De Keyser, F., and Lucas, K.G., 1968: Geology of the Hodgkinson and Laura basins, North Queensland. Dept. Nat. Dev., Bur. Min. Res., Geol. and Geophys., Bull. 84, p. 254.

Dietrich, R.V., 1962: K-feldspar structural states as petrogenetic indicators. Norsk Geol. Tidsskr., 42, pp.394-414.

Dodge, F.C.W., and Moore, J.G., 1968: Occurence and composition of biotites from the Cartridge Pass pluton of the Sierra Nevada batholith, California. Geol. Surv. Res., US. Geol. Surv. Prof. Paper 600-B, pp. 6-10.

Dodge, F.C.W., Smith, V.C., and Mays, R.E., 1969: Biotites from granite rocks of the Central Sierra Nevada batholith, California. Jour. of Petr., 10, P. 2, pp. 250-271.

Doveton, J.H., and Parsley, A.J., 1970: Experimental evaluation of trend surface distortions induced by

inadequate data-point distributions. Inst. of Min. & Met. Trans. B, 79, pp. 197-206.

Emerson, D.O., 1964: Modal variations within granitic outcrops. Am. Miner., 49, pp. 1224-1233.

Engel, A.E.J., 1968: The Barberton Mountain Land: Clues to the differentiation of the earth. Geol. Soc. S. Afr., LXXI: Symposium on the Rhodesian basement complex. pp. 255-270.

Engelhardt, W. von, 1936: Die Geochemie des Barium. Chem. der Erde, 10, p. 187.

Evernden, J.F., and Richards, J.R., 1962: Potassium-argon ages in eastern Australia. Jour. Geol. Soc. Aust., 9, pp. 1-49.

Fleischer, M., and Stevens, R.E., 1962: Summary of new data on rock samples G-1 and W-1. Geochim. Cosmochim. Acta, 26, pp. 525-543.

Foster, M.D., 1960: Interpretation of the composition of trioctahedral micas. U.S. Geol. Surv. Prof. Paper, B - 354

Gallagher, D., 1940: Albite and gold. Econ. Geol., 35, 6, pp. 618-736.

Garnett, R.H.T., 1966: Distribution of cassiterite in vein tin deposits. Inst. of Min. & Met. Trans. Sec. B, 75, Bull. No. 720, pp. 245-273.

Goldschmidt, V.M., and Peters, A., 1931: Zur Geochemie des Scandiums. Nachr. Ges. Wiss. Göttingen, Math.-Phys. Kl. III, IV, p. 257.

Goldschmidt, V.M., 1937: The principles of distribution of chemical elements in minerals and rocks. Jour. Chem. Soc., 1, pp. 655-673.

Goldsmith, J.R., and Laves, F., 1954: The microcline-sanidine stability relations. Geochim. Cosmochim. Acta, 5, pp. 1-19.

Green, T.H., 1964: Geology of the Trial Harbour district. Thesis for degree B.Sc at the University of Tasmania.

Green, T.H., 1966: Thermal metamorphism in the Trial Harbour district, Tasmania. Jour. of the Geol. Soc. of Aust., 13, P. 2, pp. 405-418.

Green, T.H., 1966: Geology of the Trial Harbour district. Papers and Proc. of the Royal Soc. of Tas., 100, pp. 1-20.

Groves, D.I., 1967: The granitic rocks associated with cassiterite-pyrrhotite mineralization. The Geology of Western Tasmania - a Symposium, pp. 5-23.

Groves, D.I., 1968: The cassiterite-sulphide deposits of Western Tasmania. Ph.D. thesis, Univ. of Tasmania.

Haack, U.K., 1969: Spurenelemente in Biotiten aus Graniten und Gneisen. Contr. Miner. and Petrol., 22, pp. 83-126.

Hahn-Weinheimer, P., and Johanning, H., 1969: Geochemical investigation of differentiated granite plutons in the Black Forest. Origin and distribution of the elements. International series of monographs in earth sciences. Editor D.E.Ingerson, 30, pp. 778-793.

Hall, G., and Solomon, M., 1962: Metallic Mineral Deposits.
        In the geology of Tasmania. Jour. Geol. Soc.
        Aust., 9, P. 2, pp. 285-309.

Hall, A., 1969: Regional variation in the composition of
        British Caledonian granites. Jour. Geol., 77,
        pp. 466-481.

Hayama, Yoshikazu, 1959: Some consideration on the colour
        of biotite and its relation to metamorphism.
        Jour. Geol. Soc. Japan, 65, No. 760, pp. 21-30.

Heier, K.S., 1962: Trace elements in feldspars - a review.
        Norsk Geol. Tidsskr., 42, pp. 415-454.

Heier, K.S., and Rhodes, J.M., 1966: Thorium, uranium and
        potassium concentrations in granites and gneisses
        of the Rum Jungle Complex, Northern Territory,
        Australia. Acon. Geol., Vol. 61, pp. 563-571.

Heier, K.S., Brooks, C., 1966: Geochemistry and the genesis
        of the Heemskirk granite, West Tasmania. Geochim.
        et Cosmochim. Acta, 30, pp. 633-643.

Hellwege, H., 1956: Zur Verteilung von Sn als Spurenelement
        in Mineralien. Hamburger Beitr. Angew. Mineral.
        Kristallphysik I, pp. 73-136.

Herz, N., and Dutra, C.V., 1964: Cobalt, nickel, chromium,
        scandium and niobium in biotite and the scandium
        geological thermometer. Boletim da Sociadade
        Brasileira de Geologia, 13, No. 1-2, pp. 23-42.

Hesp, W.R., 1971: Correlations between the tin content of
        granitic rocks and their chemical and mineralogi-
        cal composition. C.I.M. Special Volume No. 11,
        pp. 3-15.

Hietanen, A., 1963: Idaho batholith near Pierce and Bunga-
    low. U.S. Geol. Surv. Prof. Paper 344-D.

Hosking, K.F.G., 1967: The relationship between primary
    deposits and granitic rocks. A technical Confe-
    rence on tin, London, 1, pp. 269-306.

Ingerson, E., 1955: Methods and problems of geologic
    thermometry. Econ. Geol., 50th Anniversary Volume,
    P. 1, pp. 341-410.

Ivanova, G.F., 1963: O soderzhanii Sn, W, Mo v granitakh
    v svyazi s nalichiyem v nikh olovo-volframovykh
    mestorozhdeniy (content of tin, tungsten and
    molybdenum in granites enclosing tin-tungsten
    deposits). Geokhimia, No. 5.

James, R.S., and Hamilton, D.L, 1969: Phase relations in
    the system $NaAlSi_3O_8 - KAlSi_3O_8 - CaAl_2Si_2O_8 -$
    SiO_2 at 1 kilobar water vapour pressure. Contr.
    Miner. and Petrol., 21, pp. 111-141.

Jedwab, J., 1955: Granites à deux micas de Guéhenno et de
    La Villeder (Morbihan - France). Bull. de La Loc.
    Belge de Géol., 64, pp. 526-534.

Joplin, G.A., 1963: Chemical analyses of Australian rocks.
    Part I. Igneous and metamorphic. Bull. Bur.
    Miner. Resour. Geol. Geophys. Aust., p. 65.

Klomínský, J., and Groves, D.I., 1970: The contrast in
    granitic rock types associated with tin and gold
    mineralisation in Tasmania. Proc. Aust. Inst.
    Min. Met., 234, pp. 71-78.

Kohler & Raaz 1951:

Koide, Haku, 1951: An orbicular rock in andesite from
          Akagi volcano. Geol. Surv. Japan, rept. No.
          139, pp. 1-15.

Krumbein, W.C., 1959: Trend surface analysis of contour-
          type maps with irregular control-point spacing.
          Jour. Geophys. Res., 64, pp. 823-834.

Kvalheim, A., and Strock, L.W., 1939: Spectrochim. Acta,
          I, p. 221.

Larsen, E.S., 1945: Time required for the crystalization
          of the great batholith of Southern and Lower
          California. Jour. of Amer. Sci., 243 A,
          pp. 399-416.

Leake, B.E., Hendry, G.L., Kemp, A., Plaut, A.G., Harvey,P.K.,
Wilson, J.R., Coats, J.S., Autcott, J.W., Lünel, T., and
Howarth, R.J., 1969: The chemical analysis of rock powders
          by automatic X-ray fluorescence. Chem. Geol.,
          5, pp. 7-86.

Leveson, J.D., 1966: Orbicular Rocks: A review. Geol. Soc.
          of Am. Bull., 77, pp. 409-426.

Lindgren, W., 1915: The igneous geology of the Cordilleras
          and its problems; in Problems of American Geology:
          New Haven, Conn. Yale Univ. Press, pp. 234-286.

Luth, W.C., Jahns, R.H., and Tuttle O.F., 1964: The granite
          system at 4 to 10 kilobars. Jour. Geophys. Res.
          64, pp. 759-773.

Mc Dougall, I. and Leggo, P.J., 1965: Isotopic age determi-
          nations on granitic rocks from Tasmania. Jour.
          Geol. Soc. Aust., 12 (2), pp. 295-332.

Mac Kenzie, W.S., and Smith, J.V., 1956: The alkali feld-
        spars III. An optical and X-ray study of high-
        temperature feldspars. Am. Miner., 41, pp.707-732.

Mac Kenzie, W.S., 1957: The crystalline modifications of
        $NaAlSi_3O_8$. Amer. Jour. Sci., 255, p. 481.

Mantei, E.J., and Brownlow, A.H., 1967: Variation in gold
        content of minerals of the Marysville quartz
        diorite stock Montana. Geochim. et cosmochim.
        Acta, 31, p. 225.

Matheron, G., 1965: Les variables regionalises et leur
        estimation. Masson, Paris, 306 p.

Neubauer, W., 1952: Einige seltene Metalle. Berg. u.
        Hüttenm. Monatsh., 97, Hf. 7, pp. 134-135, Wien.

Nockolds, S.R., 1931: On an orbicular diorite from
        the island of Alderney. London, Geol. Mag.,
        68, pp. 499-506.

Nockolds, S.R. and Mitchell, R.L., 1948: The geochemistry
        of some Caledonian plutonic rocks: A study in the
        relationship between the major and trace elements
        of igneous rocks and their minerals. Trans. Roy.
        Soc. Edinburgh, 61, pp. 533-575.

Norrish, K., and Hutton, J.T., 1964: Preparation of samples
        for analysis by X-ray fluorescent spectrography.
        C.S.I.R.O. Aust. Div. Soils, Div. Rep., 3,
        (unpublished).

Norrish, K., and Chappel, B.W., 1967: X-ray fluorescent
        spectrography. In Physical methods in determina-
        tive Mineralogy. Ed. J.Zussman, Acad.Press,London.

Oftedahl, I., 1943: Scandium in biotite as a geologic
          thermometer. Norsk. Geol. Tiddsk., 23, No. 4,
          pp. 202-213.

Oftedahl, I., 1954: Some observations on the regional
          distribution of lead in South Norwegian granitic
          rocks. Norsk. Geol. Tidsskr., 33, pp. 154-164.

Orville, P.M., 1967: Unit-cell parameters of the microcli-
          ne - low albite and the sanidine high-albite solid
          solution series. Amer. Miner., 52, pp. 55-86.

Packham, G.H., (editor), 1969): The geology of New South
          Wales. Jour. Geol. Soc. Aust., 16, 1, p. 654.

Palfreyman, W.D., 1965: The geology of the Grenville
          Harbour area. Thesis for the degree B.Sc. at
          The University of Tasmania.

Putman, G.W., and Burnham, C.W., 1962: Trace elements in
          igneous rocks, North-western and Central Arizona.
          Geochim. et Cosmochim. Acta., 27, pp. 53-106.

Rattigan, T.H., 1963: Geochemical ore guides and techniques
          in exploration for tin. Proc. Aust. Inst. Min.
          Met., 207, pp. 137-148.

Rattigan, T.H., 1964: Geochemical characteristics of
          Australian granitic rocks in relation to the oc-
          currence of tin. Ph.D. thesis, University of
          New South Wales.

Reynolds, R.C., 1963: Matrix correlations in trace element
          analysis by X-ray fluorescence: Estimation of
          the mass absorption coefficient by Compton
          scattering. Am. Miner., 48, pp. 1133-1143.

Rimšaite, J.H.Y., 1967: Studies of rock-forming micas. Geol. Surv. of Canada, Bull. 149, p. 82.

Roeder, E., 1960: Fluid inclusions as samples of the ore-forming fluids in genetic problems of ores. Proc. 21st Intern. Geol., Congr., Norden, Pt. 16, pp. 218-229.

Sainsbury, C.L., and Hamilton, J.C., 1967: The geology of lode tin deposits. Tech. Conf. on Tin, London, 1, pp. 267-307.

Sattran, V. et al., 1966: Problemy metalogenese Českého masívu. Sbor. geol. věd., LGB, 7-112 pp., (in Czech. with English summary).

Sattran, V., and Klomínský, J., 1970: Petrometallogenic series of igneous rocks and endogenous ore deposits in the Czechoslovak part of the Bohemian Massif. Sbor. geol. ved., LG 12, Prague.

Schneiderhohn, H., 1925: Bildungsgesetze eruptiver Erzlager-stätten und Biziehungen zwischen den Metallprovin-sen und den Eruptivgesteinsprovinzen der Erde. Metall. und Erz., 22, pp. 267-274.

Serra, J., 1967: Echantillonnage et estimation locale des phenomenes miniers de transition (Thesis). Nancy, p. 670.

Slowson, W.F., and Nackowski, M.P., 1959: Trace lead in potash feldspars associated with ore deposits. Econ. Geol., 54, pp. 1543-1555.

Smith, J.V., 1956: The powder patterns and lattice para-
meters of plagioclase feldspars. 1. The soda-rich
plagioclases. Mining Mag. London, 31, pp.47-68.

Solomon M. (1965): Geology and mineralization of Tasmania.
Geology of Australian ore deposits, 2nd Edition
8th Commonwealth mining and metallurgical
congress, 1, pp. 464-477.

Solomon, M., and Griffiths, J.R., 1972: The tectonic evo-
lution of the Tasman orogenic zone, eastern
Australia. Nature, Physical Science, 234, pp.3-6.

Spurr, J.E., 1923: The ore magmas. McGraw-Hill, New York.

Taylor, S.R. and Heier, K.S., 1960: The petrological signi-
ficance of trace element variations in alkali
feldspars. Inter. Geol. Congr. Rept. 21st session,
Norden, 14, pp. 47-61.

Thomas, W.K.L, Kempe, D.R.C., 1963: Standard geochemical
sample T-1. Tanganyika Geol. Surv. Supp., 1.

Tilling, R.I., Greenland, L.P., and Gottfried, D., 1969:
Distribution of scandium between coexisting
biotite and hornblende in igneous rocks. Geol.
Soc. of Am. Bull., 80, pp. 651-668.

Tuttler, O.F., and Bowen, N.L., 1958: Origin of granite
in the light of experimental studies in the system
$NaAlSi_3O_8$- $KAlSi_3O_8$ - SiO_2 - H_2O. Geol.Soc.Am.,
Mem., 74, pp. 1-153.

Twelvetrees, W.H., 1901: Report on the mineral districts
of Zeehan and neighbourhood. Rep. Secr., Mines,
Tasm., pp. 5-108.

Twelvetrees, W.H., and Ward, L.K., 1910: The ore-bodies
of the Zeehan field. Geol. Surv. Bull., Dept.
of Mines Tasmania, No. 8, p. 165.

Van Moot, J.C., 1966: Les roches cristallophylliennes des
Cévennes et les roches plutoniques du Mont Lozére.
Annales de la Faculté des Sciences de L'Université
de Clermont, Nu. 31, Geologie, Mineralogie,
14 fascicule, p. 272.

Vendel, M., 1949: Zusammenhänge zwischen Gesteinsprovinzen
und Metallprovinzen I. Mitt. berg. - und hütten-
män. Abt. Univ. Sopron (Ungarn), 17, pp. 206-324.

Vendel, M., 1956: Zusammenhänge zwischen der Substituier-
barkeit der Ionen und der Lagerstättenbildung.
Berg. - und hüttenm. Mschr., 101, pp. 44-45, Wien.

Vendel, M., 1958: Die Substituierbarkeit der Ionen und
Atome von geochemischen Gesichtspunkte aus II.
Über eine annähernde Bestimmung der Diadochieneigung.
Acta Geol. Hungarica, 5, pp. 381-433.

Viewing, K.A., 1968: Regional geochemistry and the Rhodesian
Basement Complex. Geol. Soc. S. Afr., LXXI;
Symp. on the Rhodesian basement complex, pp. 21-31.

Vogt, T.H.L., 1898: Über die relative Verbreitung der Ele-
ments, besonders der Schwermetalle, und über die
Koncentration des ursprünglich feinvertailten
Metallgehalts zu Erzlargerstätten. Ztsch. f. pract.
Geol., pp. 225-238, 314-327, 374-392, 413-420.

Wager, L.R., Brown, G.M., 1968: Layered igneous rocks.
Oliver & Boyd Edinburgh and London.

Waller, G.A., 1902: Report on the tin ore deposits of
          North Dundas.   Rep. Sec. Min. Tas., pp. 139-158.

Waterhouse, L.L., 1916: The south Heemskirk tin-field.
          Geol. Surv. Bull. Tasm., 21.

Wedepohl, K.H., 1956: Untersuchungen zur Geochemie des
          Bleis.   Geochim. Cosmochim. Acta, 10, pp. 69-148.

Whitten, E.H.T., 1959: Composition trends in a granite:
          Modal variation and ghost stratigraphy in part
          of the Donegal granite, Eire.   Jour. Geophys. Res.,
          64, pp. 835-848.

Whitten, E.H.T., 1960: Quantitative evidence of palimpses-
          tic ghost-stratigraphy from modal analysis of
          a granitic complex.   Rep. 21st Int. Geol. Congr.
          Copenhagen, Berlingske Bogtrykkere, 14, pp.182-193.

Whitten, E.H.T., 1963: Application of quantitative methods
          in geochemical study of granitic massifs.   Roy.
          Soc. Can., Spec. Pub. 6, pp. 76-123.

Winkler, H.G.F., 1961: On coexisting feldspars and their
          temperature of crystallization.   Instituto Lucas
          Mallada (Madrid) Cursillos y Conferencias,
          fasc. 8, p. 9.

Wyllie, P.J., and Tuttle O.F., 1961: Hydrothermal melting
          of shales.   Geol. Mag. 93, pp. 56-66.

PLATES

Plate 1

Steep slopes of mountainous part of the Mt.
Heemskirk massif (between sampling points
2 and 4) looking north from the Trial Harbour
- Grenville Harbour road.

Plate 2.

View from the summit of Mt.Heemskirk looking
southeast. Mt. Agnew (2769 feet) is highest
point of the far horizont.

7/9/94

Plate 3

1 - Outcrops of the white granite with tourma-
   line nodules on the summit of Gap Peak (100
   nodules per 1 m^2).

2 - Detail of the outcrop of the medium-grained
   white granite with tourmaline nodules stand-
   ing out in relief.

70/9/193+188

Plate 4

1 - Opencut of the Federation mine (Black Face).
   The main quartz-tourmaline vein (up to 5 me-
   ters in thickness) accompanied by system of
   parallel quartz-tourmaline and greisen vein-
   lets.

2 - Contact between medium-to fine-grained red
   granite and coarse-grained red granite in
   the vicinity of sampling point 5 (see the
   map I).

701 9 l192 + 196

Plate 5

1 - Contaminated porphyritic red granite (s.p.12).
    natural size.

2 - Contaminated porphyritic white granite (s.p.1)
    natural size.

70/9/199

Plate 6

1 - Coarse-grained red granite (s.p. 48) natu-
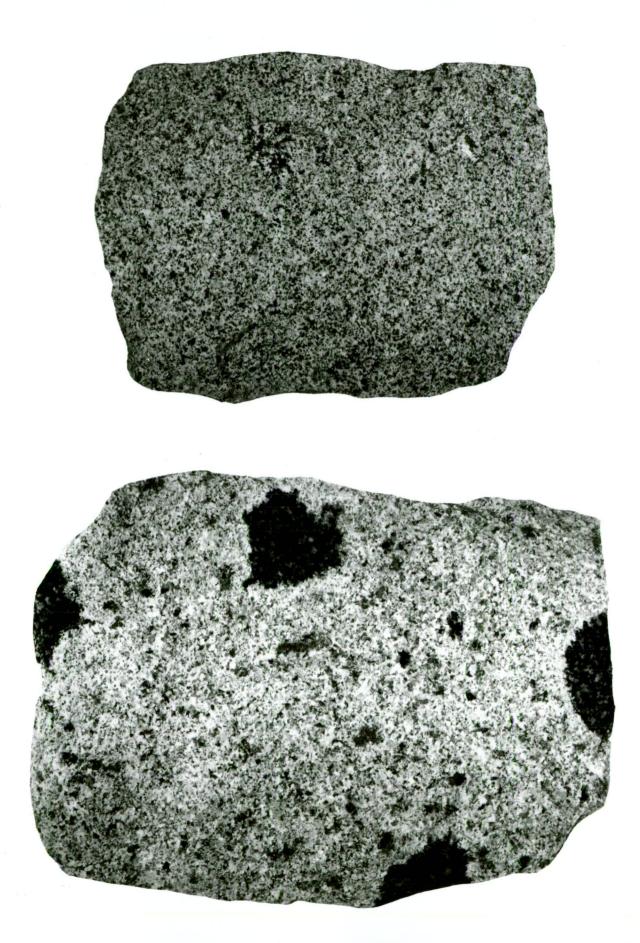   ral size.

2 - Coarse-grained white granite (s.p. 89),
    natural size.

Plate 7

1 - Coarse-grained red granite (s.p.52),
   natural size.
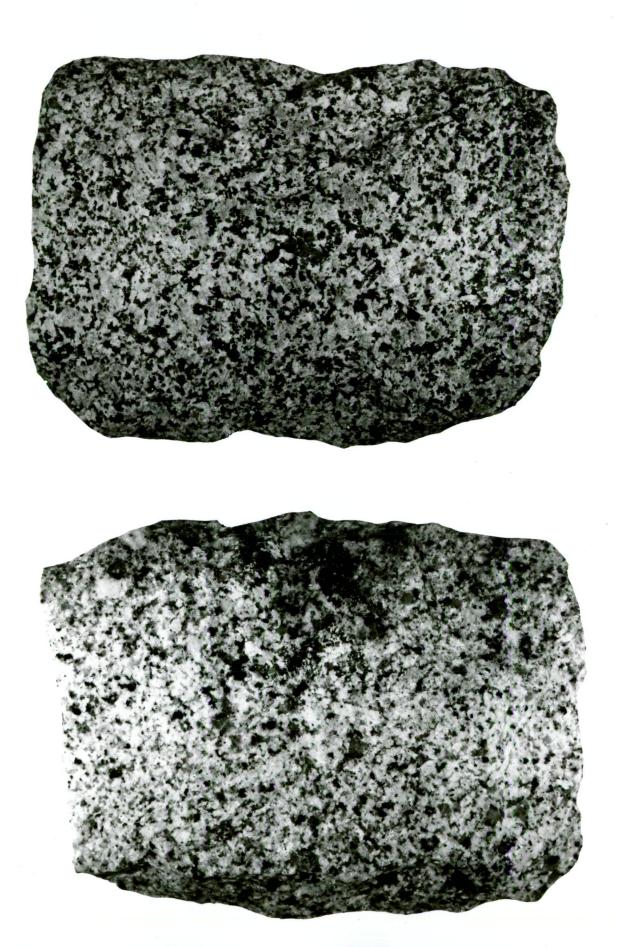
2 - Coarse-grained white granite (s.p.97),
   natural size.

Plate 8
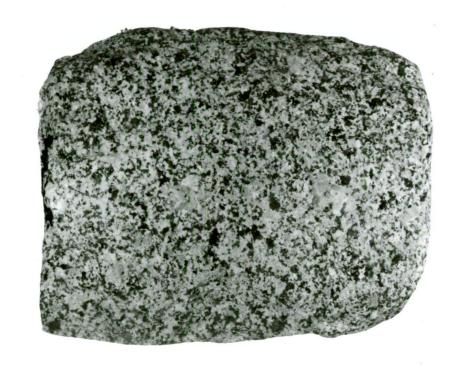
1 - medium-grained red granite (s.p. 19),
    natural size.
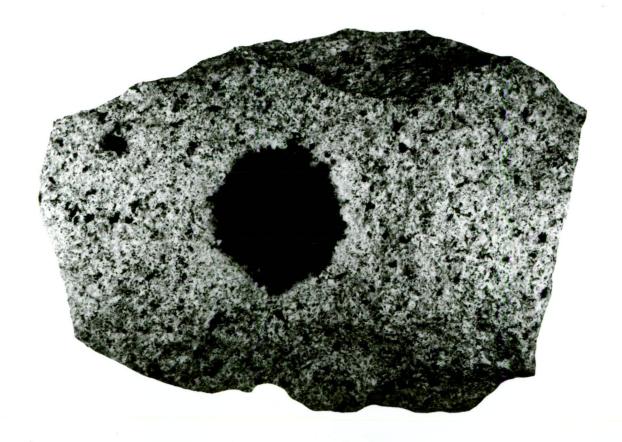
2 - medium-grained white granite (s.p. 90),
    natural size.

Plate 9

1 - medium-grained red granite (s.p. **6**7),
   natural size.

2 - medium-grained white granite (s.p. 85),
   natural size.

Plate 10
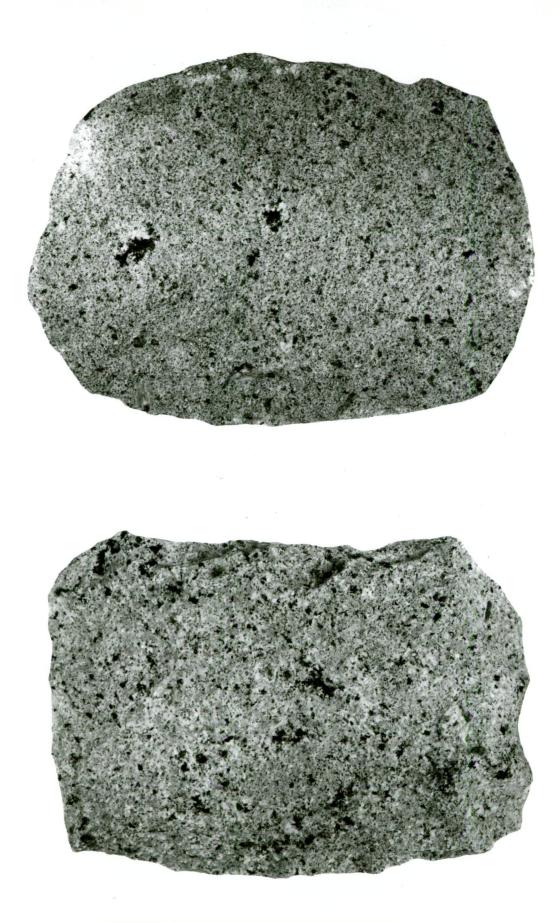
1 - fine-grained red granite (s.p. 24),
   natural size.

2 - fine-grained white granite (s.p. 13),
   natural size.

Plate 11
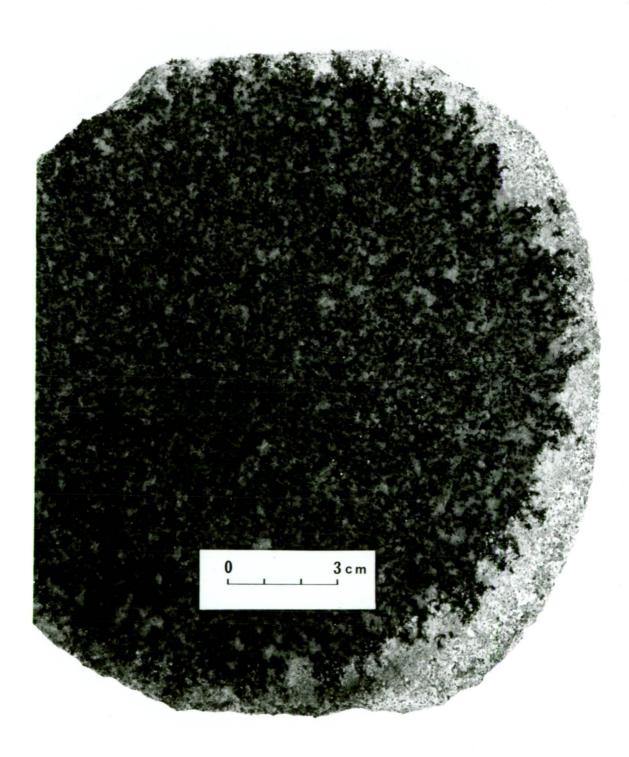
1 - fine-grained red granite (s.p. 37),
   natural size.

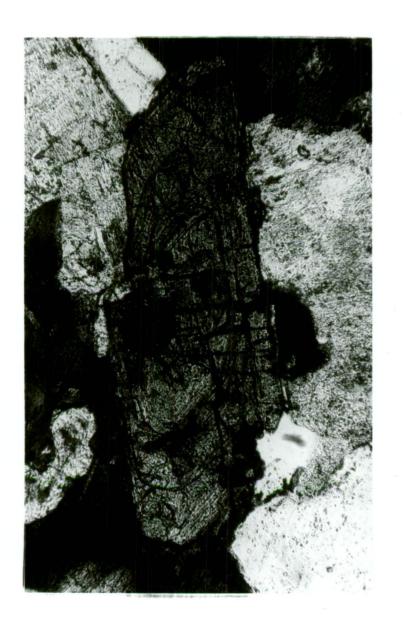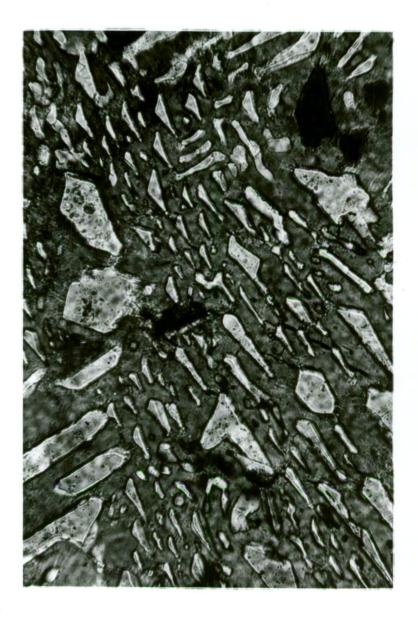2 - fine-grained white granite (s.p. 38);
   natural size.

Plate 12

Section through quartz-tourmaline nodule from
fine-grained white granite. The rim around the
nodule has metasomatic nature with protuberances
of quartz and tourmaline into the country rock.
Natural size.

0   3 cm

70/9/198

Plate 13

1 - Graphic intergrowths of K-feldspar (dark
    gray) and quartz (pale gray) in the medium-
    to fine-grained red granite.
    Thin section, X N, x 100.

2 - Zonal crystal of allanite in coarse-grained
    red granite.
    Thin section, X N, x 100.

Plate 14

1 - Relationship between tourmaline and K-feld-
    spar. Automorph crystal of K-feldspar is
    surrounded by younger tourmaline in medium-
    to fine-grained granite.
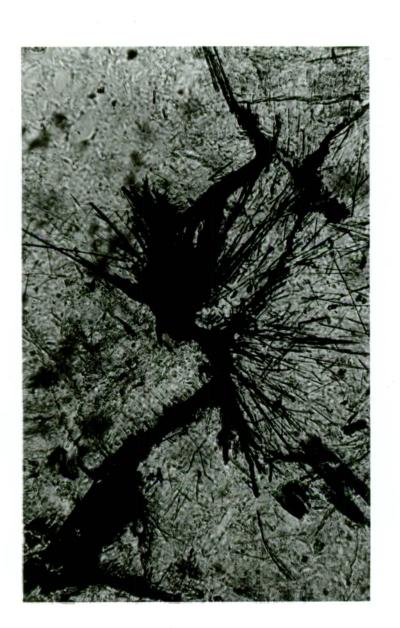   Thin section, // N, x 100.

2 - Relationship between tourmaline and K-feld-
    spar. Space among the quartz crystals (pale
    gray) is filled by tourmaline. Quartz -
    - tourmaline nodule from fine-grained white
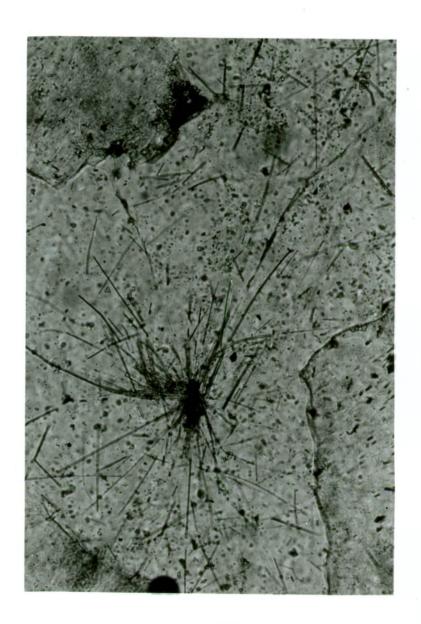   granite. Thin section, // N, x 100.

Plate 15

1 - Cluster of radially orientated needle-like
   crystals of tourmaline in the quartz of
   the coarse-grained red granite.
   Thin section // N, x 100.

2 - Tourmaline filling in the fracture following
   the grain boundaries in quartz agregate in
   the coarse-grained red granite. Needle-like
   crystals show radial arrangement.
   Thin section, // N, x 100.

Plate 16

1 - Shear fracture in the K-feldspar. Magnetite
    crystals are concentrated along or in close
    vicinity of the fracturing. Coarse-grained
    red granite.
    Thin section, // N, x 100.

2 - Selective tourmalinization of the quartzitic
    schists in the vicinity of the granite contact.
    The lamines of mudstones are replaced by tourma-
    line and quartzites remain intact.
    Thin section, // N, x 100.
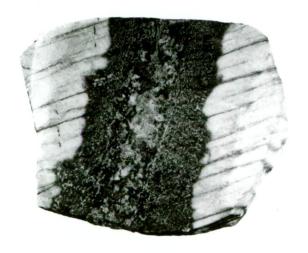
Plate 17

1 - Selective tourmalinization of the quartzitic
    mudstones from the granite contact (see Plate
    16-2), natural size.

2 - Cross section of the quartz-tourmaline veinlet
    orientated perpendicularly to the schistosity
    of Precambrian quartzites, in the vicinity of
    the granite contact. Crystals of cassiterite are
    accumulated in the centre of the veinlet.
    The margins of veinlet are marked by efect of
    the metasomatic reactions between the hydro-
    thermal fluids circulated along the fracture and
    quartz of the country rock. Natural size.
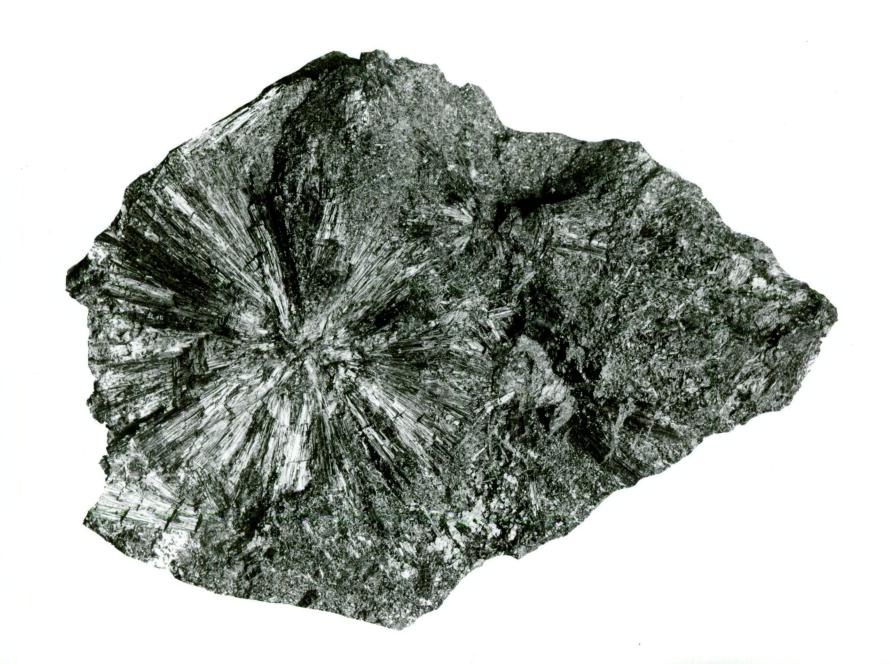
Plate 18

Breccia from the quartz-tourmaline vein intruding
Precambrian rocks in close vicinity of the granite
contact. The fragments of tourmalinised mudstones
are cemented by white quartz. The clusters of
tourmaline crystals are grouped around the rock
fragment and on the wall of the fracture.
Natural size.

Plate 19

Tourmaline "sun" in the coarse grained tourmaline
agregate from quartz-tourmaline vein in Cliff Mine,
2 km southwest of Trial Harbour. Natural size.

Plate 20

Zircon crystals from coarse-and medium-grained
red granite.

1 - Simple crystals of magmatic zircon type

2 - 3 - Zonal crystals of magmatic zircon type

4 - Older zircon crystal closed in the younger
    crystal of magmatic zircon type.
    // N, x 100.

1   2   3   4

Plate 21

5 - 8 - Zircon crystals from the contaminated
porphyritic red granite. Magmatic
zircons contain rounded inclusions of
older zircons which may be derived from
the assimilated country rocks.
// N, x 100.

5 6 7 8